PETROLEUM RESEARCH JOURNAL

TECHNICAL PAPERS

ENGINEERING

Estimation of recovery factor of Libyan carbonate oil reservoirs,..... *A.Y. Zekri and M.S. Nasar.* 3

The application of gridrefinement, gridgathering and moving grid in EOR simulation,.... *Z.E. Heinemann and C. Brand.* 10

Constraints on enhanced oil recovery development,..... *P. Simandoux and E. Valentin.* 22

EXPLORATION

Geochemical investigation of the Bahi Formation in the western part of the Sirt Basin, Libya,.... *A.M. Sghair.* 33

Evaluation of bentonic clays of Umm ar Rizam area, Libya, as potential drilling muds,.... *D.M. Watson and M. Rahuma.* 46

CHEMISTRY

Kinetics of orthovanadate catalysed epoxidation of maleic anhydride by hydrogen peroxide,.... *I. Ahmad and M. Degam.* 52

Characterization of methanol-utilizing bacteria and yeast as a single cell protein product,.... *M. Bushwereb, A. Al-Misuraty and S. Al Jelani.* 56

SHORT NOTES

A computer program to simulate two-phase pipeline flow,... *M.M. Elgarni, H.H. Beck and N.A. Faruqi.* 59

Butadiene reactions using the EROS 5.0 computer program,.. *T. Elgomati and K. Rafeiner.* 63

Study of corrosion damage to Cu/Ni chlorinator line by sea water,..... *M.L. Mehta and A.T. Hassan.* 68

Determination of trace metals in some gas oil fractions of Libyan crude oils by electrothermal atomic absorption spectrometry,..... *I. Busheina, I. Ahmad, H.M. Kut, N. Bawash and S. Zayed.* 72

VOLUME 4–1992

Petroleum Research Centre
P.O. Box 6431 Tripoli
Great Socialist People's Libyan Arab Jamahiriya

PRJ, Vol. 4. (January 1992); P. 3–9, 5 FIGS, 3 TABLES.

ESTIMATION OF RECOVERY FACTOR OF LIBYAN CARBONATE OIL RESERVOIRS

A.Y. Zekri*, M.S. Nasar*

تقدير الإحتياطي النفطي لمكامن الصخور الكربونية الليبية

عبد الرزاق يوسف زكري ومحمد السنوسي نصر

يعتبر تقدير الإحتياطي النفطي الممكن إنتاجه بواسطة الطرق المتبعة حالياً وخاصة الحقول المكتشفة حديثاً والتي لم يتم وضعها على الإنتاج من أهم المعلومات التي يتم بناء عليها إستكمال الدراسات المختلفة لتحديد إقتصاديات ذلك المكمن.

وبالقاء نظرة فاحصة على المراجع العلمية الخاصة بتقدير الإحتياطي النفطي للمكامن الحديثة المكتشفة بناء على المعلومات الأولية البسيطة، نجد عدد محدود جداً على المستوى العالمي. فقد تم إستنتاج علاقة متبادلة للإحتياطي وعدد من خواص الصخور والموائع للمكامن ذات الصخور الرملية باستخدام معلومات تم تجميعها من الحقول النفطية بالولايات المتحدة الأمريكية.

تم من خلال هذه الدراسة إستنتاج وإستخلاص علاقة متبادلة بين عدداً من خواص صخور وموائع المكامن النفطية الليبية ومعامل الإستخراج أو الإحتياطي. فباستخدام المعلومات الخاصة بالمسامية، اللزوجة، التشبع، النفادية والسمك لعدد أربعون حقل نفطي ليبي ذات الصخور الكربونية وباستعمال طرق التحاليل بالمضاهاة (MULTIPLE CORRELATION ANALYSIS) تم تحديد علاقة بين الإحتياطي وتلك الخواص، مما يمكن من تقدير الإحتياطي لمكامن الصخور الكربونية المكتشفة حديثاً والمتواجدة عادة في المناطق العربية.

إن إستخدام العلاقة المستخلصة في هذه الدراسة ستمكن من تقدير الإحتياطي لمكامن الصخور الكربونية بدقة أكبر عنها من إستخدام العلاقات المستنتجة سابقاً والخاصة بالحقول الرملية.

ABSTRACT

Estimation of recovery factor of any newly discovered reservoir is an important piece of information needed to assess the economical viability of that reservoir. Therefore, it is essential to be able to predict as accurately as possible the reservoir reserves based on limited data available on hand for newly discovered reservoirs.

In this study, data collected from forty Libyan oil reservoirs were utilized to generate a correlation between reservoir future recovery factor and basic reservoir data of porosity, permeability, saturation, oil viscosity and net formation thickness. This correlation will provide a useful tool for any engineer dealing with carbonate oil reservoirs to predict with more confidence its recovery factor after drilling a wildcat well and collect limited data.

INTRODUCTION

Our current life has been influenced by oil and gas more than any other natural resource, and indications are that oil and gas reserves will increase in importance in the remainder of this century. Oil and gas provide an inexpensive source of energy.

Reserve estimates have dictated actions of different Governments, entire industries, individual companies and lending institutions. Many people working in the petroleum industry, especially petroleum engineers spend a major part of their professional lives developing estimates of reserves together with new methods and techniques for improving these estimates. The confidence levels and the technique utilized by the petroleum engineer depend on the quantity, reliability and the maturity of the data available. The

*Petroleum Engineering Dept., Al Fateh University, Tripoli, G.S.P.L.A.J.

data quality, therefore, indicate the confidence one should have in the reserve estimates.

There are various methods used by the oil industry to estimate recovery factor such as analogy, volumetric calculations and performance techniques (numerical simulation models, material balance and decline curve analysis).

Before a reservoir is drilled, prospective reserves are usually estimated on the basis of analogy. On the other hand, if little or no production from the target formation exists, then statistical data from wells completed in the formation is used to predict the recovery factor of that reservoir. When performing a statistical analysis for prediction purposes, a simple average of various rock and fluid data needed to be employed in the technique is normally required.

By searching the literature regarding recovery factor estimate based on limited rock and fluid data obtained from a newly discovered oil field, one notices that limited work has been done. In a reservoir study made by Craze & Buckley [1], 70 of 103 fields analysed produced wholly or partially by water-drive conditions.

Arps [2] indicated that data obviously is related to the reservoir oil viscosity and permeability. He obtained average correlation between oil viscosity and oil residual saturation, and took into consideration another variable, reservoir permeability.

Guthrie & Greenberger [3] conducted a statistical study using multiple correlation analysis methods. They found a correlation between water-drive recovery and five variables, permeability, saturation, viscosity, porosity and net formation thickness for water-drive sandstone reservoirs. They indicated that 50 percent of the fields had recoveries within ± 6.2 percent of the predicted recovery by the correlation. This correlation is used extensively for sandstone or carbonate reservoirs to obtain a rough estimate of recovery efficiency despite its limitations.

Since most of the Libyan oil reservoirs and Middle East oil reservoirs are of carbonate type (limestone and dolomite type of lithology), it is essential to utilize data from fields representing Libyan reservoirs. In this study, data from 89 carbonate and sandstone Libyan reservoirs were employed to try to develop different correlations between recovery factor and various fluid and rock data. Most useful correlation developed using multiple regression analysis for water-drive carbonate reservoir was 40 Libyan reservoirs data representing different carbonate horizons with water influx mechanism.

Results indicate that 0.113 standard deviation exists in this type of reservoir. Meanwhile, if only reservoirs with recovery factors of 20 percent or higher are used, we observe improvement in correlation results. A substantial reduction in standard deviation from 0.113 to 0.079 percent is observed, i.e. a more reliable correlation.

DISCUSSION

Reserve estimates are just those estimates which can be no better than the data on which they are based and are subjected to the experience of the estimator. Unfortunately, reliable reserve figures are most needed during the early stages of a project, when only a minimum amount of information is available. As the field is put on production, more data and information become available. As the project matures, this increase in data with which to work, changes the method or methods used to predict the recovery factor and improves the confidence in the reserves estimates. Recovery factor is estimated during various stages of oil reservoir life. These stages are before drilling, or any subsurface development, after drilling few wells, before producing the reservoir, after some performance information is available and after performance trends are well established. In this study, the main period of the life of the reservoir in recovery efficiency could be estimated after drilling few wells and before producing the reservoir.

Various types of reservoirs were analysed to develop a correlation between recovery factor and various fluid and rock properties, porosity, permeability, saturation and viscosity. The main correlation developed for water-drive carbonate oil reservoirs were data from 40 Libyan oil reservoirs, see Table 1, which were utilized to develop the correlation. The empirical correlation obtained was:

$$RF = 0.0554 + 0.6065 \text{ porosity} + 0.0955 \log\left(\frac{K}{\mu}\right) - 0.0571 S_w - 0.0426 \log H$$

As shown in Fig. 1 data is scattered mostly below the chosen line for recovery factor of 20% or higher and above the line for points with recovery factor below 20% with a standard deviation of 0.114. Therefore, elimination of data points of RF below 20% were tested and results were plotted in Fig. 2. As shown in Fig. 2, more fair distribution of data was obtained with a standard deviation of 0.079.

The correlation between oil recovery and various data for water-drive carbonate reservoirs with RF greater than 20% is:

$$RF = 0.3251 - 0.1287 \text{ porosity} + 0.0745 \log\left(\frac{K}{\mu}\right) - 0.046 S_w - 0.0433 \log H$$

Table 1. Water Drive-Carbonate Reservoirs Data

Field	POR frac.	K md	U cp	Sw frac.	Reported Empirical H ft.	Reported Empirical RF frac.	RF frac.	Without H RF frac.
Ali NC29B	0.230	90.0	0.650	0.460	37.0	0.480	0.306	0.307
Almas NC29C	0.236	16.0	0.580	0.455	58.0	0.490	0.235	0.244
Intisar 103E	0.190	190.0	1.100	0.440	17.0	0.200	0.307	0.290
103D Elgiza	0.266	43.0	3.200	0.287	30.0	0.270	0.245	0.239
Intisar 103B	0.200	490.0	0.024	0.230	33.0	0.49	0.510	0.502
Sabah Beda C(I)	0.241	353.0	0.800	0.185	36.2	0.491	0.377	0.371
Sabah Beda C(II)	0.272	353.0	0.800	0.354	26.3	0.491	0.392	0.386
W. Sabah Beda C(I)	0.206	200.0	0.800	0.236	33.0	0.302	0.331	0.322
W. Sabah Beda C(II)	0.203	100.0	0.800	0.494	44.0	0.302	0.281	0.284
E. Sabah Bedac	0.182	200.0	0.800	0.197	29.5	0.131	0.321	0.308
Elgiza E &W	0.260	150.0	1.400	0.430	32.0	0.350	0.318	0.317
Gialo	0.222	153.0	3.080	0.310	98.0	0.377	0.249	0.264
Choboc (Kalash)	0.388	520.0	0.540	0.450	27.3	0.300	0.489	0.492
Tagrifet (Farrud)	0.250	35.0	2.030	0.270	35.0	0.120	0.244	0.239
Farrud (Mabruk)	0.246	145.0	0.790	0.450	38.0	0.375	0.328	0.330
Bouri	0.150	300.0	3.490	0.200	500.0	0.150	0.204	0.242
Ed Dib (Gir/Fach)	0.240	100.0	0.700	0.350	85.0	0.150	0.304	0.318
Um-Farroud	0.240	40.0	0.700	0.270	38.0	0.330	0.286	0.283
Field 4Z DOL	0.240	40.0	2.600	0.270	38.0	0.148	0.231	0.228
BuMras(Mabruk) LS	0.260	340.0	13.000	0.450	7.4	0.391	0.286	0.258
Daba (Farr UD)	0.220	45.0	1.650	0.570	53.0	0.200	0.220	0.230
Facha (Mabruk)	0.250	23.0	0.940	0.770	24.0	0.140	0.240	0.242
103E Elgiza B	0.050	250.0	6.500	0.500	49.0	0.040	0.136	0.134
103E Elgiza A	0.268	370.0	6.500	0.410	18.6	0.060	0.308	0.297
103E Gir B	0.246	200.0	1.700	0.311	30.8	0.304	0.321	0.315
103E Gir A	0.245	16.0	1.700	0.300	56.0	0.233	0.205	0.210
Bahi PL7 LS	0.280	150.0	0.700	0.445	103.2	0.400	0.336	0.359
Bahra PL7 LS	0.301	34.5	1.230	0.448	28.8	0.330	0.288	0.288
Nasser	0.186	5000.0	0.880	0.220	122.0	0.461	0.425	0.440
Gialo	0.200	45.0	3.000	0.520	18.0	0.099	0.206	0.193
"Paleocene LS	0.252	14.5	0.670	0.301	49.6	0.340	0.246	0.249
"4B Paleocene	0.195	400.0	0.840	0.555	85.0	0.300	0.320	0.332
Barash P'cene LS	0.200	388.0	1.190	0.471	16.6	0.450	0.338	0.322
Kasrab P Basel D	0.237	27.1	2.400	0.440	29.0	0.300	0.212	0.208
Warid Field	0.220	2.0	3.700	0.500	40.0	0.034	0.066	0.069
Beda Field	0.200	60.0	2.800	0.500	60.0	0.300	0.199	0.208
Kotla Field	0.220	60.0	2.000	0.350	150.0	0.130	0.217	0.240
Umm-Faroud	0.240	40.0	0.700	0.270	38.0	0.330	0.286	0.283
Facha (Gir) Dol	0.240	25.0	1.400	0.330	42.0	0.140	0.232	0.232

Empirical Recovery Factor, including H, fraction = 0.0554 + 0.6065 (porosity) + .0954 (log(k/μ) − 0.0571 (Sw) − 0.0426(log(H)) Standard Deviation = 0.114 Empirical Recovery Factor, without H, fraction = −0.0358 + 0.6603 (porosity) + 0.0957(log(k/μ)) − 0.0304 (Sw) Standard Deviation = 0.113

Another correlation was obtained for solution gas drive carbonate-oil reservoirs. Data from only 7 Libyan reservoirs were utilized, with the following result:

$$RF = 0.3514 - 1.1967\ \text{porosity} + 0.00955 \log\left(\frac{K}{\mu}\right) + 0.0205\ S_w - 0.0434 \log H$$

With standard deviation of 0.035, due to limited data used in the correlation, not much confidence is given to this result, (see Fig. 3, and Table 2).

From the analysis of data from 9 Libyan carbonate oil reservoirs with water injection, see Table 3, the following correlation was obtained, where standard deviation is 0.073:

$$RF = -0.2224 + 0.1262 \log\left(\frac{K}{\mu}\right) - 0.0163\ S_w + 0.1722 \log H$$

Again, not much confidence is given to this correlation due to the limited data used (Fig. 4).

The effect of using limited data, i.e. no pay thickness was utilized in the analysis, was also examined

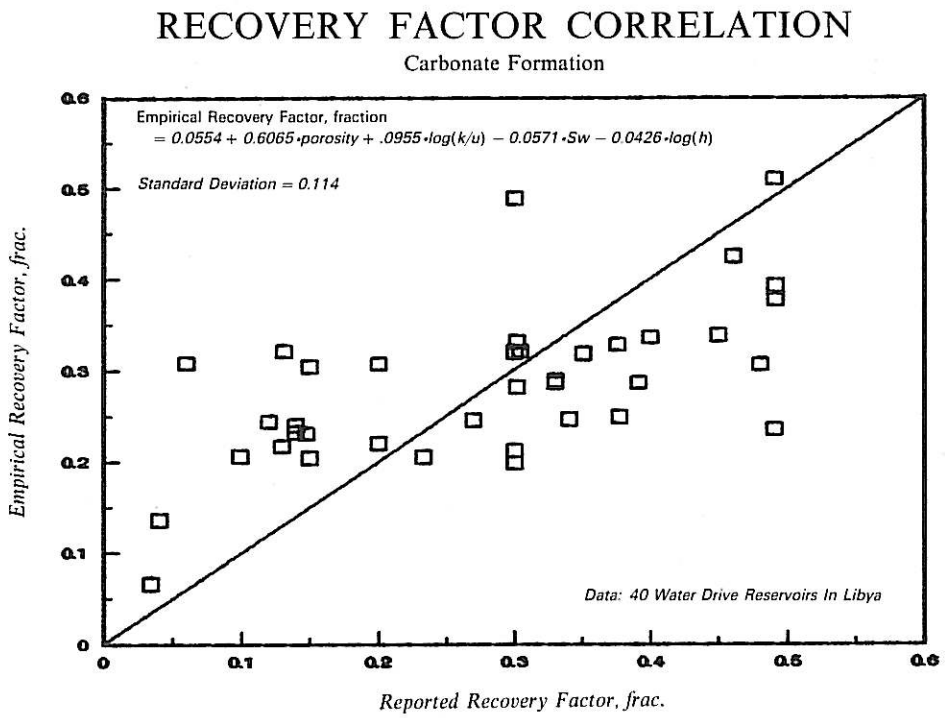


FIG. 1. Relationship between empirical and reported recovery factors for carbonate formation – water drive reservoirs.

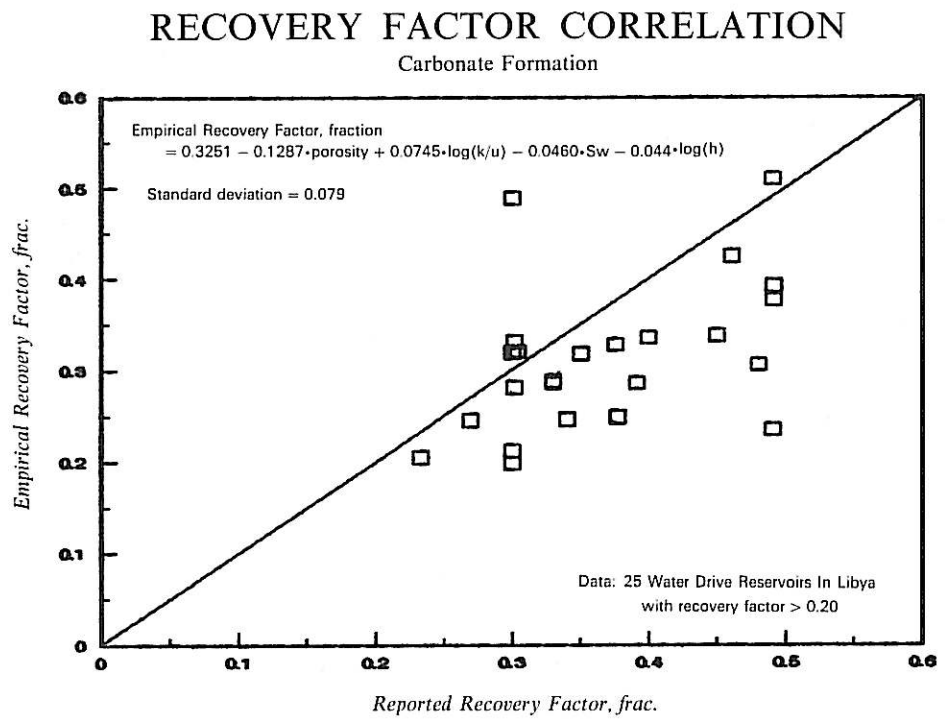


FIG. 2. Relationship between empirical and reported recovery factors for carbonate formation – water drive reservoirs.

for the case of water-drive carbonate reservoirs and the following empirical correlation was obtained:

$$RF = -0.0358 + 0.6603\ \text{porosity} + 0.0957 \log\left(\frac{K}{\mu}\right) - 0.0304\ S_w$$

With standard deviation of 0.113, the data and the distribution of the results are presented in Table 1 and Fig. 5 respectively.

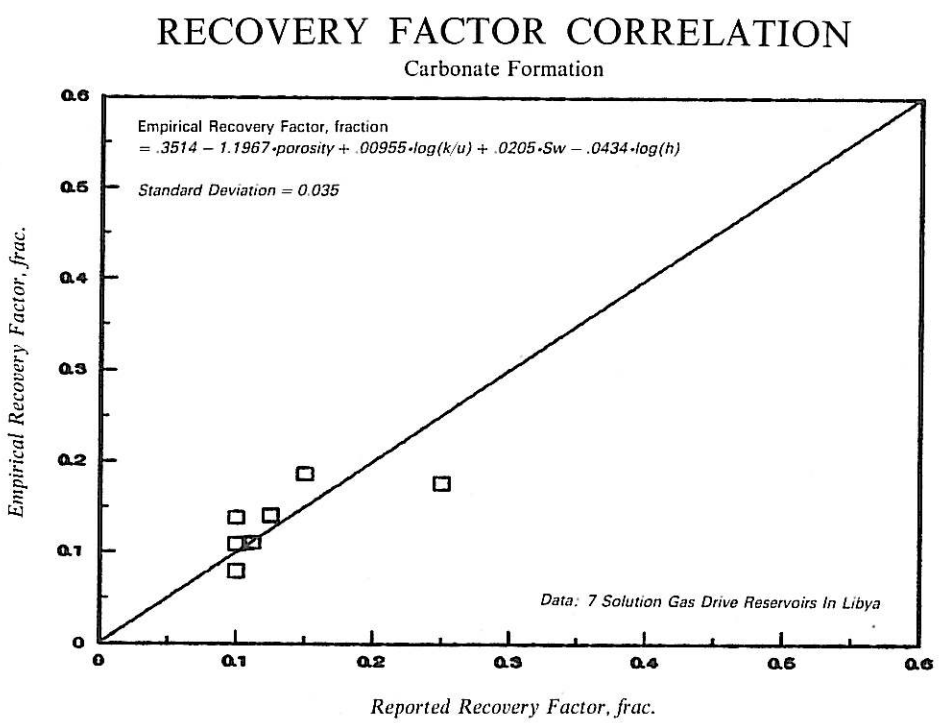


FIG. 3. Relationship between empirical and reported recovery factors for carbonate formation – solution gas drive reservoirs.

Table 2. Solution Gas Drive- Carbonate Reservoir Data

					Reported Emperical		
FIELD	POR frac.	K md	U cp	Sw frac.	h ft	RF frac.	RF frac.
Hofra (Thalita)	0.170	6.0	0.580	0.330	32.0	0.150	0.186
Dahra B	0.330	150.0	0.630	0.420	17.6	0.100	0.138
Mellugh (Facha)	0.250	25.0	0.354	0.390	25.0	0.250	0.176
Defa LS	0.160	3.2	1.600	0.320	94.0	0.112	0.110
AA Area LS	0.244	14.7	1.200	0.400	27.7	0.100	0.109
Hofra – Dahra B	0.320	25.0	0.620	0.360	14.2	0.100	0.079
Hofra Dahra B & Mabruk	0.330	150.0	0.600	0.420	17.6	0.125	0.140

Empirical Recovery Factor, frac. = .3514 – 1.1967 (porosity) + .00955(log(k/μ)) + .0205 (Sw) – .0434(log(h)
Standard Deviation = 0.035

Table 3. Water Injection-Carbonate Reservoir Data

					Reported Emperical		
FIELD	POR frac.	K md	U cp	Sw frac.	h ft	RF frac.	RF frac.
Intisar C103 Reef	0.220	85.0	0.560	0.494	141.0	0.550	0.414
Intisar A103 Reef	0.198	18.0	0.160	0.113	648.0	0.472	0.518
Zella NC74B Facha	0.195	7.7	0.176	0.199	117.0	0.350	0.338
Fidaa Facha	0.209	125.0	0.970	0.370	67.0	0.300	0.343
North Hakim Facha	0.204	14.0	0.150	0.222	29.0	0.300	0.276
South Hakim Facha	0.216	27.0	0.420	0.251	46.0	0.300	0.285
Gham Farrud	0.250	50.0	0.400	0.250	50.0	0.300	0.328
Gham Farrud	0.270	50.0	0.400	0.250	55.0	0.300	0.335
Zeuad	0.270	50.0	0.400	0.250	55.0	0.300	0.335

Empirical Recovery Factor, frac. = 0.2224 – .1262(log(k/μ) – 0.0163(Sw) + 0.1722(log(h)) Standard Deviation = 0.073

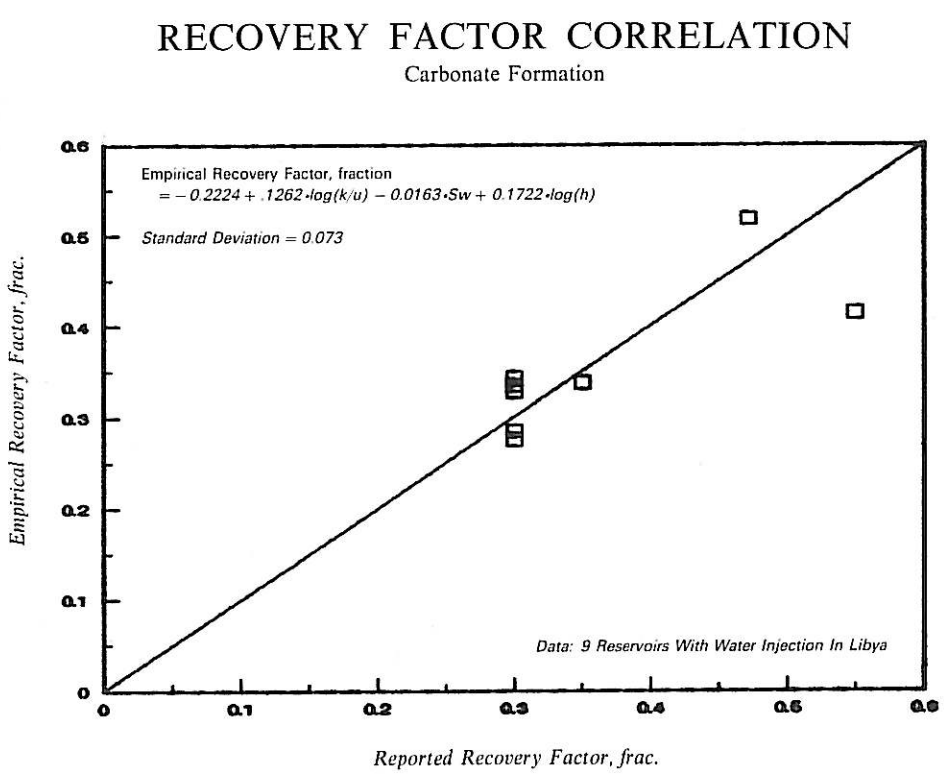


FIG. 4. Relationship between empirical and reported recovery factors for carbonate formation – water injection reservoirs.

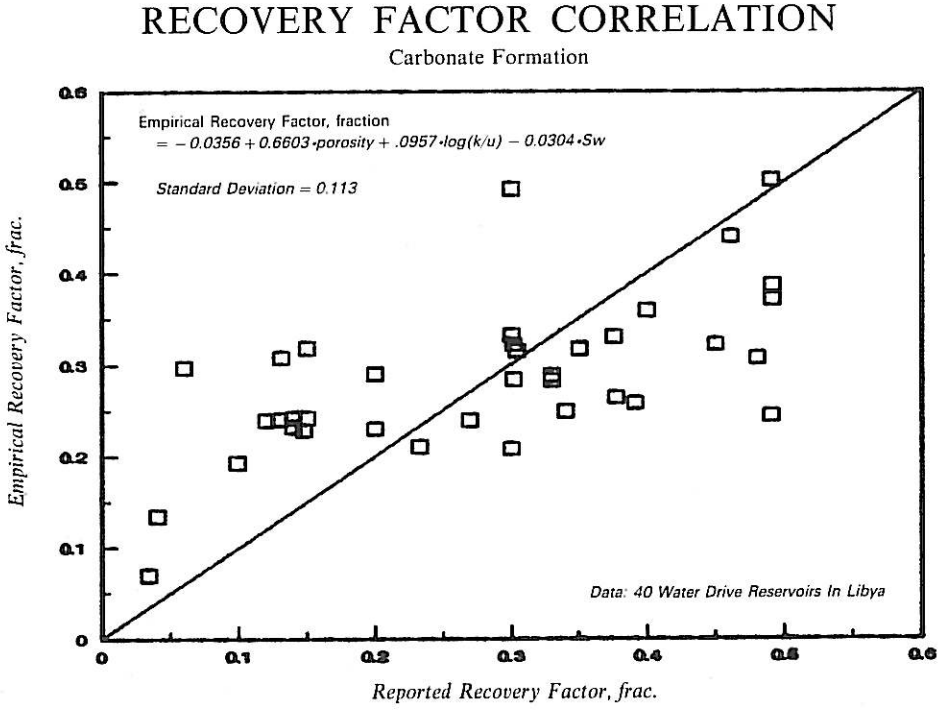


FIG. 5. Relationship between empirical and reported recovery factors for carbonate formation – water drive reservoirs excluding pay thickness.

CONCLUSIONS

1. A new correlation for Libyan carbonate oil reservoirs to estimate RF using limited data was developed.
   This correlation could be used in estimating the oil recovery factor for all newly discovered Middle East water-drive carbonate oil reservoirs.
2. A correlation for solution-gas drive carbonate oil reservoirs was obtained to be used as a rough estimate of RF.
3. Libyan sandstone water-drive reservoirs correlation was also developed.

ACKNOWLEDGEMENT

The authors would like to thank all Libyan Oil Companies and NOC Production Department for providing the data used in this study and for their permission to publish the work. Thanks are also extended to WAHA Oil Company for granting permission to use their computer facilities.

REFERENCES

[1] Craze R.C. and Buckley S.E., 1945, "Actual Analysis of the Effect of Well Spacing on Oil Recovery", Drilling and Production Practice, API, pp. 144–155.

[2] Arps J.J., 1956, "Estimation of Primary Oil Reserves", Trans. AIME, 207, 183–186.

[3] Guthrie R.K. and Greenburger Martin K., 1955, "The use of Multiple Correlation Analysis for Interpreting Petroleum-Engineering Data", Drilling and Production Practice, API, pp. 135–137.

[4] Garb F.A., 1985, "Oil and Gas Reserves Classification Estimation and Evaluation", Journal of Petroleum Technology, pp. 373–390.

[5] "World Petroleum Congress Study Yields Reserves Classification", 1983, Oil and Gas Journal.

[6] "Proven Reserves Definition", 1981, Journal of Petroleum Technology, 2113–14.

[7] Petroleum Engineering and Production Handbook, 1962, T.C. Frickem McGraw-Hill Book Co. Inc., New York City, Vol II, Chapters 37 and 38.

PRJ, Vol. 4. (January 1992); P. 10–21, 19 FIGS.

THE APPLICATION OF GRIDREFINEMENT, GRIDGATHERING AND MOVING GRID IN EOR SIMULATION

Z.E. Heinemann* and C. Brand*

تطبيقات تحسين وتجميع وتغيير التقاسيم المكنية في محاكاة الإسترداد الإضافي

ز. هينمان وك. براند

يصل طول ضلع شبكة التقسيم في نظام محاكاة النفط الثقيل إلى 100 م في المكامن ذات طاقة الدفع المستنفذة ، الذاتية . كما أن طرق الإسترداد الإضافي مثل الإزاحة المتجانسة والإزاحة البخارية والغمر الكيميائي والإحراق الداخلي تتطلب تقسيم المكمن إلى مساحات صغيرة بطول ضلع يتراوح ما بين 0.5 إلى 10 أمتار. غير أن هذه التقسيمات تعتبر مستحيلة فنياً وعملياً عند تطبيقها في محاكاة المكامن النفطية .

تشير هذه الدراسة ، التي تعتمد على طريقة التحكم في الحجم التفردي للمكمن ، على أن تحسين شبكة تقسيم محاكاة المكمن هي إمتداد للطرق المتبعة عملياً في محاكاة المكامن النفطية . وحيث أن التقاسيم الصغيرة للمكمن النفطي مطلوبة فقط عند مقدمة سوائل المكمن المزاحة ، لذلك فأن تحسين حجم المكمن مطلوبة فقط في هذه المنطقة .

ABSTRACT

In black oil simulation, the areal block size can have a magnitude of 100 m by water drive and can extend to 1000 m by depletion drive. EOR displacement processes such as miscible and steam drive, surfactant flooding and in situ combustion require 10 to 0.5 m grid spacing. This is technically impossible in field scale simulation which uses a conventional Cartesian grid.

This paper, based on the control volume discretization technique, shows that local grid refinement is a straightforward extension of industry standard methods. Applying some simple rules, the locally refined grid is strictly orthogonal, even at the fine-coarse grid transition. This orthogonality is a fundamental requirement to make sure that the numerical solution converges to the true one if the grid size is reduced.

Since small block size is only required at the displacing front, local grid refinement is applied only in this area and moves forward in time. With dynamic grid refinement, the down-streams block ahead of the front are subdivided before the displacing front arrives and they are gathered again when the front has passed them. By gathering the blocks outside the EOR area, the overall block number can be reduced considerably without neglecting the influences of the environment.

An example for missible hydrocarbon gas drive illustrates the combination of dynamic grid refinement and gathering, showing that a field scale EOR displacement can be simulated with small block size without exceeding the technical and economic limits.

INTRODUCTION

Numerical simulation has become one of the most important tools to solve complex reservoir engineering problems. Based on a mathematical description of the physical system, a set of non linear differential equations are solved numerically and the result is compared with the observations. By tuning reservoir parameters, called history matching, a numerical reservoir model is created which is able to reproduce the real reservoir performances and gives the possibility of predicting future behaviour. A good fitting neither confirms the mathematical description nor proves the accuracy of the numerical

*HOT Engineering Ges.m.b.H., Austria

solution or genuine reservoir data. Inaccuracies on one side are counterbalanced by deviations on other side. This circumstance does not restrict the applicability of the model provided that no greater change in the reservoir mechanism takes place.

In black oil simulation, the mathematical description is simple and well defined. The result is not seriously influenced by the numerical solution techniques in use. The number of system variables is limited and identical in time and space. However, it is important that enough observations are available to confirm the reliability of the numerical reservoir model.

When dealing with enhanced recovery processes, the situation is rather different. A large variety of methods exists and the possibilities in mathematical description are wide spread. The physical and chemical natures of the ongoing processes change dramatically in time and space, differing fundamentally from the primary ones. The history matching based on black oil type simulation gives no or very limited guarantee for realibility of the EOR prediction. In most of the cases is it inaccurate to speak about simulation, because no possibility is given to compare the model with observations of the real reservoir. What normally is done is simply mathematical-numerical modelling the reliability of which can only be based on the complete and correct mathematical formulation, on the accurate numerical solution and the complete and proper accounting of the influence of reservoir properties.

This paper focuses on gridding to show the neccessity and practical applicability of grid refinement and gathering. Local grid refinement is necessary to get enough small blocks at the area of interest and gathering makes it possible to consider the environment without spending computer time and money to calculate unneccessary details. The possibility to change the grid over time, by the user or automatically, increases the flexibility of these techniques considerably. The methods are applicable for modelling of miscible drive, polymer and surfactant flooding, steam drive and in situ combustion and also for conventional black oil and compositional simulation.

FINITE CONTROL VOLUME FORMULATION OF THE FLOW EQUATION

The reservoir system is formed by the formation rock given the frame for the pore space and K chemical components. The pore space is filled out by P phases, may be vapor, liquid or solid. Each fluid phase contains up to K chemical components.

The first and most fundamental step in the development of any reservoir simulator is the description of the physical phenomena by a set of equations. This equation system contains mole (or mass) balances for each component and one energy balance equation. Additional information, in the form of constitutive equations is needed to define the intrinsic response of the material in question. They formulate the relations between driving forces and transport velocities and the mathematical properties (as densities and viscosities) to the state variables. In reservoir simulation, conditions of thermodynamic equilibrium are commonly assumed. The assumption of equilibrium, while questionable in many situations, plays an important role in the derivation of the final form of the mathematical model.

The equation system in question is very complex and non linear. Analytical solution is possible only after strong simplifications, thereby losing the applicability to real reservoir problems. Though a number of numerical techniques have been tried, almost all such problems are solved through the finite difference method. For this reason, the discussion in this paper is limited to this method.

The finite difference method, especially in the form of the finite volume technique, has some theoretical and numerical advantages. The difference equations can be easily identified with the corresponding differential equations and the solution of the finite difference equations is more straightforward. Most importantly it is possible to identify the numerical terms with the reservoir ones. The control volume represents a defined part of the reservoir and all properties and variables assigned to the grid point are averages for this volume.

Before going on to solve the equation system, certain substitutions are made to reduce the number of unknowns and equations per grid point. The phase pressures, except one, are eliminated through the capillary pressure equations, a part of the mole fractions are eliminated using mole constraints and phase equilibrium conditions. Darcy's law is substituted to eliminate phase velocities as variables. The variables eliminated by substitution are called secondary. They do not eliminate primary variables. Some of the primary variables existing only in equations belonging to one grid point can be eliminated by partial elimination. The variables solved simultaneously for all grid points are the implicit variables. The eliminated the explicit ones.

With growing complexity of the mathematical description, increases the variety for selection of primary-secondary and implicit-explicite variables and the resulting equations bring advantages and disadvantages by the numerical solution (more or less stability, higher or lower convergence rate by the Newton iteration, etc.). One of the advantages of the finite difference method is that substitution and partial elimination can be done before and after discretisation. It is possible to do it algebraically or

numerically assuring great flexibility, especially important when dealing with EOR models. The wide range of EOR technologies and possible description of the physical phenomenon requires such a flexibility.

An integral approach similar to the one described by Nghiem [1], and Pedrosa and Aziz [2] is applied to derive the multiphase flow equations.

The conservation of mass for the component k:

$$-\iint_{A_I}\left[\sum_{p=1}^{P}\vec{u}_p\xi_p x_{pk}M_k\right]\vec{n}dA+\iiint_V q_k M_k dV$$
$$=\frac{\partial}{\partial t}\iiint_V\left[\phi\sum_{p=1}^{P}S_p\xi_p x_{pk}M_k\right]dV. \tag{1}$$

V is a finite control volume around the grid point I (Fig. 1). The first term on the left-hand side is the *convection term*. Its physical meaning is very easy to understand. $\vec{u}_p$ is the phase velocity with dimension $m/s = m^3/(s\ m^2)$ and gives the phase volume flowing per second through a unit surface perpendicular to the flow direction. ξ_p is the mole density $mole/m^3$ of the phase, and the product $\vec{u}_p\xi_p$ is the mole velocity in $mole/(s\ m^2)$. This is the number of moles flowing through the unit surface. Multiplying by the mole fracture x_{pk} and the mole weight M_k $kg/mole$ one gets the mass velocity $kg/(s\ m^2)$ of component k. On the surface of the control volume, the mass velocity can be split into two components: one parallel to the surface, the other orthogonal on it. We obtain the orthogonal component by multiplying the velocity with the normal unit vector $\vec{n}$. The expression

$$\sum_{p=1}^{P}[\vec{u}_p\xi_p x_{pk}M_k]\vec{n}dA \tag{2}$$

is the mass flow rate kg/s of component k through the elementary surface dA. The summation over all phases is necessary, because the given component can be present in, and transported by, several phases. The integral over the closed surface A_I is the total mass flow rate of component k, flowing in or out from the control volume. Because the normal vector is oriented outwards, the integral is positive if more mass is flowing out than flowing in.

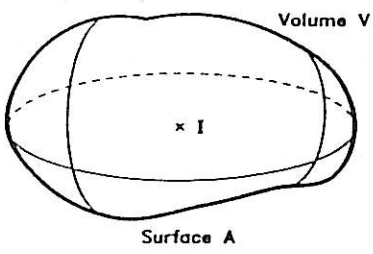


FIG. 1. Control volume around the grid point.

The second term is the *source* (or sink) rate. It determines how much mass of component k directly will be taken out of, or supplied into, the control volume per time unit. In the case of a point source, interpreted as a well within the volume, the volume integral can be replaced by the value Q_{kI}. The left-hand side of Eq. 1 is also the mass exchange rate between the control volume and the outside world. The right-hand side of Eq 1 is the *accumulation* term. The volume of phase p per unit rock volume is $\phi S_p m^3$. It contains $\phi S_p\xi_p$ moles and $\phi S_p\xi_{pk}x_{pk}M_k$ mass kg of the component k. The summation over all phases and the integral over the whole control volume gives the mass of component k within the control volume. The derivative with respect to time is the mass accumulation rate for component k in the control volume.

Eq. 1 is a mole balance. As a matter of fact, mass and mole balances are equivalent. This will be evident by cancelling the constant mole mass M_k from both sides of Eq. 1. In petroleum engineering, standard volumes are often used to express material quantities. Let ϱ_k^0 be the standard density of the pure component k (which is a constant). Dividing both sides of Eq. 1 by ϱ_k^0, it becomes a volume balance. Such a formulation is commonly used in the so called *black oil models* with three components: oil, gas and water. It is easy to show that the integral form of the flow equation is equivalent to the commonly used differential form. The permeability of the porous medium is defined *via* the Darcy law, which we write immediately for a multiphase case:

$$\vec{u}_p=-\frac{k_{rp}}{\mu_p}\bar{\bar{k}}\nabla\Phi_p=-\lambda_p\bar{\bar{k}}\nabla\Phi_p, \tag{3}$$

$$\nabla\Phi_p=\nabla p_p-\varrho_p\vec{g}. \tag{4}$$

In general, the permeability $\bar{\bar{k}}$ is a symmetrical tensor:

$$\bar{\bar{k}}=\begin{bmatrix}k_{11}&k_{12}&k_{13}\\k_{21}&k_{22}&k_{23}\\k_{31}&k_{32}&k_{33}\end{bmatrix}, \tag{5}$$

where $k_{ij}=k_{ji}$.

Substituting the flow term of Eq. 1 for velocity according to Eq. 3, and splitting up the integral into a sum over all the surfaces connecting block I with its neighbours $J=1,\ldots NJ$, one obtains

$$\iint_{A_I}\sum_{p=1}^{P}\xi_p x_{pk}\lambda_p(\bar{\bar{k}}\nabla\Phi_p)\cdot\vec{n}dA$$
$$=\sum_{J=1}^{NJ}\iint_{A_{IJ}}\sum_{p=1}^{P}\xi_p x_{pk}\lambda_p\nabla\Phi_p(\bar{\bar{k}}\vec{n})dA$$
$$=\sum_{J=1}^{NJ}Q_{IJk}, \tag{6}$$

where Q_{IJk}, the flow of component k from I to J, is

$$Q_{IJk} = -\iint_{A_{IJ}} \sum_{p=1}^{P} \Lambda_{pk} \nabla \Phi_p (\bar{\bar{k}} \vec{n}) dA \tag{7}$$

$$\Lambda_{pk} = \xi_p x_{pk} \lambda_p. \tag{8}$$

The sequence of multiplications in the term $\bar{\bar{k}} \nabla \Phi_p \vec{n}$ can be changed, because $\bar{\bar{k}}$ is a symmetrical tensor. Eq. 1 can be written in the following form:

$$\sum_{J=1}^{NJ} Q_{IJk} + \iiint_{V_I} q_k dV = \iiint_{V_I} \frac{\partial}{\partial t} \left[\phi \sum_{p=1}^{P} S_p \xi_p x_{pk} \right] dV. \tag{9}$$

Discretization

Looking for approximative values of the solution only on a set of grid points and only for discrete time-levels, the differential equations are reduced to a finite-dimensional system of algebraic equations. The process is called discretization. It involves the construction of an appropriate grid system and the set up of proper equations, one or more per grid point.

Consider the grid block shown in Fig. 2. The volume of the block is V_I, x_I is the gridpoint in the centre of the block, and x_J is the grid point in the J-th neighbour block. A_{IJ} denotes the communication surface between blocks I and J. In the general case, the block is confined by curved surfaces which can be approximated by planes.

For the *flow terms* (Eq. 7)

$$Q_{IJk} = \iint_{A_{IJ}} \sum_{p=1}^{P} \Lambda_{pk} \nabla \Phi_p (\bar{\bar{k}} \vec{n}) dA \tag{10}$$

- the surface A_{IJ} connecting the block I with its J-th neighbour
- the scalar product $\nabla \Phi_p (\bar{\bar{k}} \vec{n})$
- the component mobility Λ_{pk}

have to be approximated.

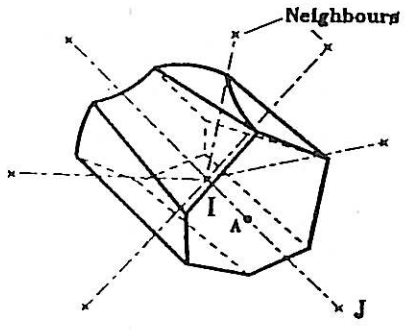


FIG. 2. A grid block.

The surfaces A_{IJ} and the orientation of the unit normal vectors $\vec{n}_{IJ}$ are determined by the rules of grid construction. Once the grid is given, area and orientation can be computed exactly by means of geometry.

For the approximation of the scalar product $\nabla \Phi_p (\bar{\bar{k}} \vec{n})$, an isotropic porous medium has to consider at first. In this case, the tensor can be replaced by a scalar value k.

In the general case, all grid points forming tetrahedrons with intersection with the individual block surface have to be taken into consideration (Fig. 3). However, the scalar product $\nabla \Phi \cdot \vec{n}$ can be approximated by a more simple formula if the vector $\vec{n}$ is parallel to the vector h_{IJ}, *i.e.* the surface connecting blocks I and J is orthogonal to the straight line connecting the grid points I and J. Therefore,

$$\nabla \Phi \cdot \vec{n} = \frac{\Phi_J - \Phi_I}{h_{IJ}}. \tag{11}$$

For the orthogonal case, flow terms are therefore given by

$$Q_{IJk} = \tau_{IJ} \sum_{p=1}^{P} (\Lambda_{pk})_{IJ}^{n+1} (\Phi_J - \Phi_I)_p^{n+1}, \tag{12}$$

where

$$\tau_{IJ} = \frac{A_{IJ}}{h_{IJ}} k_{IJ} \tag{13}$$

is the interblock transmissibility. Eq. 13 is often used if the block surface is non orthogonal to the connection line h_{KJ}. This is erroneous, because the calculated flow rate does not converge to the true value if $h_{IJ} \to 0$. That means the approximation is not consistent. In the following, grid refinement will be proposed as a possibility to improve the accuracy, but this only makes sense if the grid is orthogonal.

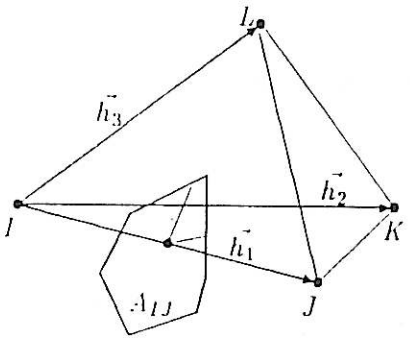


FIG. 3. Grid element and communication surface between blocks I and J.

In cases where a scalar permeability cannot model the flow behaviour in a porous medium, a tensor $\bar{\bar{k}}$ is introduced. The Darcy law, Eq. 3, establishes a linear relationship between the potential gradient $\nabla\Phi$ and the flow velocity $\vec{u}$. In general, this linear dependence alters the absolute value of $\nabla\Phi$ and its direction. Flow velocity is no longer parallel to the potential gradient.

By using *finite volume techniques* the flow term $\nabla\Phi_p(\bar{\bar{k}}\vec{n})$ can be calculated in the same manner as for the isotropic case. The only difference is that $\nabla\Phi_p$ is multiplied with the vector $\bar{\bar{k}}\vec{n}$ instead of $k\vec{n}$. Or for general grids, the grid-block must be constructed so that the communication surfaces are $\bar{\bar{k}}$-orthogonal (orthogonal in a general sense, defined by $\bar{\bar{k}}\vec{n}$ parallel to $\vec{h}$) on the straight lines connecting adjacent blocks. In analogy to the derivation of Eq. 12,

$$\nabla\Phi\cdot(\bar{\bar{k}}\vec{n})=|\bar{\bar{k}}\vec{n}|\frac{\Phi_J-\Phi_I}{h_{IJ}}. \tag{14}$$

Fig. 4 shows how an orthogonal Cartesian block system is altered by the concept of $\bar{\bar{k}}$-orthogonality. In this example,

$$\bar{\bar{k}}=\begin{pmatrix}3 & 1\\ 1 & 3\end{pmatrix}, \tag{15}$$

the principal axes are oriented diagonally. Note that for this reason, the surfaces connecting the block to its diagonal neighbours are orthogonal (in the usual sense) to the connecting line.

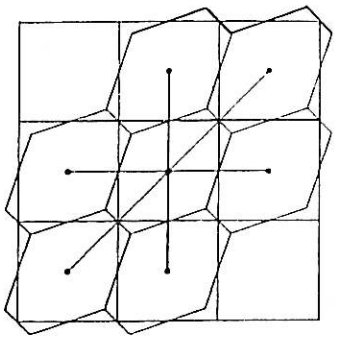


FIG. 4. $\bar{\bar{k}}$-orthogonal block system.

The Component Mobility

Since Q_{IJk} given by Eq. 7 is a surface integral, the component mobility Λ_{pk} is required on A_{IJ}, which lies somewhere between grid points I and J. However, the state variables are assigned to the grid points. To get approximate values for Λ_{pk}, some sort of averaging between the values at points I and J is necessary. It can be demonstrated that midpoint weighting has lower truncation error, but both Peaceman [3] and Russel and Wheeler [4] point out that midpoint weighting may lead to oscillations and overshoot in the solution upstream of the front. The easiest is to take the value for the upstream grid point, leading to the industry standard up-stream weighting. The up-stream weighting is stable when variables are taken at the current time level (implicit mobility) and conditionally stable when calculated at the old time level (explicit mobility). However, upstream weighting does have a serious price related to its higher truncation error, smearing out the sharpness of the front. Ewing [5] discusses some of the disasterous effects of up-stream weighting. Many proposals have been made to reduce this numerical dispersion, including the use of dynamic weighting, but only one possibility is practical namely reducing the distance between the grid points and increasing the number of blocks between injection and production wells.

Perry and Herron [6] and Snyder [7] showed that by immiscible gas displacement under practical conditions, the saturation distribution is wrong for 3 blocks on the head of the displacement front (Fig. 5). This smearing out effect leads to early breakthrough and overestimate of the overall *GOR*, but has no significant effect on the cummulative oil production. With most *EOR* displacement, the composition through determination of the existing phases and their properties as viscosity, interfacial tension etc., plays a decisive role. The numerical dispersion smears out not only the saturation profile, but also the composition one. As a consequence, in a given point (or block) between the injection and production wells, the concentration required for miscibility will be achieved later in a numerical simulation as in reality.

A good example for this error was published by Coats [8]. The length of the linear model reservoir was 60 m. The reservoir oil composed of methane, butane and decane (20/20/60 mole %) was displaced by a methane and butane mixture (68.4/31.6 mole %). The numerical simulation was performed using 80, 40 and 20 grid blocks. The block lengths were 1, 2 and 4 m.

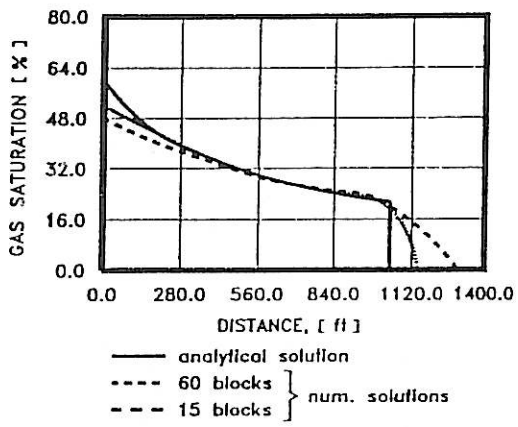


FIG. 5. Numerical solution of a linear gas displacement with different block sizes [7].

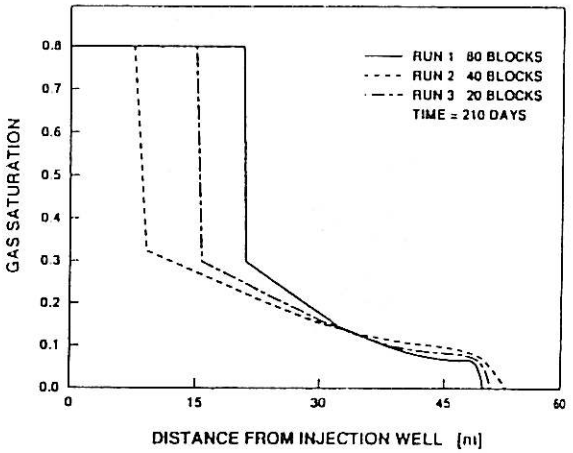


FIG. 6. Calculated gas saturation vs. distance for multicontact miscible gas drive [8].

Fig. 6 shows the calculated gas saturation profiles vs. distance at 210 days. The discontinuities show the position of the miscible front. It is clear, that a correct calculation of the displacement process requires a block width in magnitude of $1m$.

Similar results were published by Nghiem and Li [9]. In a low temperature CO_2 flooding, 0.3 m block size gives satisfactory matching for slim-tube displacement. The reduction of size to 0.15 m showed no significant changes.

Accumulation Term

In the accumulation term of Eq. 1,

$$\iiint_{V_I} \frac{\partial}{\partial t}\left[\phi \sum_{p=1}^{P} S_p \xi_p x_{pk}\right] dV, \tag{16}$$

we replace the time derivative by a difference approximation. The volume integral is evaluated approximately as the value of the integrand at point I, times the block volume. This results in

$$\left(\iiint_{V_I} \frac{\partial}{\partial t}\left[\phi \sum_{p=1}^{P} S_p \xi_p x_{pk}\right] dV\right)^{n+1}$$

$$\approx \frac{V_I}{\Delta t}\left(\left[\phi \sum_{p=1}^{P} S_p \xi_p x_{pk}\right]_I^{n+1} - \left[\phi \sum_{p=1}^{P} S_p \xi_p x_{pk}\right]_I^{n}\right) \tag{17}$$

where V_I denotes the volume of gridblock I, n is the index for the time level, $t^{n+1} = t^n + \Delta t$. In the discretization for this term and also for the source term, an irregular shape of the gridblock has no influence as long as the block volume is evaluated correctly.

The accumulation term for the energy balance equation has a similar form. By simulation of in situ combustion this term plays a critical role. The high temperature burning zone has an extension of 0.3 to 1 m. If the block size is larger than this, the average temperature of the block will be lower than the reaction temperature. Consequently, the burning front extinguishes. Chu [10] showed that the grid block size would have to be in the order of half-a-meter.

BLOCK SIZE IN NUMERICAL SIMULATION OF EOR PROCESSES

In black oil simulation, the areal block size can be in the magnitude of 100 m by water drive and can be extended to 1000 m by depletion drive. That means 2000–10,000 blocks per layer in the case of an average oil reservoir. Taking 3–10 layers vertically means 6000–100,000 blocks in a conventional Cartesian grid. The upper limit is nowadays the maximum which can be handled with the largest and fastest computers.

Reducing the block size to 10 m, the number of blocks explodes to 0.5 to 10 million and 10 m is still to large for some important EOR displacement processes. This is the reason that most of simulation studies were limited to symmetry elements of pilot areas.

Theoretically there are two possibilities to overcome this difficulty:
- local grid refinement, and
- front trucking.

Local grid refinement is an extension of the generally used finite difference technique. In front trucking, the steady-state pressure distribution is calculated for fixed saturation and composition distribution. This determines the velocity of the displacing fronts and it is possible, taken into consideration the overall material balances, to determine their new position a time step later. Recent publications [11] presented results for two phase immiscible displacement. Future investigations have to show the applicability for more realistic cases. In this paper, only local grid refinement will be discussed, already applied in commercial simulators.

Local Grid Refinement

A simple Cartesian grid, also when using variable grid spacing, is frequently not sufficient for supplying a good description of particularly interesting areas, e.g. in the vicinity of the displacing front.

In order to achieve a high resolution by means of as few blocks as possible, selected area or individual blocks can be subdivided by means grid refinement. This method was used for reservoir simulation by Von Rosenberg [12] and Heinemann *et al.* [13–15] at first.

The initial block system is called fundamental and its blocks are referred to as fundamental blocks (Abbreviate: F-blocks). They are defined by three indices $I1$, $I2$, $I3$ for the 3D-space. Three divisor numbers ($KI1$, $KI2$, $KI3$) are assigned to every F-block. They indicate the number of partial blocks into which the F-block is to be subdivided in the corresponding direction. In this

way, sub-coordinates ($I1T$, $I2T$, $I3T$) are defined in every F-block, having the same direction as the main coordinates (Fig. 7).

In this way each partial block can be addressed by specifying the coordinates ($I1$, $I2$, $I3$). Partial blocks are referred to as R-blocks (refinement) in the following.

For a correct calculation of the transmissibility it is necessary to modify the block boundaries on the transition surface of the coarse and refined grid. Fig. 8 shows a correct refinement.

The communication surface between F- and R-blocks is orthogonal on the grid line $\overline{IJ}$ and so, as shown previously the difference approximation will be consistent.

It is easy to understand that this solution has some limitations. It is applicable only if the refinement is 1:2 (Fig. 9) for each direction. The second problem is if there is a refinement on both sides of a grid block, one gets complications in the calculation of the transmissibilities. For blocks with stretched shape it is not possible to construct such a geometry. The last problem rises when regarding the vertical directions. In consequence the following rules have to be considered for subdivision of fundamental blocks:

1. If the neighbouring F-blocks of an F-block in one coordinate direction are looked at, the divisors for the two other coordinate directions are not allowed to increase for both of the neighbouring F-blocks.

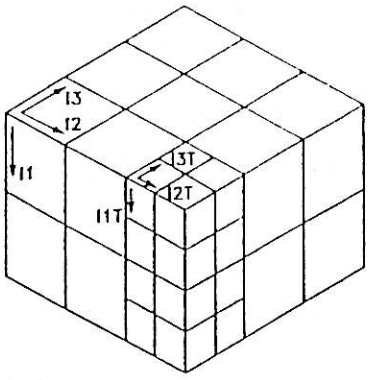


FIG. 7. Determination of subcoordinates.

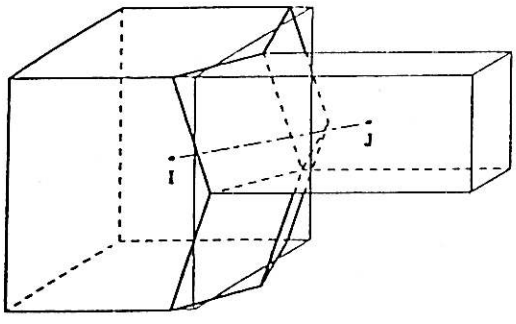


FIG. 8. Distortion of block interfaces in a three-dimensional grid. The fundamental block (left) has a neighbouring block divided into four subblocks.

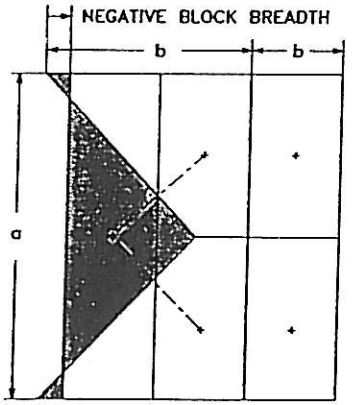


FIG. 9. No orthogonal refinement possible by stretched blocks.

2. At any section through the block system, one block may only have one or two neighbouring blocks on each side.
3. The division in the vertical direction must be continuous within communicating layers, *i.e.* the divisor for the directions $I2$ and $I3$ are the same for neighbouring F-blocks lying one below the other.
4. If two F-blocks in one coordinate direction are looked at, it is not allowed that one of the divisors of the two other coordinate directions increases and the other decreases.

In a conventional Cartesian block system using a five-point differential scheme, a block has a maximum of four neighbours in the two-dimensional case, and a maximum of six neighbours in the three-dimensional case.

For a local grid refinement, a block can have a maximum of twelve neighbours, taking into consideration rules 1–4.

True and Patch Refinement

Two different type of local grid refinements have been applied in reservoir simulation:

- True refinement
- Patch refinement

The first technique is a true local grid refinement where an arbitrary level of refinement can be applied at any region or point of space. With true refinement, all grid points are integrated into the same equation system. A conventional Cartesian grid with natural ordering (follow the coordinate axis) leads to a linear algebraic equation system with regular band matrix with uniform bandwidth. The solution algorithm for these types of equations is well known and a good vectorisable. Local grid refinement disturbs this regularity and needs special matrix solvers. They cannot be so fast because the position of the non zero coefficients are not known a priori. This type of refinement cannot be adapted to conventional

simulators because a different algorithm and code structure are required. It was mentioned [16], that the overhead associated with the data structures and the grid generation can dominate the overall computation time. This statement does not fit with the experiences of the author. Developping new matrix solvers, special for irregular linear equation systems, can reduce the overhead considerably [17].

The performances are the same as for the conventional block model with the same grid size. Experiences have shown that the true refinement is general applicable and has no limitation in respect to flow direction, saturation, distribution etc. In this paper all discussion are related to truly refinement.

By patch refinement the equations are solved on the coarse grid at first. This coarse grid overlap the refined area. Afterwards, some of the grid points serve as boundary points to solve a second system of equations for the refining grid points. The advantage of this type of refinement is that the matrix remains regular and can be solved faster. The decoupling of the refined part of the grid leads to serious instabilities and cannot be used if the flow is directed from the refined grid towards the coarse one. In this case the upstream block is refined and has different saturations and overall composition as the corresponding coarse block. If any, then the patch refinement can be used but only if the transition surface between the coarse and fine grid is far enough from the place of interest.

Gathering

Applying grid refinement one can get a higher resolution in the vicinity of the wells, boundaries and discontinuities. Practical applications have shown that the reverse procedure, *i.e.* constructing a block system by block gathering, may be very useful. This technique was introduced by Heinemann and Munka [18].

Fig. 10 shows one part of a fundamental Cartesian grid. Once 8 blocks and twice 2 blocks where gathered. The same block system can be constructed through refinement. In Fig. 10 one block was subdivided 4 times and two blocks twice. A gathered block system is consistent under the same conditions as the refined block system. The rules of that are given in the previous section.

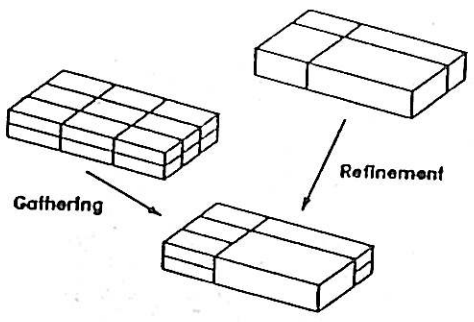


FIG. 10. Construction of a block system by block gathering and refinement.

Primary and Secondary Grid

The reservoir is known through the structure map, gross and net thickness, porosity distributions *etc.* We apply a block system which approximates more or less the geometry. We assign parameters to the blocks which are average values for that part of reservoir represented through the block volume. The average pressure and saturations will be calculated for each block under consideration of the phase contact, the PVT and rock properties. In this way the block system is initialized. The average reservoir pressure and the petroleum in place can be compared with the forgoing volumetric reserve estimation. If the initialization is right, the model will be in hydrodynamic equilibrium. The grid model is called *primary grid.*

We can change the block system through subdivision of the blocks or through gathering. The combination of these, that means construction of new blocks from subdivided ones, can be used, even when it is a little bit complicated. Such a rebuilding of the block system has to conserve the mass. That means no change in the amount of fluid in place is allowed. The parameters of the blocks have to be calculated from the previous block system and not from the maps. The new system is called *secondary block system.*

Our expectation is that if the primary grid was in a hydrodynamical equilibrium the secondary has to be near this stage.

Dynamic Grid Refinement

Refinement and gathering can be done in every stage of the simulation run. The only problem is to assign the right pressure, saturations and compositions to the new blocks. Fig. 11 shows a linear

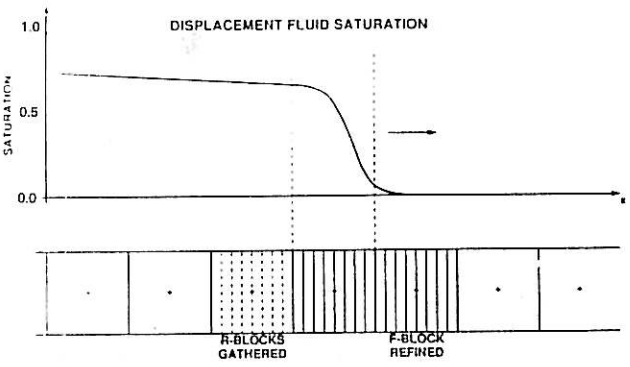


FIG. 11. Linear displacement with dynamic grid refinement.

displacement with pressure and saturation distribution. Ahead of the displacement front the saturation is homogeneous. If the coarse grid is refined here before the displacement front arrives, the same saturation to all refined block, equal to can be assigned themselves of the coarse grid. The pressure is not critical because it is calculated implicity in the next time step and the assigned values have no influence on that.

Behind the front saturation (and composition) gradient is moderate. Blocks can be gathered and the volume average values can be assigned to the new ones. The automatic and continuous application of this procedure leads to the moving grid. The grid is refined only on the displacing front and moves with it.

The refinement and gathering of the blocks is regulated by two sets of parameters:

- Maximal pressure, saturation and concentration gradients before a fundamental block
- Maximal pressure, saturation and concentration between refined blocks within a fundamental block.

After every time step it will be shown if at least one of the gradients is higher than the limit. If this is the case, the downstream block will be refined for the according coordinate direction. Afterwards, it will be proved if the rules of refinement are satisfied or not and supplementary refinement done if necessary in the surrounding blocks. It is assured that the displacement front is always placed in the refined area. The second condition will be proved only in given time points to avoid a continuous jump between refinement and gathering.

Dynamic grid refinement brings a certain overhead in the numerical calculation, but this is not very much. This will be demonstrated by a simple example which is well documented by Odeh [19]. Areal and cross-section views of the reservoir are given in Fig. 12. The reservoir is initially undersaturated. A gas injection well is located at the grid point (1,1,1) and a producing well at (3,10,10). Pertinent data, PVT properties and relative permeabilities can be taken from the original Odeh paper.

A $3 \times 5 \times 5$ grid was taken with 2×2 refined blocks at the well location. The number of blocks are 93 compared with the 300 blocks in the original $3 \times 10 \times 10$ grid. The same data and constraints were used as in the original example (Case A).

For every block a 2×2 horizontal dynamic refinement was allowed. A block would be refined if the difference between two neighbouring blocks exeeds in saturation 0.05 or in pressure 20 bars. For case B the block gathering, that means the reconstruction of the original blocks, was not allowed. In case C this happens if the maximal saturation and pressure differences between the refined blocks within a fundamental one become less then 0.05 and 10 bars.

Fig. 13 shows number of blocks vs. production time. Fig. 14 gives the block systems of cases B and C at gas breakthrough. The results were in every respect practically identical and as good as for the basic case. Fig. 15 compares the CPU-times and gives an impression of the advantages of dynamic grid refinement.

To evaluate the computational efficiency of local refinement the 10 years producing period with time step 90 days is simulated. The simulation was run on the DEC Microvax-II computer. For both cases the finite difference equations are solved respectively by IMPES, semiimplicit, and fully implicit (Newton-Raphson Iteration) solution methods. The matrix is solved by an iterative solver. The production results

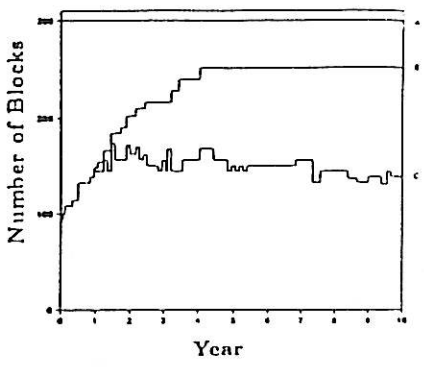
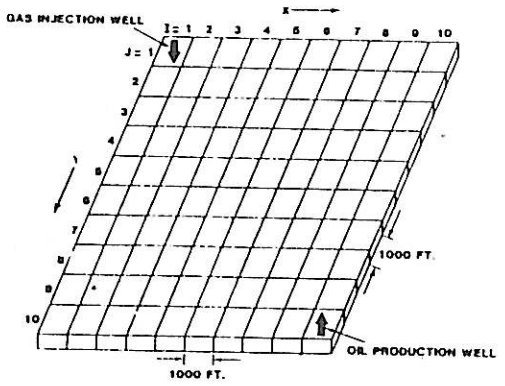


FIG. 13. SPE First Comparative Solution Project. Number of blocks vs. production time.



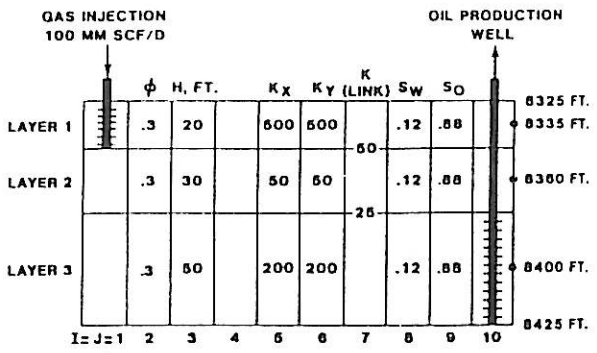


FIG. 12. SPE First Comparative Solution Project. Grid system and diagonal cross section [19].

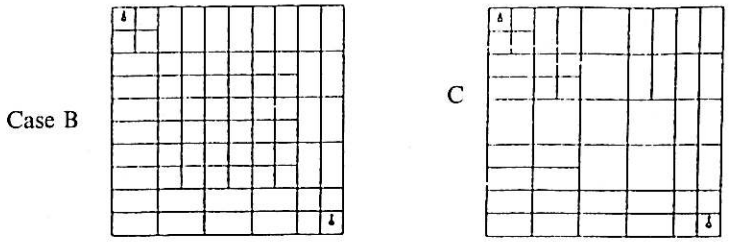


FIG. 14. SPE First Comparative Solution Project. The blocksystem at gas breakthrough for cases B and C.

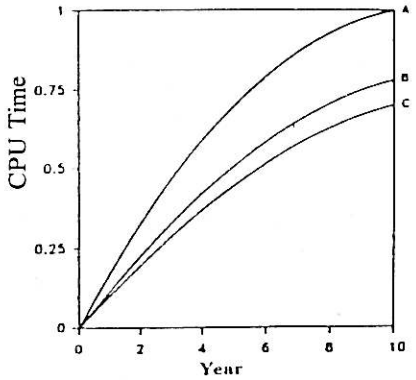


FIG. 15. SPE First Comparative Solution Project. Comparison the CPU time for dynamic refinement.

in both cases were in good agreement for all three solution methods.

The CPU time per matrix-solution and per variable of case B is larger than that of case A. This is caused by the irregular matrix structure of case B, but is compensated by the reduction of block number. In the average, 23% reduction of block number could save 10% of CPU time.

EXAMPLE

To transmit the idea of combined application of dynamic grid refinement and gathering by EOR simulation studies, an example will be presented.

The fundamental block system has an extension of $5 \times 30 \times 40 = 6000$ blocks. The block size in the productive area is 100×100 m. Rich *HC* gas is injected on the top of the relatively flat anticlinal in one well with 300.000 sm^3/d rate. The area of interest was refined 2×2 to get 50×50 m block size and outside the blocks are gathered to save CPU-time. The block model is shown in Fig. 16. Note that in the area which will not be touched by miscible drive, the blocks are gathered vertically as well, leading to a two dimensional model for this part of the reservoir. The surrounding of the EOR area is described just coarsly, but still the whole hydrodynamic unit is included in the calculations. This refined/gathered model has 3660 blocks. The conventional model with the same block size in the central area, shown in Fig. 17, would have 8640 blocks.

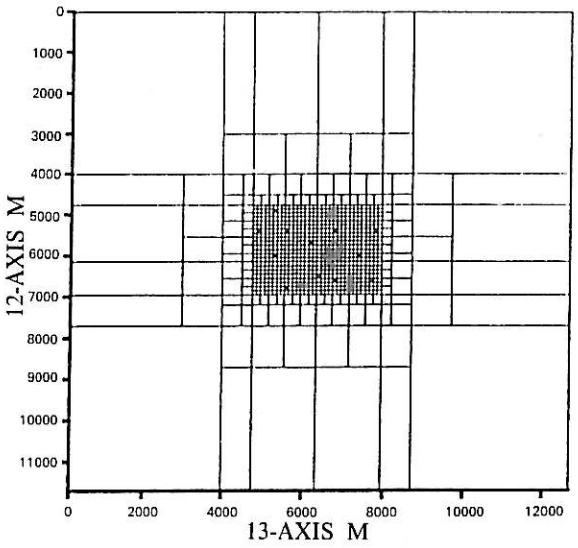


FIG. 16. Field scale miscible gas drive. Refined and gathered grid.

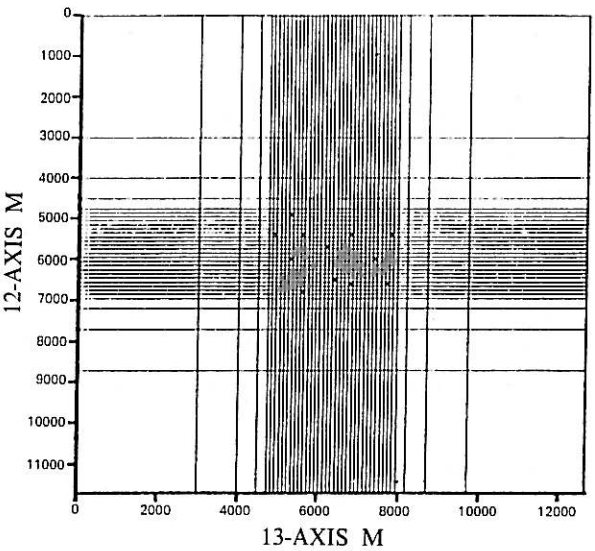


FIG. 17. Field scale miscible gas drive. The conventional Cartesian grid.

A 4×4 dynamic grid refinement was used on the edge of the miscible front. A $50 \times 50\,m$ block was refined if the gas saturation difference between the two upstream partial blocks (in the already 4×4 refined 50×50 m block), exceeded 0.2. The dynamic refined blocks were gathered if in the initially $50 \times 50\,m$ block the maximum saturation difference

between any partial blocks became less than 0.05. Fig. 18 shows the resulting block system after 3 years of injection. The actual block number is at this time 6640. A static conventional grid with the same block size in the EOR area requires 49,608 blocks already beyond the technical limit of compositional simulation. In Fig. 19 only the refined area is plotted showing more detail of it.

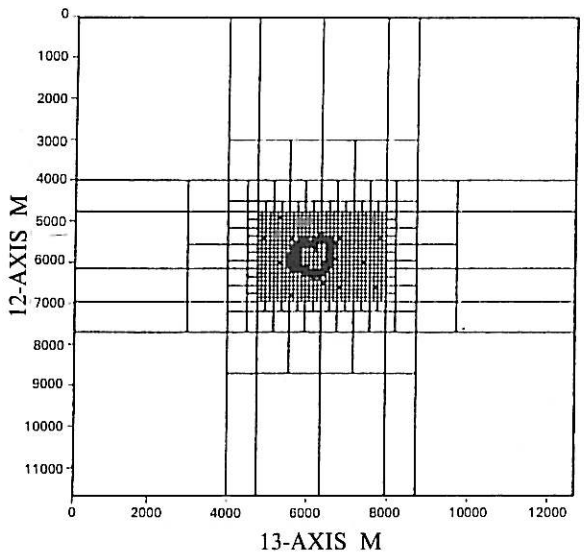


FIG. 18. Field scale miscible gas drive dynamic grid refinement after 3 years production.

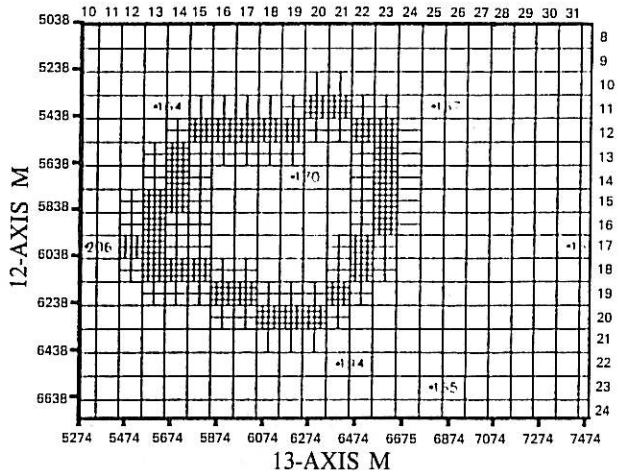


FIG. 19. Field scale miscible gas drive. Dynamic grid refinement after 3 years production focused on the EOR area.

CONCLUSIONS

1. Numerical simulation of EOR processes based on finite difference methods requires small block size. Depending on the displacement process the range is somewhere between 0.5 and 10 m. In full scale simulation, this is not applicable with conventional gridding for such a model would have some millions of grid blocks.
2. The grid must be orthogonal to make sure that the numerical solution converges to the true one if the grid size diminishes. By applying some simple rules, local grid refinement satisfies this requirement even at the fine-coarse grid transition zone for a Cartesian grid.
3. True refinement is robust and generally applicable, but requires new numerical algorithm and computer codes. Batch refinement can be adapted to conventional simulators, but its applicability is limited.
4. Small block size is only required at the displacing front. A dynamic grid refinement makes it possible to divide the downstream blocks ahead of the front and gather them in the upstream area.
5. The block gathering technique can be used outside the EOR area, reducing the block model to a two dimensional one. In this way, the influence of the environment (aquifer, other producing areas) is taken into account without wasting computing time for uninteresting detail.
6. Combining block gathering and dynamic grid refinement techniques an EOR displacement can be simulated with some meter block size on the front without exceeding the technical and economic limits.

NOMENCLATURE

A	surface of control volume in balance equation
A_{IJ}	surface common to grid blocks I and J
$\vec{g}$	gravity acceleration
h	grid spacing
K	number of all components
$\bar{\bar{k}}$	permeability tensor
k_{ij}	component of the permeability tensor
k_{rp}	relative permeability for phase p
M_k	mole mass of component k
NJ	number of neighbours communicating with gridblock J
$\vec{n}$	unity normal vector on surface A
P	number of all phases
$P_{cpp'}$	capillary pressure for phase p and p'
p_p	phase pressure
Q_{IJ}	flow terms defined in Eq. 7
S_p	phase saturation
t	time
$\vec{u}_p, u_p$	filtration velocity of phase p
V	volume
x_{pk}	mole fraction, component k, phase p

Greek letters

Λ_{pk}	$\xi_p x_{pk} \lambda_p$
λ_p	phase mobility
ξ_p	specific mole density of phase p
ρ_p	phase density

τ_{IJ} interblock transmissibility
ϕ porosity

Subscripts

p phase
k component
rp relative permeability for phase p
I, J gridblocks

REFERENCES

[1] Nghiem, L., 1983, An Integral Approach to Discretizing the Reservoir Flow Equations, CMG technical report.

[2] Pedrosa, O.A. and Aziz, K., 1985, Use of Hybrid Grid in Reservoir Simulation, paper SPE 13507 presented at the Middle East Technical Conference, Bahrain.

[3] Peaceman, D.W., 1977, Fundamentals of Numerical Reservoir Simulation. Development in Petroleum Science 6. Elsevier, Amsterdam, Oxford, New York.

[4] Russel, T.F. and Wheeler, M.F., 1983, The Mathematics of Reservoir Simulation, Chapter II: Finite Element and Finite Difference Methods for Continuous Flows in Porous Media, Society for Industrial and Applied Mathematics, Philadelphia.

[5] Ewing, R.E., 1983, The Mathematics of Reservoir Simulation, Chapter I: Problem Arising in the Modelling of Processes for Hydrocarbon Recovery of Processes for Hydrocarbon Recovery, Society for Industrial and Applied Mathematics, Philadelphia.

[6] Perry, J.H. and Herron, E.H. Jr., 1969, Three-Phase Reservoir Simulation, J. Pet. Eng., pp. 211–210.

[7] Snyder, L.J., 1969, Two-Phase Reservoir Flow Calculations, Soc. Pet. Eng. J., pp. 170–182.

[8] Coats, K.H., 1980. An Equation of State Compositional Model, Soc. Pet. Eng. J., pp. 171–184.

[9] Nghiem, L.X. and Li, Y.K.. 1986, Effect of Phase Behavior on CO_2 Displacement Efficiency at Low Temperatures: Model Studies with an Equation of State, SPE Res. Eng., pp. 414–422.

[10] Chu, C., 1981, The Course of Grid Size, AOS-TRA: Workshop on Computer Modelling.

[11] Rian, D.T., 1988, Modelling and Simulation of Fluvial Geological System by Application of Front Tracking Methods, Case Study presented on the First International Forum on Reservoir Simulation, Alpbach.

[12] Rosenberg von, D.U., 1982, Local Grid Refinement for Finite Difference Methods, paper SPE 10974 presented at the 57th Annual Fall Technical Conference, New Orleans.

[13] Heinemann, Z.E., Gerken, G. and Meister, S., 1983, Anwendung der Localen Netzverfeinerung bei Lagerstaettensimulation, Erdoel und Erdgas, pp. 199–204.

[14] Heinemann, Z.E., Gerken, G., Hantelmann, G., 1983, Using Grid Refinement in a Multiple-Application Reservoir Simulator, paper SPE 12255, presented at the 7th Symposium on Reservoir Simulation, San Francisco.

[15] Heinemann, Z.E. and Brand, C., 1989, Gridding Techniques I in Reservoir Simulation, Proceeding of First and Second International Forum on Reservoir Simulation, Alpbach.

[16] Ewing, R.E. and Lazarov, R.D., 1988, Adaptive Local Grid Refinement, paper SPE 17806, presented at the Rocky Mountains Regional Meeting, Casper, WY.

[17] Brand, C. and Heinemann, Z. E., 1989, A New Iterative Solution Technique for Reservoir Simulation Equations on Locally Refined Grids, paper SPE 18410, presented 1989 at the 10th Reservoir Simulation Symposium on Reservoir Simulation, Houston.

[18] Heinemann, Z.E. and Munka, M., 1986, Reservoir Simulation with Block Gathering, paper SPE 15097, presented at the 56th SPE California Regional Meeting, Oakland, CA.

[19] Odeh, A.S., 1981, Comparison of Solutions to a Three-Dimensional Black-Oil Reservoir Simulation Problem, J. Pet. Tech., pp. 13–25.

PRJ, Vol. 4. (January 1992); P. 22–32, 15 FIGS, 6 TABLES.

CONSTRAINTS ON ENHANCED OIL RECOVERY DEVELOPMENT

P. Simandoux* and E. Valentin*

القيود المتحكمة في تطوير عمليات الإسترداد الإضافي النفطي

ت . سيماندو وأ . فالنتين

تغطي التقنيات المختلفة لعمليات الإسترداد الإضافي النفطي مجالات تطبيقية واسعة بالنسبة للنفط الخفيف والثقيل . وقد وصل إنتاج الإسترداد النفطي في عام 1988م إلى 1.5 مليون برميل يومياً ، ويمثل هذا حوالي 3 % من جملة إنتاج النفط في العالم .

وتمثل العمليات الحرارية والحقن الغازي على التوالي 55 % و43 % من الطرق المستخدمة في إنتاج الإسترداد النفطي . ومن وجهة النظر الفنية ، تعتبر الأبحاث التي تنفذها شركات النفط والمتعلقة بإنتاج الإسترداد النفطي من أكثر المشاريع تعقيداً .

فعمليات الإسترداد الإضافي تتطلب أوقات ومصاريف كثيرة من أجل القيام بالأبحاث والتطوير المطلوب . وقد تطورت هذه العمليات تقنياً في السنوات الأخيرة ، غير أن التدهور الحاد في أسعار النفط الخام عام 1986 أكد مرة أخرى على التأثير الحاسم لتكاليف تلك الطرق عند تنفيذها .

تناقش هذه الدراسة السبل المختلفة للتقليل من المخاطر الفنية والإقتصادية لطرق الإسترداد الإضافي النفطي بواسطة التحكم في العوامل الرئيسية المؤثرة في هذه الطرق .

ABSTRACT

The different techniques of enhanced oil recovery (EOR) cover a wide range of applications from light to heavy crudes. In 1988, EOR production reached 1.5 million bbl/d, representing about 3% of the total amount of oil produced in the world. North America is the main actor in this domain, ensuring half of the total EOR production. Thermal processes and gas injection represent respectively 55% and 43% of EOR production by the various processes that are widely used in the world.

From a technical point of view, research on EOR processes is among the most complex projects carried out by the oil industry. Process tailoring itself requires long lead times to do the necessary research and development. All the processes have evolved technically in recent years and steady progress has been made, but the sharp drop in the price of crude oil in 1986 again emphasized the crucial influence of the cost of these methods on their implementation.

This paper discusses the different ways of decreasing the technical and economic risks of EOR methods by mastering the main parameters of the processes thanks to extensive research and development in laboratories, by improving reservoir characterization or their performance to be predicted with some degree of confidence, and lastly by searching for synergy with new technologies that have emerged in the meantime, such as horizontal drainholes.

*Institut Francais du Petrole, France

PRESENT STATUS

The different techniques of EOR cover a wide range of applications from light to heavy crudes. They are widely used around the world, but some processes are better suited to the general characteristics of specific fields, depending on where they are located.

Out of pure necessity, North America was and still is the proving ground of the various EOR concepts. Its large oil demand and declining oil fields have forced the United States and Canada to search for

new ways to more efficiently recover the oil that was being left behind. In 1974, tertiary oil recovery (nearly all thermal) accounted for 3% of total oil production. Today, it accounts for 8%. The trend is inexorably toward secondary and tertiary oil production, because oil fields in North America are aging, new discoveries are much smaller in size and increased reliance is being put on low productivity "stripper" wells. The 1980's saw a very rapid growth of both oil production and the number of active EOR projects in North America (Fig. 1). In 1988, the USA and Canada produced 637,000 bbl/d and 145,000 bbl/d respectively by EOR. The popularity of EOR techniques in the United States and Canada differs significantly (Fig. 2).

In the former USSR, about 95% of domestic oil production was coming from oil fields developed with artificial waterflooding. However, recent years have been characterized by an increase in applications of enhanced oil recovery techniques (Table 1).

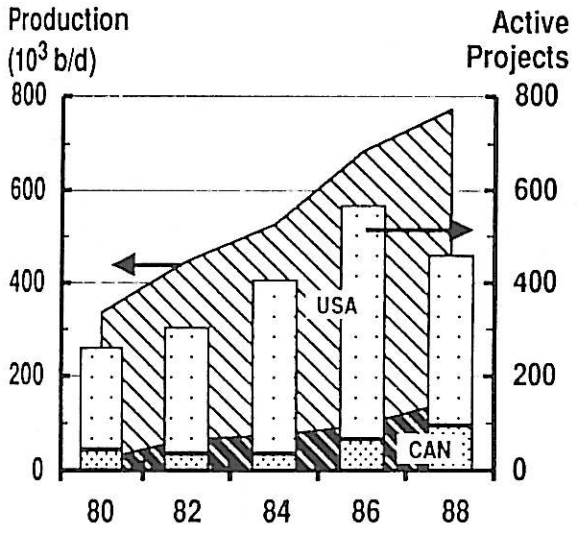


FIG. 1. EOR trends in North America.

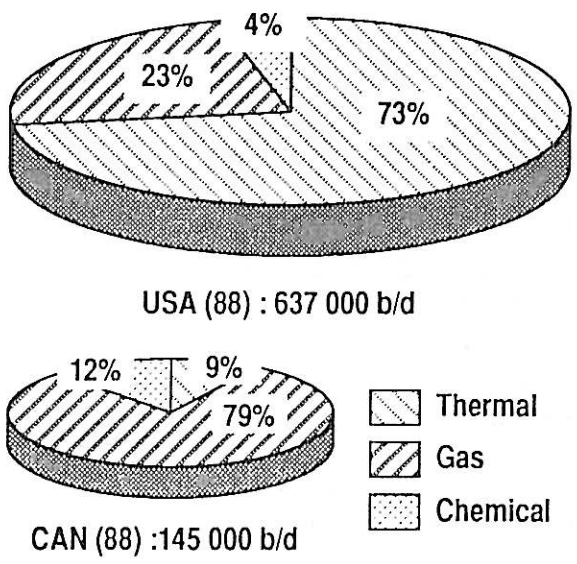


FIG. 2. Breakdown of EOR production in N. A.

Table 1. EOR Projects in the former USSR

EOR Techniques	1976 Total	1976 Active	1987 Total	1987 Active
Thermal	19	16	52	40
Gas	6	5	20	12
Chemical	56	56	165	128
Total	81	77	237	180

EOR techniques are used in various regions of the former Soviet Union. Mostly these techniques are widely used in Kazakhstan, representing 46% of the total oil in place, Tataria (23%) and West Siberia (11%). Thermal methods are applied mainly in Kazakhstan, chemical ones in Tartaria, gas and chemical methods in West Siberia. In 1988, the production was 160,000 bbl/d of oil by EOR application. The oil production in time for thermal, gas and chemical methods is shown in Fig. 3.

Venezuela is the second largest EOR producer with a production of 215,000 bbl/d in 1988, achieved essentially with the aid of thermal processes. Among other thermal producers, China, Indonezia, Romania, and Trinidad can be mentioned. Thermal production in China is achieved essentially through huff-and-puff steam injection in 3 oil-bearing areas: Liaohe, Xinjiang and Shengli. EOR in Indonezia is essentially provided by steam flooding. It should also be noted that the major producers include Algeria and

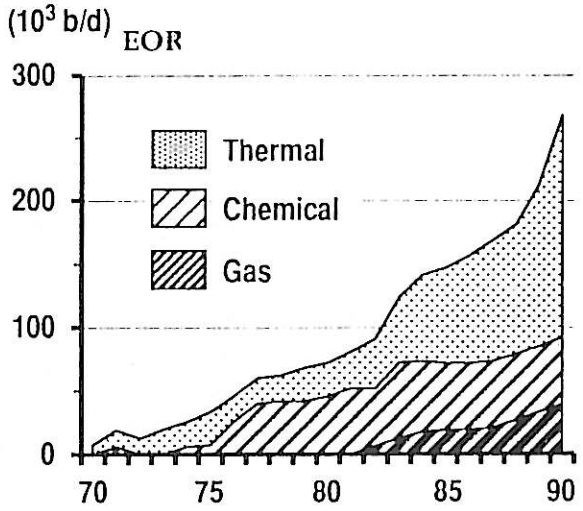


FIG. 3. EOR production in the former USSR.

Libya, due to the importance of the miscible gas operations on their respective Hassi-Messaoud and Intisar fields.

The overall EOR production worldwide can thus be evaluated at about 1.5 Mbbl/d of which thermal processes represent 55% and gas flooding 43% (Table 2).

Commercial applications of different EOR processes evolve at various rates and depend strongly on local conditions such as the suitability of reservoirs to a particular technology (steam flooding in California), the availability of injectants (natural gas in Alberta, carbon dioxide in the Permian Basin, Texas) local market conditions, and economic incentives.

Table 2. World Oil Production by EOR Methods

(10^3 b/d)

	Thermal	Gas	Chemical	Total
USA	465	150	22.5	637.5
Canada	13	115	17.5	145.5
Venezuela	207	9	-	216
USSR	20	90	50	160
Other (estimated)	107	280 (*)	1.5	388.5
Total	812	644	91.5	1547.5

* Mainly Hassi-Messaoud (Algeria) and Intisar (Libya) IFP/Economics Department/89

Table 3. Criteria for Selecting EOR Processes

CRITERIA	THERMAL		MISCIBLE	CHEMICAL	
	STEAM	IN SITU COMBUSTION	GAS	POLYMER	SURFACTANT
LITHOLOGY	N.C.	SANDSTONE	N.C.	SANDSTONE	SANDSTONE
FRACTURING	N.C.	NUL or WEAK	NUL or WEAK	NUL or WEAK	NUL or WEAK
TRANSMISSIBILITY (KH/μ)	>100	>20	N.C.	N.C.	N.C.
MOBILITY (K/μ)	N.C.	N.C.	N.C.	>25	>25
VISCOSITY (cp)	N.C.	N.C.	<10	<40	<20
DEPTH (m)	300-1500	<1500	>700	N.C.	N.C.
SALINITY (g/l)	N.C.	N.C.	N.C.	N.C.	<50
TEMPERATURE (°C)	N.C.	N.C.	N.C.	<100	<80

N.C.: Non Critical

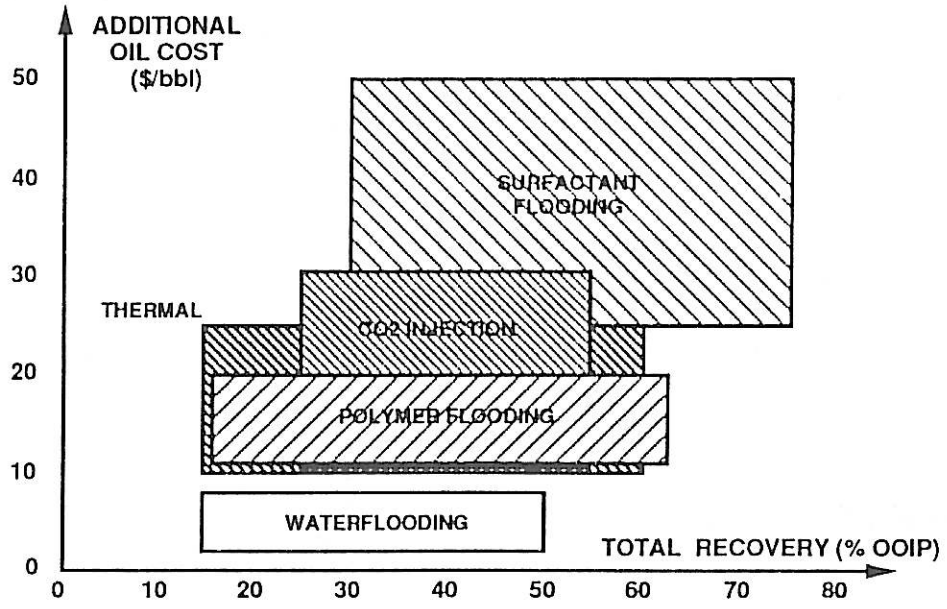


FIG. 4. Technico-economic performances of EOR Methods.

Each of these EOR processes has a specific range of application depending on the main parameters of the field (Table 3).

The technical and economic performances of the main EOR techniques, that have been scaled up to the industrial level, are shown in Fig. 4. These assessments were made in the economic conditions of early 1986 in Western Europe.

The lessons gleaned from past experience lead to the following conclusions that illustrate the actual constraints on EOR development:

(1) in most cases, the cost of the additional oil recovered through the use of any EOR method is above $ 10/bbl;

(2) thermal processes are the only EOR processes whose use is sometimes obligatory to recover a high viscosity oil. In all other cases, the use of EOR processes is restricted to fields where they can be implemented under good economic conditions, and where it is assumed that they will lead to a significant increase in the final oil recovery compared to conventional techniques such as waterflooding. In addition this increase in recovery must be achieved at the same time and the risk of failure must be reduced.

As a consequence the development of EOR techniques implies that risk and cost must be fully mastered during their implementation. The experience gained in the past now makes it possible to understand the different ways of attaining this goal.

UNDERSTANDING THE MAIN PARAMETERS OF EOR PROCESSES

From a technical point of view, research on EOR processes is among the most complex projects carried out by the oil industry. For each process both the reservoir parameters and operating parameters must be fully understood in order to reduce financial risks.

For thermal methods, the most important and often poorly understood variable is the displaceable-oil content (Fig. 5). Another source of uncertainty, especially for in-situ combustion, is linked to the understanding of the heterogeneities of the reservoir. Regarding the operating parameters and especially for steam injection, well spacing has the greatest impact on oil recovery and hence on production costs (Fig. 6).

For surfactant processes, most of the reservoir parameters and operating parameters have a strong influence. This is certainly one of the major difficulties in the designing of such a project. The imperfect chemical stability and the uncertainty as to how much product will be consumed by retention are what introduce the greatest errors in estimating

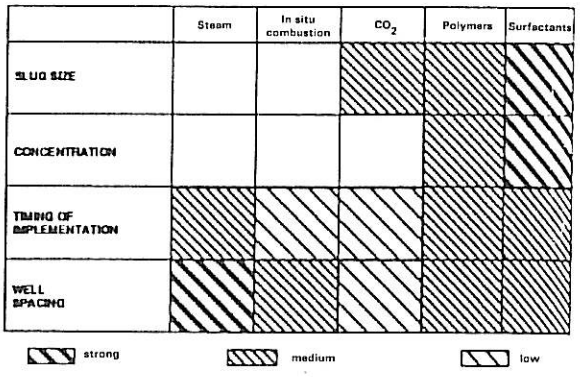


FIG. 5. Influence of operating parameters.

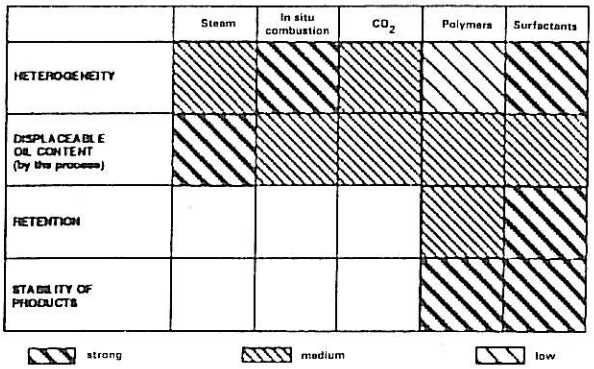


FIG. 6. Influence of operating parameters.

recovery and cost for surfactant flooding. However, uncertainties as to the residual oil saturation and the heterogeneity of the reservoir may also be of major importance.

Taking into account Libyan field characteristics, special attention must be paid to gas injection, for instance CO_2, and polymer flooding.

The following analysis was made specifically for Western European economic conditions. But the tendencies are general and can be extrapolated to other areas.

CO_2 Flooding

At economic optimum, additional recovery (Fig. 7) varies between 5 and 15% for specific CO_2 consumptions of 1 to 10 t of CO_2/t. The most sensitive parameters are heterogeneity and oil saturation at the start of the project.

Fig. 8 shows the marginal cost of the additional oil for different costs of CO_2, as a function of CO_2 requirements expressed in relation to the tons of CO_2 injected per ton of oil recovered. It can be seen that, in a first approximation, the cost of the oil is an increasing linear function of the CO_2 requirements. The scattering of the results around this straight line is slight. This can be explained by the fact that the cost of CO_2 supplies makes up the principal item in the production cost of the oil (50 to 70% of the technical production cost).

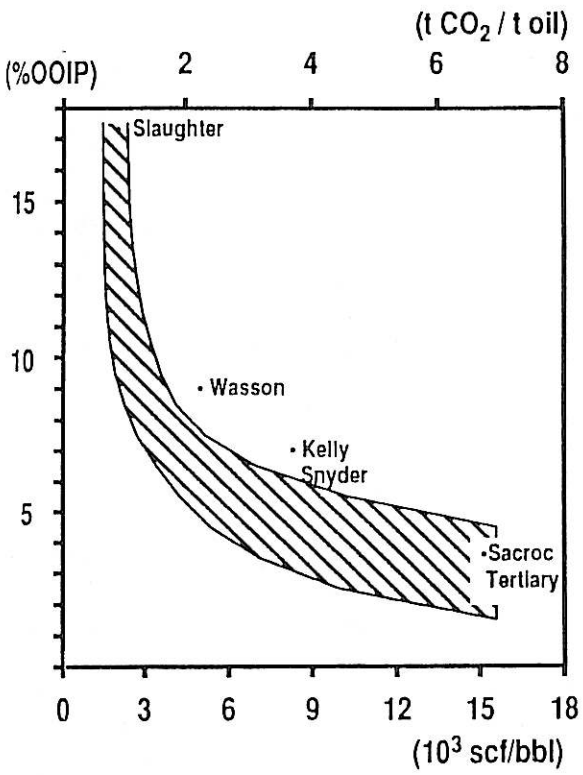


FIG. 7. Oil recovery versus CO_2 efficiency.

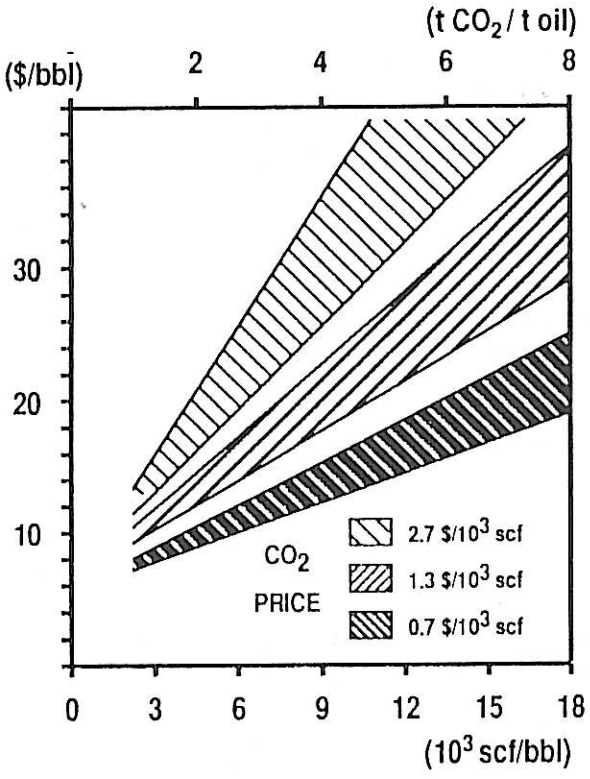


FIG. 8. Price per barrel versus CO_2 efficiency.

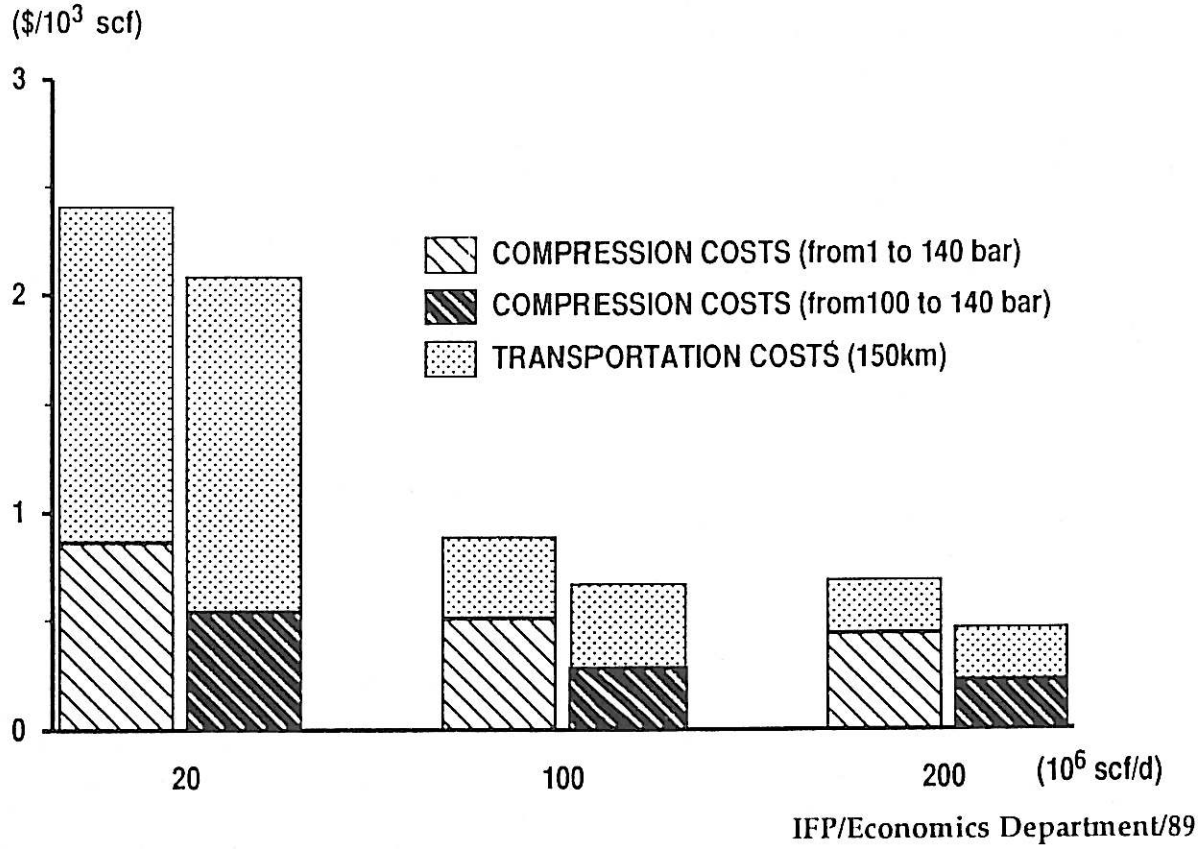


FIG. 9. Cost of CO_2 from natural deposits.

Values of $ 1.3 and 2.7/10^3 scf, considering the recycling of produced gas (economically advantageous), respectively represent the case of a source rich in CO_2 (natural deposit or ammonia plant) or poor in CO_2 (power-plant fumes in particular).

These Western European economic conditions could be adapted to the specific case of Libya. As a matter of fact, the figures can be very different if large amounts of CO_2 from natural deposits can be injected at a very low cost, depending on the plant capacity and on the initial pressure of CO_2 (Fig. 9).

When the mobility of the CO_2 is reduced by alternating water and gas flooding or by the addition of foaming agents, production increases in quite appreciable proportions, whereas the specific cost of this operation is slight when compared to the additional oil produced in relation to CO_2 flooding alone. Therefore, the higher the cost of the additional oil recovered by CO_2 flooding, the more advantageous it will be from the economic standpoint to use foaming agents. Indeed, for all the additional oil produced, the effect of foaming agents will be all the greater as drainage efficiency by CO_2 is low. Presently the use of foaming agents is limited by the poor technical behavior of available chemicals.

In the case of hydrocarbon gases, the results are also greatly influenced by the local value of the gas. They could be very similar if this gas is close enough to a gas market, with a price in the range of $2 to 4/$10^3$ scf similar to the high level mentioned for CO_2 cost. If not, the cost of the gas is the production cost which can be very low. In this specific case the cost of the additional oil produced is much less sensitive to the hydrocarbon gas requirement.

Polymer Flooding

Additional oil recovery due to polymer flooding amounts to about +5 to +20% of the oil in place at the start of chemical flooding, and the cost is fairly stable, between $10 to 20/bbl. With regard to the breakdown of the technical cost, it can be seen that the product item still represents 40 to 50% of the end cost of production. This process is particularly suitable for heterogeneous reservoirs or ones having an unfavorable water/oil mobility ratio. Under optimized conditions, the greatest improvement in the recovery corresponds to a high mobility ratio and medium heterogeneity.

An increase in polymer retention reduces the increase in recovery. This decrease is always fairly low as long as retention is no greater than about 100 to 200 ug/g, but increases rapidly above these values. In addition, the stability of the polymer solution under the reservoir conditions obviously has a strong influence on the oil recovery and the production cost.

The operating parameters generally have a moderate influence. It can be emphasized that the optimum situation corresponds to large size slugs with a high polymer concentration.

If compared to the main pilot operations carried out, this situation of economic optimum corresponds to the injection of a large amount of polymers. Despite higher specific polymer consumption, this results in considerably greater recovery, with approximately the same cost per barrel of oil.

SEARCHING FOR POTENTIAL IMPROVEMENTS FROM RESEARCH AND DEVELOPMENT

For thermal processes, improvement of sweep efficiency using surfactant additives to generate foam and reduce fingering of steam is required. Research must be carried out to find agents consistant with temperatures as high as 300°C.

For gas injection, improvement of sweep efficiency through WAG (Water Alternating Gas) or foaming agents is necessary since many reservoirs have only a low dip that is insufficient for gas oil gravity stabilization.

Looking towards ideal viscous flooding, additional research on polymer flooding should aim at:

(1) Improving the control of polymer adsorption and retention, particularly in reservoirs containing a high proportion of clay and carbonates;

(2) ensuring polymer stability especially in high temperature and salinity reservoirs.

For micellar polymer processes, the quantity of surfactants per cubic meter of oil recovered must be optimized by reducing losses due to retention together with preserving the efficiency of the micellar slug. One method consists in preflushing the reservoir with alkaline agents. An alternative solution consists in injecting a desorbing agent together with chase water behind the micellar slug.

The resulting improvement in the economics could reach 25 to 30% of the technical cost of the processes as shown in Table 4.

IMPROVING RESERVOIR CHARACTERIZATION

The experience accumulated about the application of EOR processes, especially when implementing pilots, has shown the extreme importance of reservoir heterogeneity on the technical and economic results.

In practice, if the external geometry of the reservoir must be determined accurately, above all, its internal architecture must be described quantitatively in terms of porosities, permeabilities and saturations so that this description can be integrated into reservoir simu-

Table 4. Reduction of EOR Costs

Methods	Mean costs ($/bbl)	Optimized costs ($/bbl)	Action
Thermal	15	11	- Optimizing drilling - Optimizing sweep efficiency - Improving energy balance
CO_2	20	13	- Optimizing cost and amount of CO_2 - Improving sweep efficiency
Polymers	17	12	- Optimizing products - Controlling retention
Surfactants	30	15	- Reducing the share of product in the technical cost (at present 65 to 80%) - Reducing adsorption

lators. The dynamic behavior of the field during its production life has to be followed up.

Traditional reservoir engineering techniques for data acquisition (tests and well logging) are continuing to evolve and to improve. Nevertheless, a satisfactory answer to the above problem can come only from a multidisciplinary approach that is progressively implemented by associating reservoir engineers with geologists and geophysicists, whose knowledge and know-how have made considerable progress in their disciplines.

One of the difficulties is the scale factor between the size of heterogeneities (tens of meters) and the spacing between wells (hundreds of meters or more).

Today, developments aim is interpolating between wells or extrapolating around one well. Among the different possible tools, geostatistics appears very promising. Even though the quantitative data on

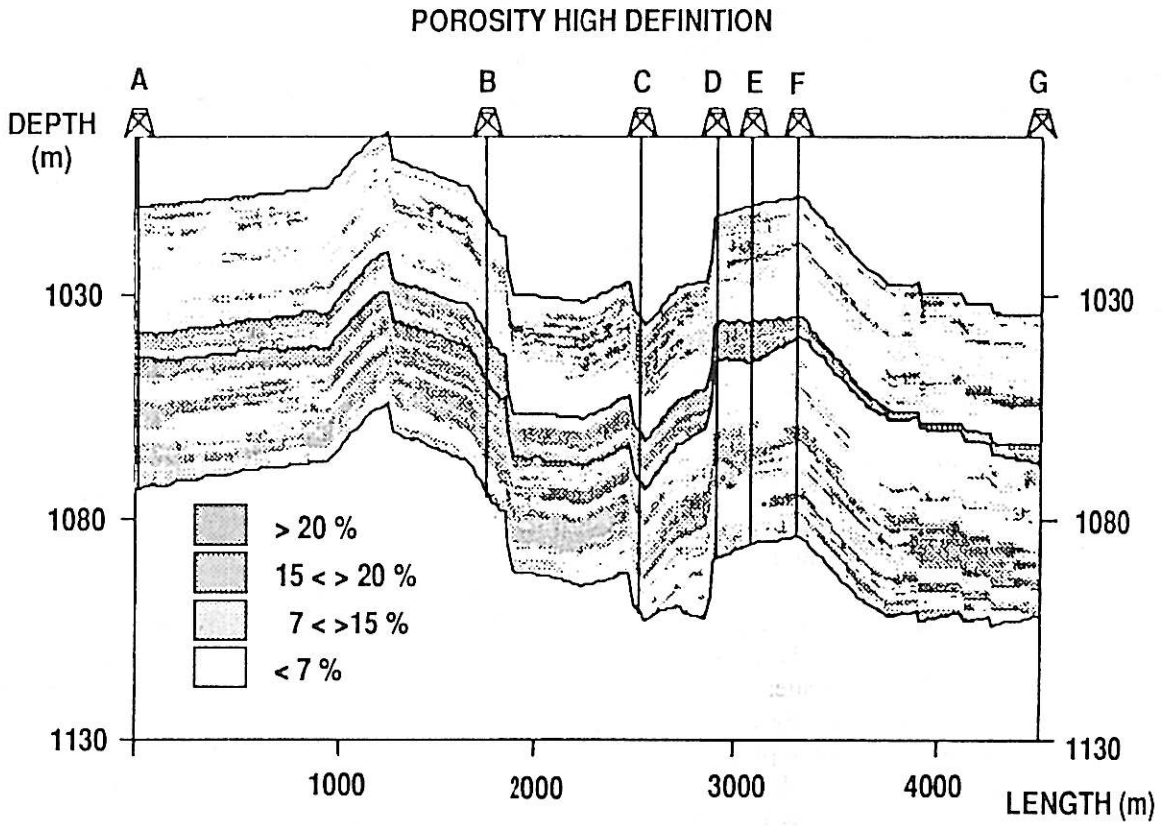


FIG. 10. Geostatistical interpretation with HERESIM®.

heterogeneities are of a statistical nature, their spatial distribution is not completely random, and the understanding of the depositional environments can be very useful. In the method, rather than defining sedimentary bodies having a given geometry, the goal is to incorporate information about "sequences". These sequences are characterized by variograms deduced from field observations of the same type of depositional environment.

The method of geostatistical interpretation can then be used to generate a series of equiprobable models. These models are progressively constrained by well data as well as by additional constraints such as seismic data, dynamic data or any other pertinent data. The resulting reservoir images are supplied to the geologist, who can select the models that are most likely to represent reality (Fig. 10). The models selected are then at the disposal of the reservoir engineer, giving him a quantitative description of the heterogeneities. His task is then to transfer this quantitative geological model to the typical grid-block model for reservoir calculation.

SEARCHING FOR SYNERGISM WITH NEW TECHNOLOGIES

Horizontal Drainholes

The technology of horizontal drilling, for which the principle is not new, was taken up again in the late 1970s by Elf Aquitaine/IFP to substantially boost production from the Rospo Mare field in the Adriatic Sea (Fig. 11). This field consists of a fractured and vuggy limestone reservoir containing a very heavy oil located above an active aquifer.

The problem was first to demonstrate the feasibility of drilling drainholes several hundred meters long horizontally in the reservoir. The results exceeded anticipations, because productivity rose by a factor of more than 10 with production over a long period of more than four times that from vertical and slanted wells close to it.

However, horizontal well costs are about 1.4 to 2 times those of a vertical well. Depending on the method selected, completion costs could also increase the differential. Do enhanced production, more efficient drainage, and ultimate recovery compensate for the added drilling, completion, and operating expenses of going horizontal? The answer lies in a cost-benefit analysis that must be performed on a case-by-case basis.

Horizontal economics is most compelling in: (1) thin formations, (2) relatively isotropic (homogeneous) reservoirs, (3) naturally fractured reservoirs, (4) formations with gas or water coning problems (Fig. 12).

In a thick pay zone, the incremental benefit from drilling horizontally through the formations is reduced.

Concerning drilling technology, two main technologies have emerged:

(1) a lung turning radius: This is the most spread out technique using conventional drillstring rotation and standard equipment;

(2) a short turning radius: This method requires the rotating of the drillstring and the use of articulated drill collars in the deviated section. So far the drain length is limited to 1000 ft.

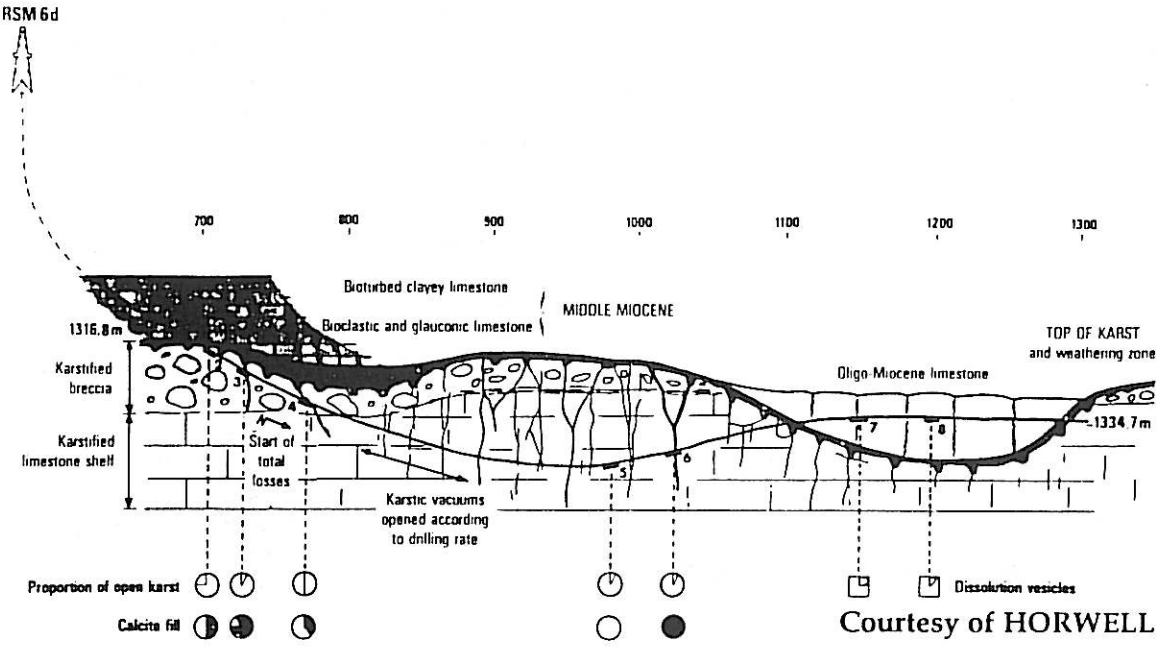


FIG. 11. ROSPO MARE 6D (Interpretive section of the reservoir).

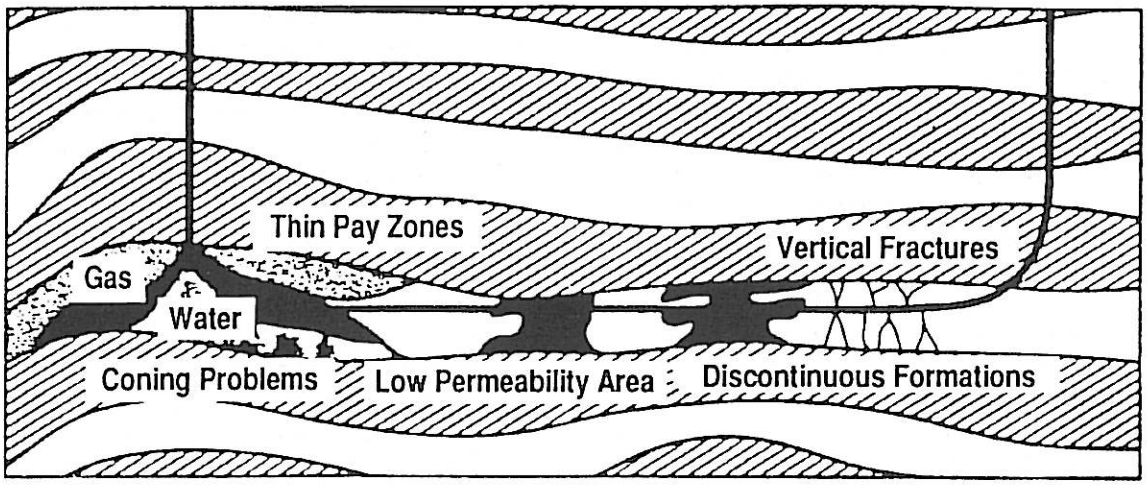


FIG. 12. Horizontal drainholes applications.

The first technique is more advantageous for improving recovery. Several dozen wells of this type have been drilled in recent years in a wide variety of fields (Fig. 13). They have generally demonstrated gains in productivity over vertical wells by a factor of 2 to 5 (Fig. 14), to the point where this technique must now be considered as a general technique for improving production. Even more importantly, horizontal wells appear to be a new technique for production, as achieved for the first time at Rospo Mare, where a complete zone has been developed at Elf Aquitaine exclusively with horizontal wells drilled from a rig. Offshore situations such as this one are very attractive, because horizontal wells reduce the number of wells needed, thus drastically reducing the size of the platform, or allowing some slots to be kept for future wells such as infill wells or injection wells.

Drainholes measuring 1500 to 3000 ft long can be drilled today at any depth, under most conditions. Core samples can be taken and any type of well log plotted. Completion can be achieved including cementing, which is certainly a delicate technique with this geometry.

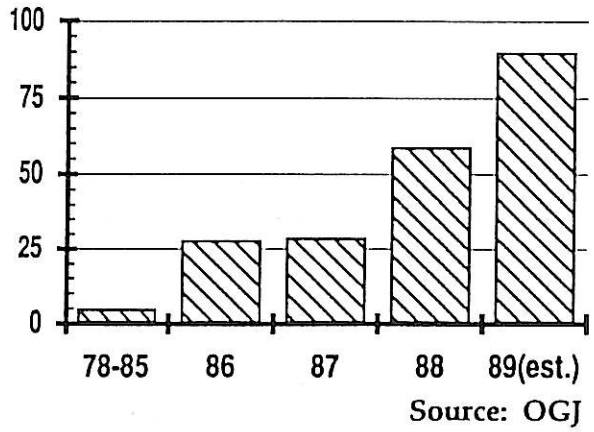


FIG. 13. Horizontal drilling activity (Drainholes longer than 1000 ft).

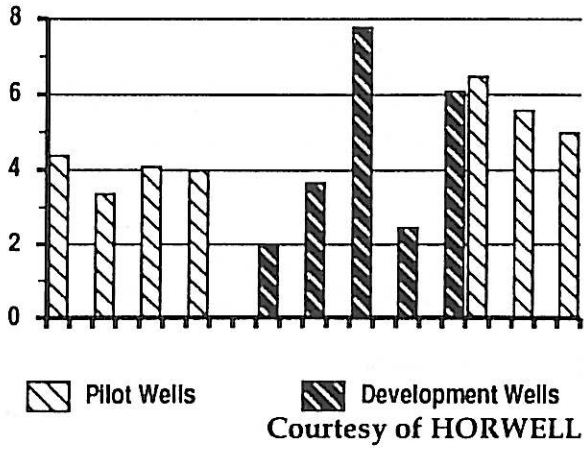


FIG. 14. Production ratio: Horizontal vs vertical.

Recent experiments have shown that the potential of these wells can be further increased by multiple hydraulic fracturing, and also by artificial pumping. Production from these drainholes can be predicted and interpreted. This technology is hence mature for intensive development, and it could represent one of the major breakthroughs in the years to come.

Synergy of EOR Processes with Horizontal Drainholes

Horizontal wells and polymer flooding

The example considered is the case of a typical oil reservoir 2000 ft deep, lying in a sandy channel system with widely contrasting permeabilities (Fig. 15). Two development schemes were considered, one having vertical wells drilled in different zones of the reservoir, and the other horizontal wells.

The simulations made for these two configurations take different types of recovery into consideration, in particular waterflooding and enhanced recovery by polymer flooding, all of which are assumed to be implemented at the start of production. Waterflooding using horizontal drainholes instead of vertical

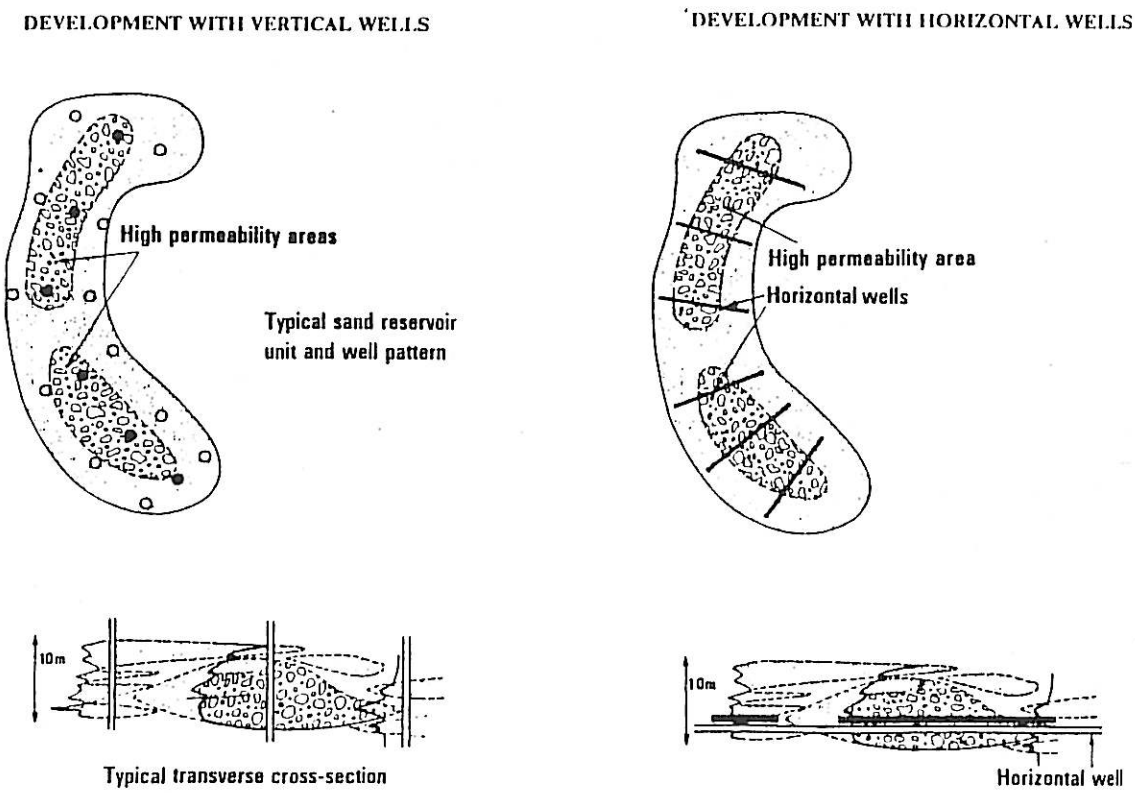


FIG. 15. Development with vertical wells versus development with horizontal wells (Case Study).

wells leads to an additional oil recovery of 0.7 Mbbl at the very low cost of $ 2.5/bbl. Moreover, combining horizontal wells with polymer flooding instead of waterflooding makes it possible to double the additional recovery compared to the results of the vertical-well scheme, with a cost of $ 6.7/bbl for the additional oil (Table 5). Therefore, the synergy between the two approaches leads to an increase of 50% from total recovery and at the same time a decrease of 20% for the average cost of the oil recovered.

Table 5. Synergy between Horizontal Wells and Polymer Flooding

Development scheme	Oil recov. after 20 y (Mbbl)	Average oil cost ($/bbl)	Addit. oil recov. (Mbbl)	Cost of addit. oil ($/bbl)*
Waterflooding				
vertical wells	2.9	13.2	-	-
horizontal wells	3.6	11.1	0.7	2.5
Polymer flooding				
horizontal wells	4.4	11	1.5	6.7

* by reference to waterflooding in vertical wells

Horizontal wells and steam injection

Two types of well configurations have been considered for the development of a 1300 ft deep reservoir: parallel horizontal-wells lines used alternately for injection and production, or five-spot patterns with vertical wells. With 300 ft spacing, the use of horizontal wells leads to an oil recovery of 25 Mbbl in 5 years, i.e. half of the time needed to reach the same amount of oil by using vertical wells (Table 6). Moreover, the optimal unit cost per barrel is 30% lower. With larger spacing (450 ft), the project life is doubled by comparison to 300 ft spacing. The unit cost in this case is only 20% lower, but the decrease remains significant.

Table 6. Synergy between Horizontal Wells and Steam Injection

Development scheme	Spa-cing (ft)	Project life (year)	Oil recov. (Mbbl)	Unit cost ($/bbl)
Vertical wells	300	10	25.3	9.6
Horizontal wells	300	6	25.0	7.0
Vertical wells	450	21	20.3	8.8
Horizontal wells	450	11	19.8	7.1

From these two specific examples, it appears that horizontal wells, as a means of boosting productivity and a new method of production, should show close synergy with enhanced recovery, by favoring the propagation of the injected fluids and the drainage of the oil mobilized.

CONCLUSION

The different technique of EOR rely on a wide variety of physical principles and cover a wide field of applications from light crudes to heavy crudes. Their implementation differs from one continent to another depending on the average characteristics of the fields and on economic factors such as the availability of low cost gases to inject.

All the processes have evolved technically in recent years, and steady progress has been made, but the sharp drop in the price of crude oil in 1986 again emphasized the crucial importance of the cost of these methods. The experience gained in the past now enables us to choose different ways for the necessary reduction of the technical and economic risks of EOR methods:

(1) by the mastery of the main parameters of the processes thanks to extensive research in laboratories and to pilot applications;

(2) by better reservoir characterization aiming essentially at determining its internal architecture in terms of porosities, permeabilities and saturations;

(3) by systematically searching for synergism with promising technology such as horizontal drainholes.

In the economic environment prevailing now, these ways of investigation appear to be the best ones that could ensure the necessary development of EOR applications in the world.

REFERENCES

[1] Simandoux P., Champlon D. and Valentin E., 1989, Managing the Cost of the EOR, IFP, Paris (France).

[2] Stosur G.L., Singer M.I., Luhning R.W. and Yurko W.J., 1989, Enhanced Oil Recovery In North America: Status and Prospects, Proceedings of the 5th European Symposium on Improved Oil Recovery, Budapest (Hungary).

[3] Surguchev L.M., Bokserman A.A. and Zhdanov S.A., 1989, The State and the Perspectives of EOR Methods Application in the USSR, Proceedings of the 5th European Symposium on Improved Oil Recovery, Budapest (Hungary).

[4] Burger J., 1988, Status of Enhanced Recovery by Thermal Methods, Revue de l'Institut Français du Pétrole, Editions Technip, Vol. 43, no. 3.

[5] Petit H., Renard G. and Valentin E., 1989, Technical and Economic Evaluation of Steam Injection with Horizontal Wells for Two Typical Heavy Oil Reservoirs, Proceedings of the SPE fall meeting, San Antonio, Texas, USA.

PRJ, Vol. 4. (January 1992); P. 33–45, 10 FIGS.

GEOCHEMICAL INVESTIGATION OF THE BAHI FORMATION IN THE WESTERN PART OF SIRT BASIN, LIBYA

A.M. Sghair*

دراسة جيوكيميائية لتكوين الباهي بالمنطقة الشمالية الغربية ، حوض سرت

عبد السلام محمد الصغير

تم دراسة 73 عينة صخرية من أربعة آبار نفطية لتكوين الباهي في المنطقة الشمالية الغربية بحوض سرت. شملت الدراسة التحليل الجيوكيميائي لعدد 26 عنصراً من العناصر الرئيسية الشحيحة والنادرة ، لمعرفة الطابع الجيوكيميائي لهذه العناصر بغرض إعطاء لمحة عن مصدر الصخور ولتسليط الضوء على المؤثرات الرجية (التكتونية) على هذه الصخور.

تبرز الدراسة أهمية توزيع العناصر في تكوين الباهي ، إذ أن النسب العالية لوجود أكسيد السيلكا دليل على درجة نضوج الرواسب في حين أن بعض العينات توجد بها نسب بسيطة من هذا الأكسيد ، ويرجع ذلك إلى وجود مواد مصاحبة مثل مواد كربونية إنهيدراتية وطفلية.

إن الإختلاف في نسبة تركيب أكسيدي البوتاسيوم والألمونيوم يعود إلى الإختلاف في توزيع معدني الفلدسبار والطفل سواء كان عمودي أو أفقي. كما أن وجود النسبة العالية لأكسيدي الكالسيوم والماغنسيوم في الجزء العلوي للتكوين ناتجة من وجود المادة اللاحمة والمتكونة من كالسيت ، ودولوميت وإنهيدرايت. ويرجع إنتشار العناصر الشحيحة والنادرة إلى العلاقة المباشرة بتوزيع أكسيدي الألمونيوم والبوتاسيوم عمودياً وأفقياً.

من تطبيق العلاقة بين العناصر الشحيحة والنادرة يتضح أن رواسب الباهي أتت أساساً من صخور رسوبية قديمة.

كذلك أوضحت العلاقة التمييزية بين الأكاسيد أن تكوين الباهي قد ترسب على حافة قارية مستقرة مغطاة بصخور رسوبية ناضجة.

ABSTRACT

Seventy three samples from the Bahi Formation from four boreholes in the western part of the Sirt Basin have been analysed for 26 elements to indicate the geochemical signature of the Bahi Formation. Variation in the major elements and the trace elements both laterally and vertically within the formation have been correlated, to give some indication of the provenance and to throw light on the tectonic setting of the sediment.

Geochemical studies of the major and trace elements distribution within the Bahi Formation showing a high SiO_2 *content, indicate a high degree of maturity in most of the samples whereas* K_2O *and* Al_2O_3 *and most of the trace elements are associated with feldspar and/or clay minerals. The relationship between the various trace elements suggests that the Bahi Formation was derived largely from pre-existing sedimentary sources. The discriminant function analysis of the major elements suggests that the Bahi Formation was derived from a craton interior and/or a passive continental margin.*

INTRODUCTION

The Bahi Formation is defined as a heterogeneous clastic rock succession known only from boreholes. The term Bahi has been used widely and rather loosely in the central and western part of the Sirt basin (Barr & Weegar, 1972). This formation occurs at the base of marine Upper Cretaceous formations. Cenomanian marine sediments have been recorded from concession 32. Maastrichtian strata occur above

*Petroleum Research Centre, P.O. Box 6431, Tripoli, G.S.P.L.A.J.

the Bahi in concession 11, 16 and in the southern part of concession 32 (Fig. 1). The formation lies unconformably upon either igneous and metamorphic Precambrian rocks, the Cambro–Ordovician Hofra Formation and the Devonian Tadrart Formation. The Bahi Formation consists essentially of two units, the lower one composed of argillaceous sandstone, and the upper being subdivisible into two tongues of coarse to very coarse sandstone with cross bedding and coarse-grained sandstone respectively, separated by a thin bed of argillaceous red siltstone. Glauconite is common in the uppermost part, but seems to be absent in the lower part (Sghair, 1990).

There have been no geochemical studies of the Bahi Formation. In this study, a detailed investigation of major and trace elements has been carried out. On the basis of vertical and lateral lithological variation of the formation a total of seventy-three samples were selected, 13, 27, 20 and 13 from cores in the A2-32, A4-32, D1-32 and F6-32 boreholes respectively. These have been analysed using an X-ray fluorescence spectrometer (Leake *et al.*, 1969; Harvey *et al.*, 1973). Ten major oxides were determined using XRF (SiO_2, TiO_2, Al_2O_3, $Fe_2^*O_3$ (total), MnO, MgO, CaO, Na_2O, K_2O, P_2O_5), and 16 trace elements (Ba, Ce, Co, Cr, Cu, Ga, La, Ni, Pb, Sr, Th, Y, Zn, Zr, U).

The major oxides FeO, H_2O, CO_2 were determined by wet chemical analysis. The FeO was determined by titration of standard dichromate solution with rock solution made by dissolving a measured amount of whole rock powder (0.5 grams) in sulphuric and hydrofluoric acids. The FeO percentage, determined by titration, was used to calculate the amount of Fe_2O_3 present. The amounts of H_2O and CO_2 in the samples were determined using the Penfield method of combustion, adsorption and gravimetry. The amount of total sulphate (SO_3) was determined by using the gravimetric method.

MAJOR ELEMENTS

Several recent studies have investigated the sedimentary geochemistry of elastic rocks in order to indicate their provenance and geotectonic setting by using variable discriminate functions based on major-element data. Bhatia (1983) used the major oxides $Fe_2O_3 + MgO$, Al_2O_3/SiO_2, K_2O/Na_2O, $Al_2O_3/(CaO + Na_2O)$ and TiO_2 as discriminating parameters to indicate the relationship between the geochemical composition of sandstones and the geotectonic settings of their sedimentary basins. He showed that the nature of continental margins and

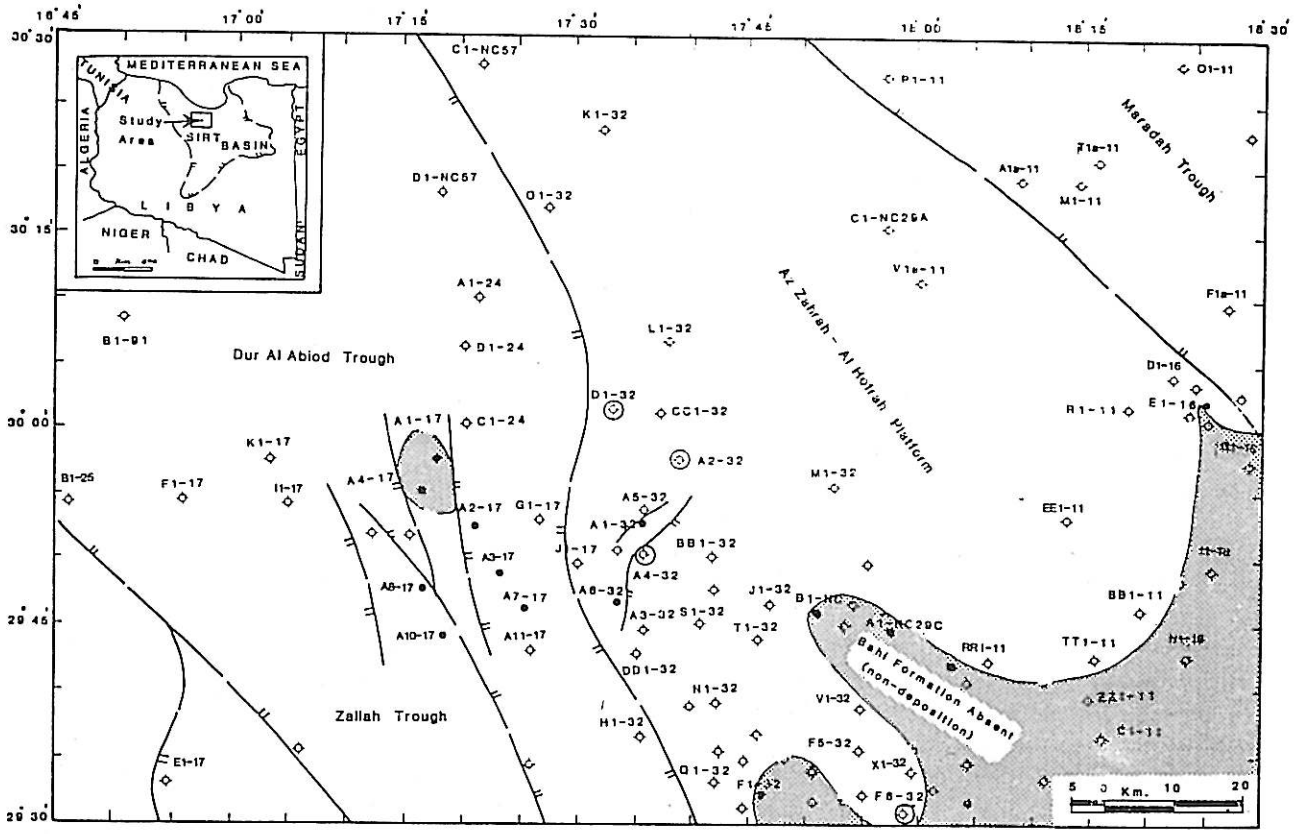


FIG. 1. Location map of the studied area in the western part of the Sirt basin, Libya.

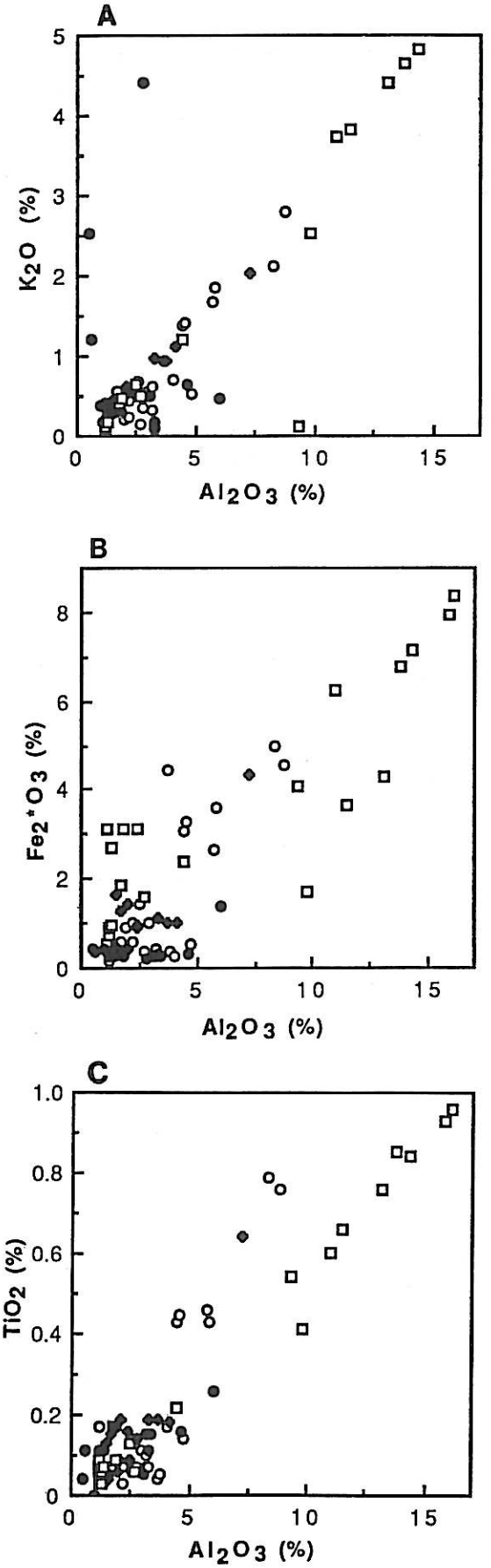


FIG. 2. Plots of Al_2O_3 vs K_2O; Al_2O_3 vs Fe_2^*O (total); Al_2O_3 vs TiO_2; K_2O vs TiO_2 and K_2O vs Fe_2^*O (total).

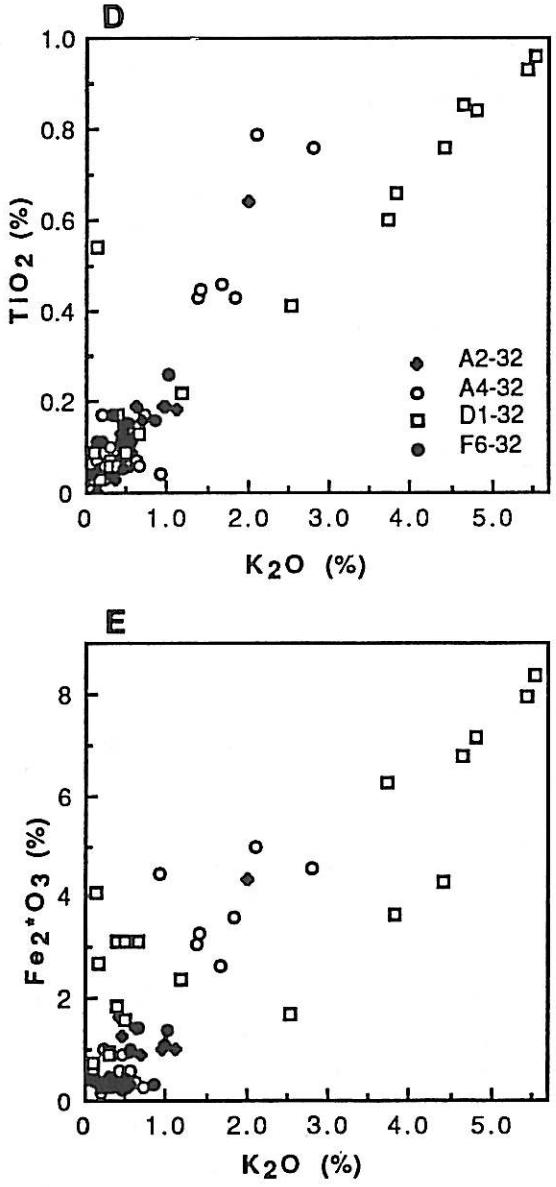


FIG. 2. *Contd.*

ocean basins can be deciphered on the basis of the major element compositions of sandstones.

In this study, the lateral and vertical geochemical variation within the Bahi Formation in the four selected boreholes reflect different mineralogical composition resulting from changes in environmental conditions at the time of deposition and/or different sources for the sediments of this formation.

Major oxides of the Bahi samples from the four boreholes, were plotted against each other on scatter plot diagrams to show the inter-relationships between these elements. The major oxides results show a high content of SiO_2 at the expense of other oxides in most of the studied samples. This suggests a more mature sediment in these samples, whereas in the upper part of the formation at A2-32, D1-32 and F6-32 boreholes, the SiO_2 content is low due to an

abundance of evaporites and carbonate as a cement or matrix. In the lower part of the formation the SiO_2 content varies inversely with the clay mineral and feldspar content.

The sources of both Al_2O_3 and K_2O in the sedimentary rocks are feldspars and sheet silicates such as micas and clays. As a result the abundance of Al_2O_3 can be directly related to the abundance of feldspar, mica and clay minerals. A plot of Al_2O_3 versus K_2O (Fig. 2A), shows a strong positive correlation. This suggests the same source for minerals containing these oxides. TiO_2 content in the sediments is due to terrigenous material consisting of: 1- wheathering residue in the form of chemically unaltered grains like rutile, or in the form of partly decomposed minerals like mica, 2- new products of weathering such as anatase and clay minerals, 3- diagenetic minerals (Wedepohl, 1978, 22-k-1). The plots of TiO_2 versus Al_2O_3 and K_2O (Fig. 2C & D), show a poor positive correlation in some studied samples. This suggests that the TiO_2 content is associated with the clay minerals and/or K-feldspar, whereas the majority of the studied samples show very low content TiO_2, suggesting that the titanium content may be concentrated in oxides or non layer silicates, opaques and rutile minerals which have been detected in the Bahi sediment. In most of the samples from the Bahi Formation in the four boreholes, the plots of Al_2O_3 and K_2O versus $Fe_2^*O_3$(total) (Fig. 2B & E), show a positive correlation suggesting that the $Fe_2^*O_3$ content is conentrated in clay minerals and/or feldspar. However, iron oxide is present in replacement minerals in the weathered feldspar and in cement materials.

Most of the calcium in the sedimentary rocks occurs in the carbonate fraction (Wedepohl, 1978, 20-k-1). The detrital components in the form of Ca-plagioclase and accessory minerals such as apatites contain significant amounts of CaO in their crystal structure. The presence of a positive correlation between CaO and CO_2(Fig. 3A), is related to enrichment of the Bahi sediment by carbonate cement composed of varying proportions of calcite and dolomite, whereas some studied samples show high CaO content with very low CO_2. This is undoubtedly related to the presence of evaporites ($CaSO_4$) in the uppermost part of the formation. Magnesium is present in the sediments mainly as dolomite and phyllosilicates such as chlorite and glauconite. Phyllosilicates are mostly present in shales and to a smaller extent in sandstones, graywackes and arkoses (Wedepohl, 1978, 12-k-1), a plot of MgO versus CO_2 (Fig. 3B), shows a positive correlation in most studied samples, suggesting that the amount of MgO is present mainly in a somewhat dolomitic carbonate cement, whereas small amonts of magnesium may indicate the presence of a phyllosilicate (glauconite).

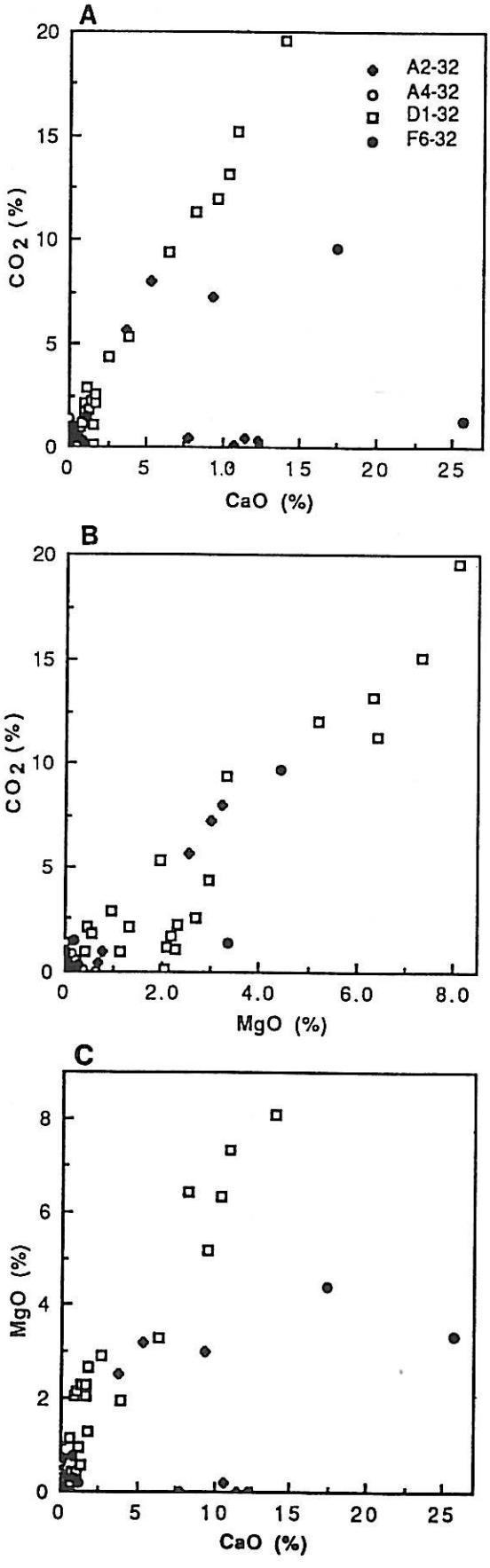


FIG. 3. Plots of CO_2 vs CaO; MgO vs CaO and MgO vs CO_2.

The uppermost part of the formation is rich in glauconite, whilest a plot of CaO with MgO (Fig. 3C), shows two trends which in some samples show a good positive correlation. This suggests that a high content of both oxides is related to an abundance of dolomite whereas in other samples there is a lack of correlation between MgO and CaO. High content of CaO is related to the presence of calcite and anhydrite.

NIGGLI NUMBERS

The use of Niggli numbers can be very useful in distinguishing between K which is derived from detrital feldspar and K from detrital illite, mica or other sheet silicate minerals. The Niggli numbers are based on taking the percentage of the sum of the molecular content of Al_2O_3(al), CaO(c), $FeO+Fe_2O_3+$ MgO(fm) and Na_2O+K_2O(alk).k$=K_2O/Na_2O+K_2O$ (Niggli, 1954, p. 13–15).

A plot of al-alk versus Niggli K has been used to distinguish between K in feldspar and K in sheet silicates such as micas and clay minerals. High al-alk(>30), indicates clay-rich rocks (shale), whereas low al-alk (<30) indicates a high feldspar content, supported by negative correlation with Niggli K if the K was largely in potassium feldspar or positive correlation if the K was largely in sheet silicates. The absence of negative or positive correlations suggests that a mixture of the two minerals is present (Van de Kamp & Leake, 1985).

A plot of al-alk versus Niggli K (Fig. 4A), shows absence of negative or positive correlation suggesting that the K occurs in a mixture of both feldspar and clay minerals. Some of the studied samples, show al-alk>30. This suggests that most of K may be related to the sheet silicates whereas the majority of the samples have al-alk <30 suggesting that K is represented in a mixture of both feldspars and clay

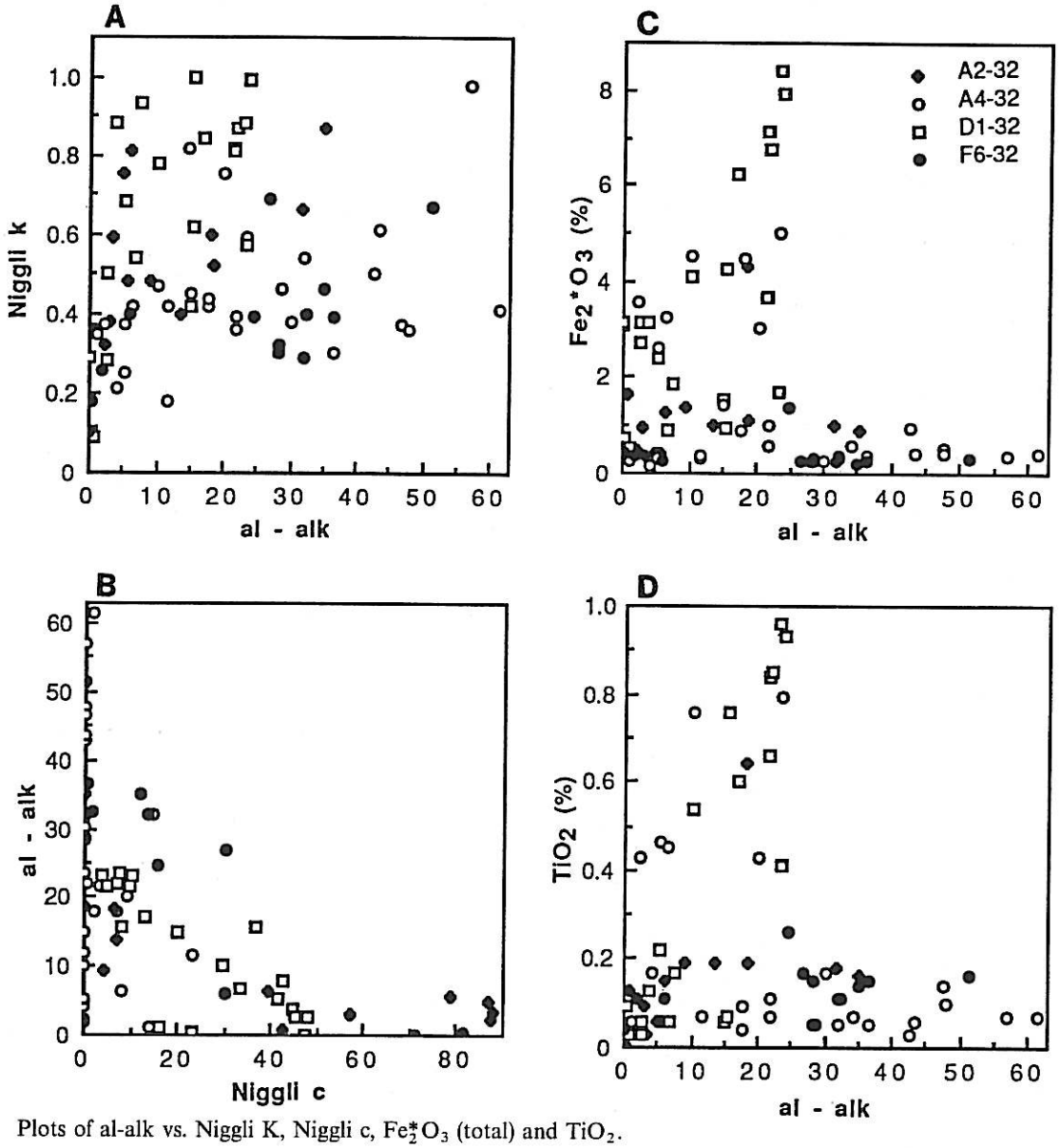


FIG. 4. Plots of al-alk vs. Niggli K, Niggli c, $Fe_2^*O_3$ (total) and TiO_2.

minerals, whereas a plot of Niggli c versus al-alk (Fig. 4B), shows three well defined trends. The dominant trend shows that c is largely related to dolomite (c=50). Another trend shows that c is largely related to calcium carbonate (c=100), whereas some samples show very low content of c (c nearly 0), and this may be related to clay minerals, while the plot of al-alk against $Fe_2^*O_3$ (total) (Fig. 4C), shows two main separate fields. One trend shows a positive correlation suggesting that the $Fe_2^*O_3$ content is largely associated with clay minerals, whereas the other field shows low $Fe_2^*O_3$ content suggesting that Fe may be related to detrital iron oxides and in a plot of al-alk versus TiO_2(Fig. 4D), most of the studied samples show very low content of TiO_2 and an undefined relationship with al-alk. This suggests that the titanium may be present in detrital minerals such as rutile and opaques and to a limited extent in a few samples it is associated with clay minerals giving a poor positive correlation.

TRACE ELEMENTS

Many attempts have been made by various workers to differentiate similar lithological units and to determine the depositional environments of the sediments and their provenance on the basis of trace element distributions. Van de Kamp & Leake (1985) state that the trace elements are useful for provenance determination. They noted that the high values of cobalt, chromium and nickel indicate detritus from mafic and ultramafic sources; barium is a good indicator of a potassium feldspar-rich provenance, and high barium content in arkoses suggests granites and monozonite in the source area. They also showed that most trace elements are concentrated in sheet silicates such as mica and clay minerals; Bhatia and Crook (1983) used the La, Ce, Nd, Th, Zr, Nb, Y, Sc and Co trace elements to distinguish provenance types and tectonic settings; Hickman and Wright (1983) used rare earth elements to determine the provenance of sediments by plotting Y+La+Ce, Ni+Cr and Sr on a triangular diagram; Loring (1981) noted that the concentration of Zn, Cu, Pb, Co, Ni, Cr, V, Se, Hg and Be is low in sands, and increases with reduction in the grain size of sediments; Fenner & Hagner (1967) established a criterion to distinguish between stratigraphical units of similar lithology on the basis of trace element variations. Trace elements have been determined in the analysed samples from the four selected boreholes, in an attempt to understand the characteristics of these elements and their distribution, and to give some indication of the provenance and depositional environment of the Bahi Formation. The following plots of trace elements against each other and versus al-alk may help in this respect.

A plot of K_2O against gallium, lanthanium, rubidium and cerium in the Bahi samples (Figs. 5B, C, E & F), show a positive correlation. This suggests that these trace elements are concentrated in the K-feldspar and/or in the clay minerals, whereas plots of barium, strontium, cobalt, nickel, lead, thorium, uranium, chromium, copper, zinc and yttrium against K_2O do not show any clear correlation. This suggests that they are not concentrated in sheet silicate or K-feldspar. Plots of Al_2O_3 against Ga and Rb in the Bahi samples (Figs. 5A and 5D), show a positive correlation suggesting that gallium and rubidium are mainly concentrated in the clay minerals or in the K-feldspar or in both.

The parameter al-alk provides a measure of the aluminium contained in the clay minerals and micas rather than in the feldspar (Van de Kamp & Leake, 1985). Plots of al-alk against the trace elements lead, chromium, cerium, zinc, yttrium, lanthanium, zirconium and rubidium (Fig. 6), show no positive or negative correlation. This suggests that these trace elements are neither concentrated in the feldspar nor in the clay minerals.

The presence of lanthanium in the sediments is related to an increase in the alkalinity of weathering solutions. It is precipitated and fixed like aluminium, galium and titanium (Wedepohl, 1978, p. 39-57-71-g-l). Cerium content in the sediments could also be due to the increase in alkalinity of weathering solutions. The presence of a positive correlation between lithanium and cerium in the Bahi Formation, suggests that these elements are contributed by the same sedimentary processes, from a source characterized by highly alkaline weathering. Plots of rubidium, yttrium and gallium versus lanthanium (Fig. 7), show a positive correlation. This suggests that these trace elements are largely concentrated in the clay minerals and/or in the feldspar.

Hickman and Wright (1983) used this relationship for the Appin Group slates (late Precambrian Dalradian Supergroup of Scoltand) to suggest their provenance. The Ni and Cr end of the diagram represents provenances composed of basic rocks, the Y+La+Ce end represents a provenance composed of granitic rocks whereas the Sr end represents a provenance containing the highest proportion of sedimentary rocks.

A plot of Y+La+Ce versus Sr for the Bahi Formation samples in the four boreholes (Fig. 8), shows a very distinct trend. Virtually all the samples fall in the Sr sector indicating that the Bahi sediment is largely derived from a preexisting sedimentary source.

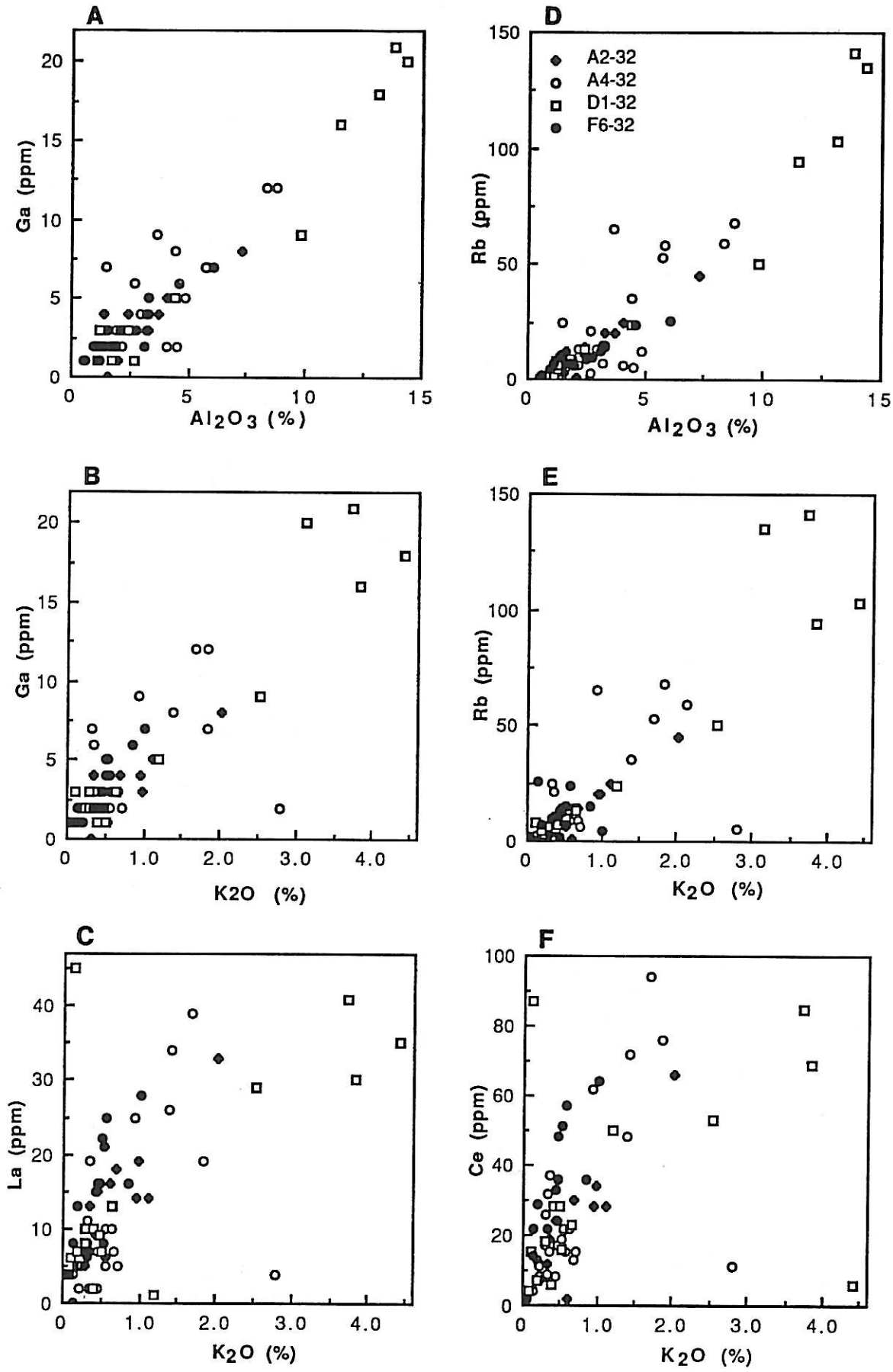


FIG. 5. Plots of Ga and Rb vs Al_2O_3 and K_2O; La and Ce vs K_2O.

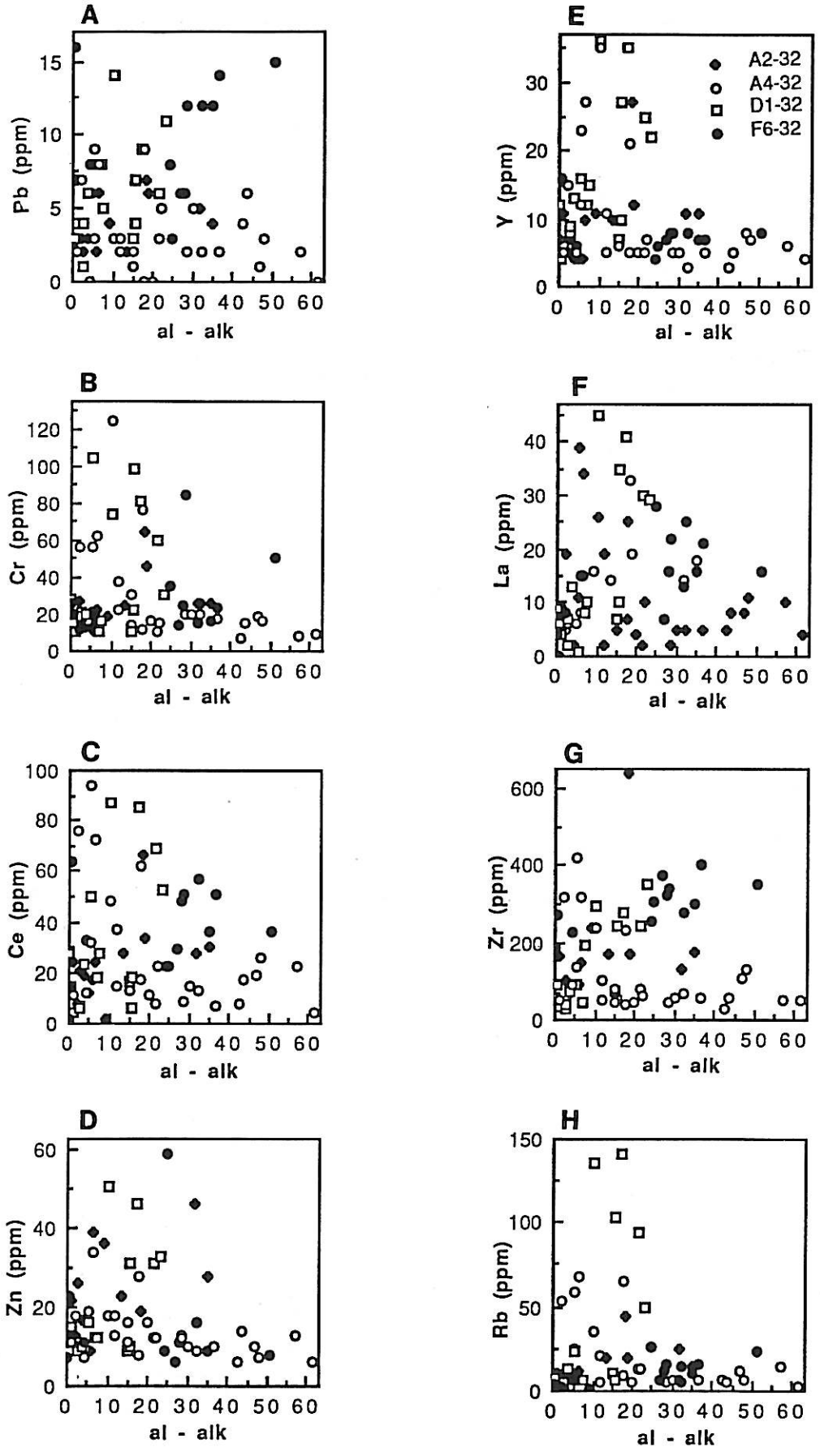


FIG. 6. Plots of al-alk vs pb, Cr, Ce, Zn, Y, La, Zr and Rb.

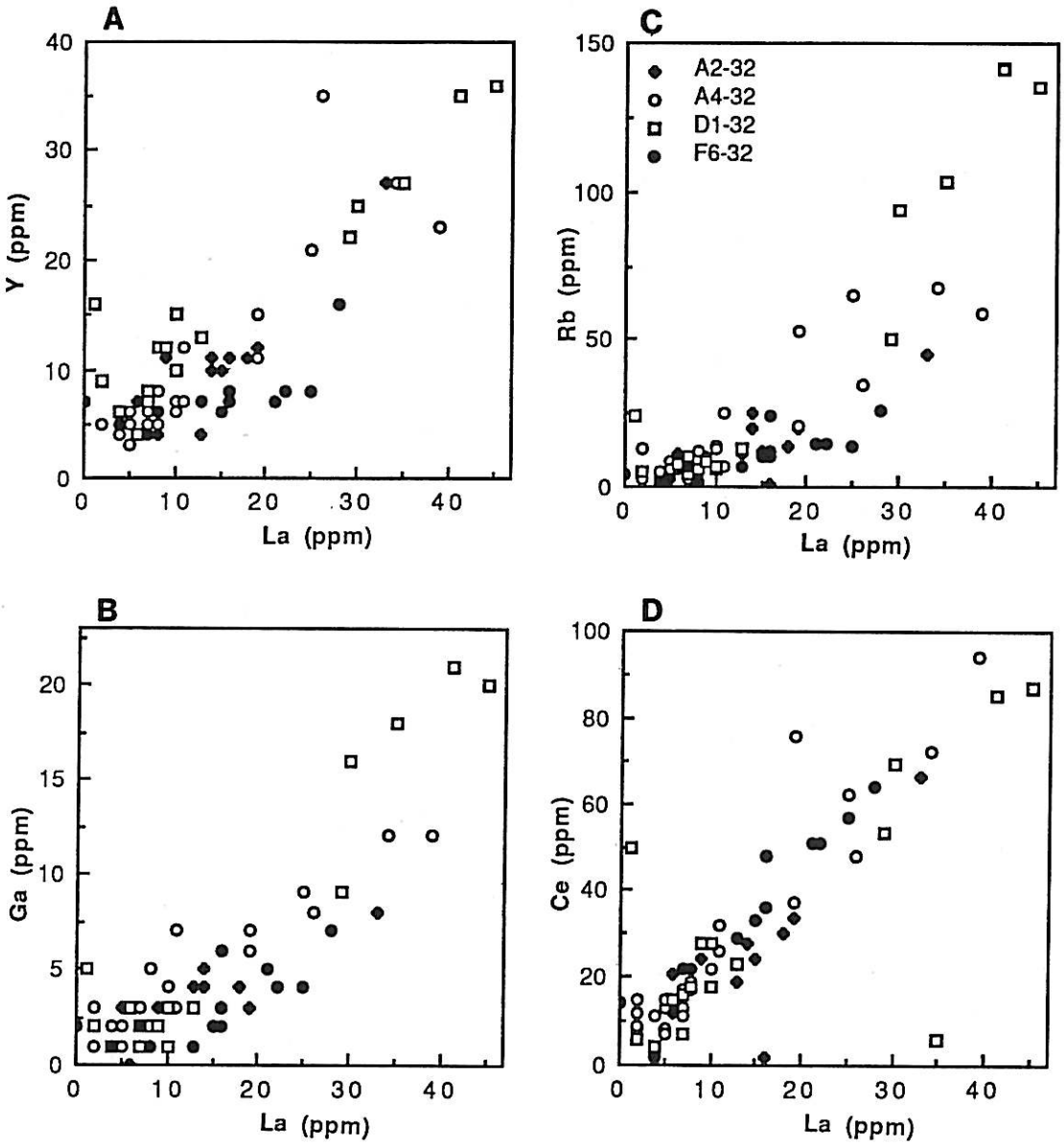


FIG. 7. Plots of La vs Y, Ga, Rb and Ce.

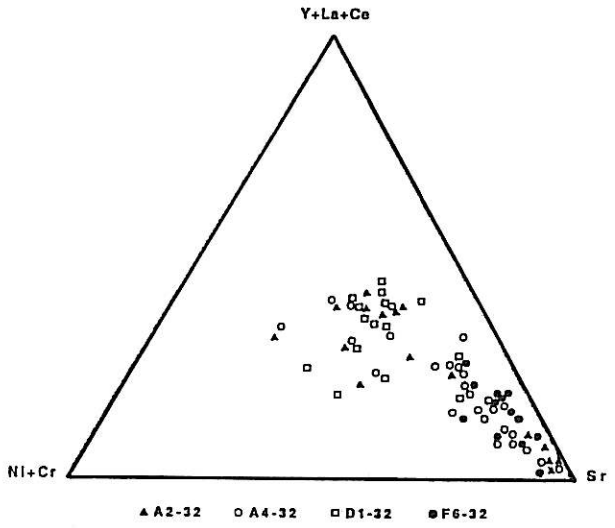


FIG. 8. Plot of Ni+Cr versus Y+La+Ce versus Sr in the four boreholes.

VERTICAL VARIATION OF BAHI GEOCHEMISTRY

The vertical variation in the major element composition, $Al_2O_2Na_2O$, K_2O and $Fe_2^*O_3$ (total) of the Bahi Formation, in the four boreholes, is related to changes in grain size and composition. This may indicate changes in the depositional environment and/or change in sediment provenance. Figs 9A-C, show the vertical distribution of the major elements and the trace elements of the Bahi Formation in boreholes A2-32, A4-32 and F6-32 respectively. In borehole A2-32, the uppermost part of the Bahi Sandstone is characterized by large amounts of clay minerals including chlorite, illite and kaolinite together with glauconite, low silica content, and high portion of the major elements (sample No. 2-1). The upper part of the formation is also characterized by a high CaO content in the form of carbonate and evaporite (samples No. from 2-2 to 2-6) and poor silica content, whereas the lower part of the formation (samples No. from 2-7 to 2-13) (below 1904m) is characterized by smaller grain size, low silica content and also a high proportion of major elements. This reflects a less mature sediment. The high concentration of the trace elements varies inversely with the grain size and thus the maturity of this sediment. However, the concentration of trace elements is high in the samples which show a high proportion of feldspar and clay minerals (Fig. 9A). In borehole A4-32, for a thickness of 7.6m down to 1845m (samples 14-16) and for a thickness of 7m down to 1880m (samples 25-27) there is a reduction in grain size and a compositional change of the Bahi Formation. There is also a decrease in silica content and an increase in other major elements and hence increase in the amount of feldspar and clay minerals. This reflect variation in major elements distribution and indicate relative mineralogical maturity of the Bahi sediments for these intervals (Fig. 9B). There is also a

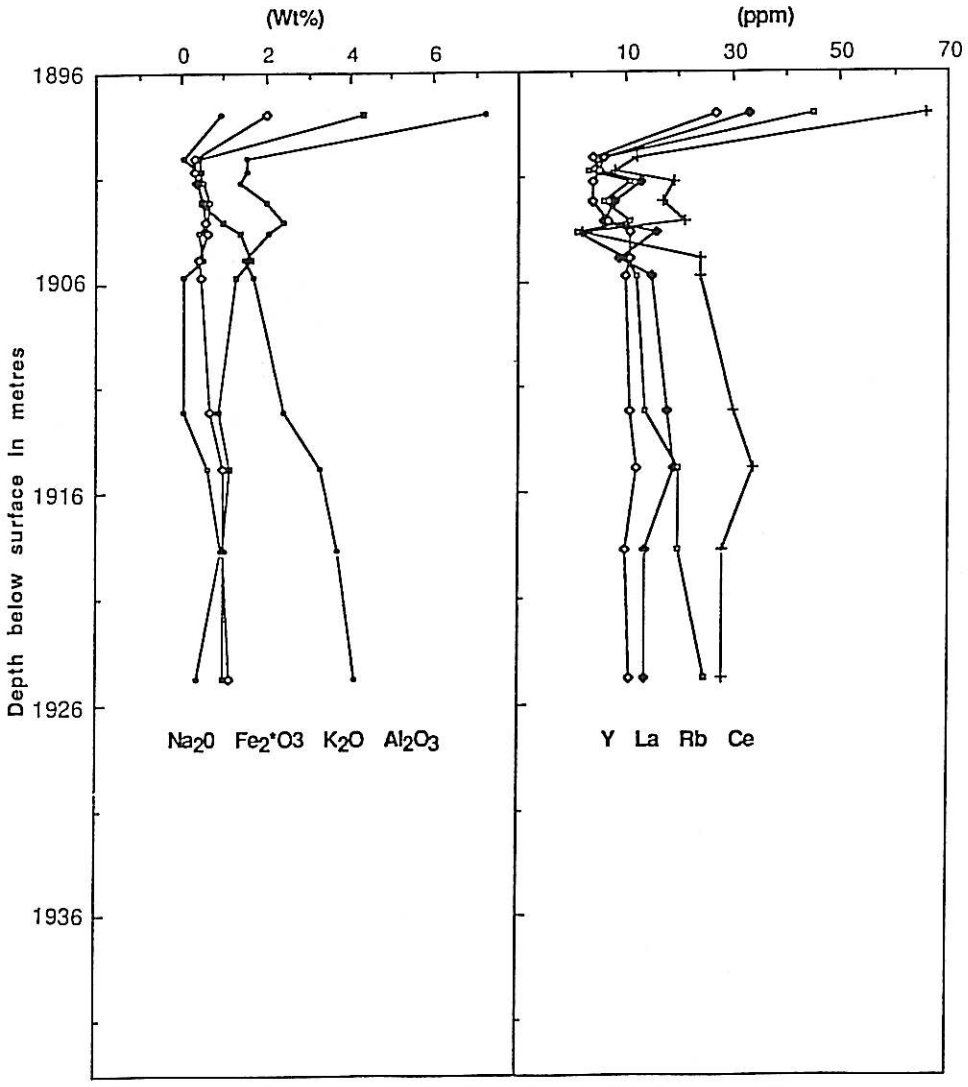


FIG. 9A. Variation in chemical composition and the concentration of major and trace elements in the Bahi Formation (A2-32 borehole). The uppermost (glauconite-bearing) part of the formation is represented by the uppermost sample.

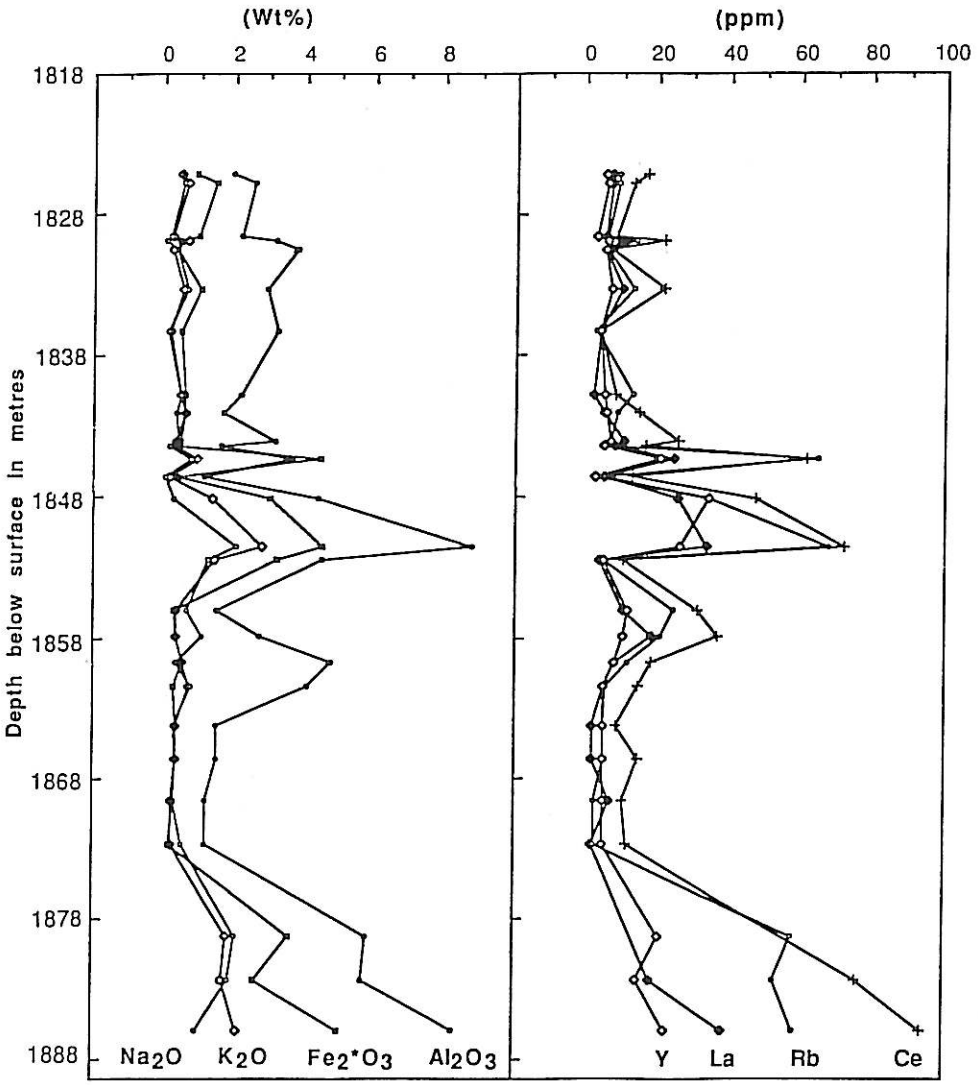


FIG. 9B. Variation in Chemical composition and the concentration of major and trace elements in the Bahi Formation (A4-32 borehole). The uppermost (glauconite-bearing) part of the formation is not represented.

change in the trace elements distribution particularly with respect to lanthanium, cerium, rubidium and yttrium, which show increasing concentration with reduction in grain size. In borehold F6-32, variation in major and trace elements is related to the low silica content and high CaO and MgO content particularly in the upper part of the section whereas the lower part is characterized by high silica content reflecting increase in quartz. This indicates a more mature sediment (Fig. 9C).

DISCRIMINANT FUNCTION ANALYSIS AND TECTONIC SETTINGS

In the past, several attempts have been made to use discriminant function analysis for sandstone geochemistry to classify individual sandstone samples into predefined groups on the basis of multiple variables in order to identify the tectonic setting of the provenance. Bhatia (1983) used discriminant function analysis to classify sandstone suites using eleven major element oxides as variables and chose five sandstone suites in eastern Australia to represent his predefined groups. Discriminant scores for the analysed Bahi samples from the four boreholes have been calculated using the unstandardised function coefficient (Bhatia, 1983), the results are plotted with respect to function I versus function II (Fig. 10).

All the studied samples in the Bahi Formation, from the four boreholes, fall into the passive margin field except for two samples from the F6-32 borehole which fall into oceanic island arc and one from the A4-32 and two from the D1-32 boreholes which fall into the active continental margin field. Passive margins are characterized by mineralogically mature sediments deposited in plate interiors, at stable

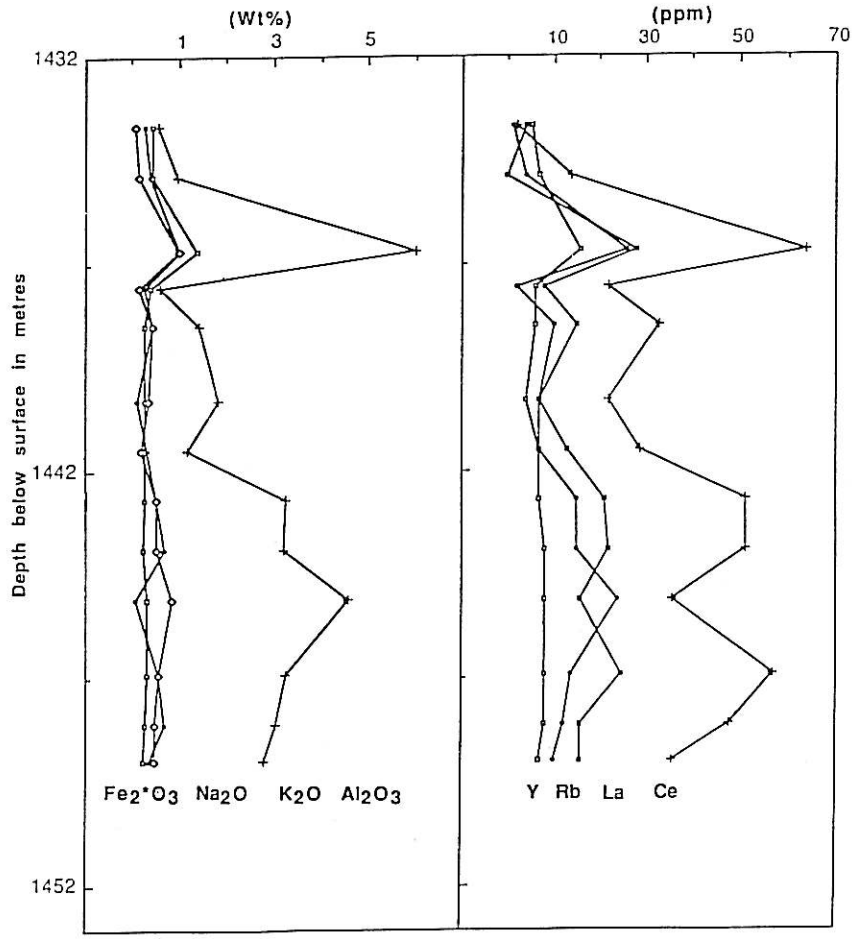


FIG. 9C. Variation in chemical composition and the concentration of major and trace elements in the Bahi Formation (F6-32 borehole). The uppermost (glauconite-bearing) part of the formation is not represented.

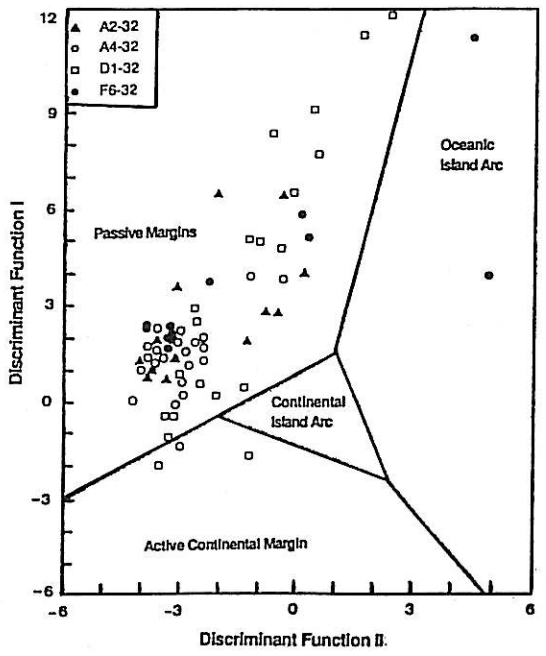


FIG. 10. Plot of discriminant scores along Function I versus Function II in the Bahi Formation in the four boreholes, using Bhatia's (1983) fields of various tectonic setting.

continental margins or in intracratonic basins. Derived sediments are characterized by recycled quartz-rich sediments originating in older adjacent continental terranes (Bhatia, 1983).

CONCLUSIONS

The significance of the major and trace element distribution within the Bahi Formation leads to the following conclusions:

The high amount of SiO_2 in most of the Bahi samples is considered to indicate a high degree of maturity. The low content of SiO_2, encountered in some samples, is probably due to enrichment of the sediment with carbonate, anhydrite and clay minerals. The variation of K_2O and Al_2O_3 is probably due to variation of feldspar and clay mineral content both laterally and vertically. The high content of CaO and MgO in some of the studied samples, particularly in the upper part of the formation, is related to enrichment with cement composed of varying proportions of calcite, dolomite and anhydrite.

Most of the trace elements (La, Rb, Ce, Zn, Ga and Y) show a positive correlation with Al_2O_3 and K_2O

but a lack of correlation with al-alk. This may be related to the presence of these trace elements in both K-feldspar and clay minerals. The relationships between Y + La + Ce, Ni + Cr and Sr, show that the Bahi sediment is derived primarily from a pre-existing sedimentary source.

Lateral and vertical distribution of the Bahi Formation show considerable variation in major and trace elements. This is related to specific lithofacies probably resulting from variation in the environmental conditions at the time of deposition of the unit. It is clear from the various geochemical plots that there is variation from boreholes involving clear correlation, particularly in boreholes D1-32 and A2-32, but which are not evident in boreoles A4-32 and F6-32. This implies slightly different depositional controls and local diagenetic variations.

The discriminant function analysis technique shows that the Bahi Formation is derived from a passive continental margin with a mature sandstone cover.

ACKNOWLEDGEMENT

I would like to express my thanks to Mr. M. Idris, General Manager of the Petroleum Research Centre for his encouragement to present this work, to the National Oil Corporation and Mr. R. Aburawi from Oasis Oil Company, Tripoli, Libya for providing the core samples. I am specially grateful to Prof. B.E. Leake from the Geology Department, Glasgow University, for his helpful support in clarifying many doubts and problems. I particularly wish to thank Dr. J.K. Ingham, who supervised this study for his help, interest, enthusiasm and continuous advice.

REFERENCES

Barr, F.T. and Weegar, A.A., 1972, Stratigraphic nomenclature of the Sirte Basin, Libya. Petrol. Explor. Soc. Libya, 179p.

Bhatia, M.R., 1983, Plate tectonics and geochemical composition of sandstones. J. Sedim. Petrol., Vol. 91, pp. 611–627.

Bhatia, M.R. and Crook, K.A.W., 1983, Trace element characteristics of gray wackers and tectonic setting discrimination of sedimentary basins. Contribs. Miner. Petrol., Vol. 92, pp. 181–193.

Fenner, P. and Hagner, A.F., 1967, Correlation of variations in trace elements and mineralogy of the Esopus Formation, Kingston, New York. Geochim. cosmochim. Acta., Vol. 31, pp. 237–261.

Harvey, P.K., Taylor, D.M., Hendry, R.D. and Bancroft, F., 1973, An accurate fusion method for the analysis of rocks and chemically related minerals by X-ray flourescence spectrometry. X-ray Spectrometry, pp. 33–44.

Hickman, A.H. and Wright, A.E., 1983, Geochemistry and chemostratigraphical correlation of slates, marbles and quartzites of the Appin Group, Argyll, Scotland. Trans. Roy. Soc. Edinb: Earth Sci., Vol. 73, pp. 251–278.

Leake, B.E. *et al.* (9 authors)., 1969, The chemical analysis of rock powders by automatic X-ray fluorescence. Chem. Geol., Vol. 5, pp. 7–86.

Loring, D.H., 1982, Geochemical factors controlling the accumulation and dispersal of heavy metals in the Bay of Fundy sediments, Can. J Earth Sci., Vol., 19, pp. 930—944.

Niggli, P., 1954, Rocks and mineral deposits, W.H. Freeman and Co. San Francisco, 559p.

Sghair, A.M., 1990, Stratigraphy, lithofacies and environmental analysis of the Bahi Formation in the northwestern Sirt basin, Libya. MSc Thesis, Geology Dept., Glasgow Univ., 171p.

Van de Kamp, P.C. and Leake, B.E., 1985, Petrography and geochemistry of feldspatic and mafic sediments of the northeastern Pacific margin. Trans. Roy. Soc. Edinb. Earth Sci., Vol. 76, pp. 411–449.

Wedepohl, K.H., (ed.), 1978, hand book of geochemistry. II/1-5. Springer-Verlage, New York.

PRJ, Vol. 4. (January 1992); P. 46–51, 3 FIGS, 4 TABLES

EVALUATION OF BENTONIC CLAYS OF UMM AR RIZAM AREA, LIBYA AS POTENTIAL DRILLING MUDS

D.M. Watson* and M. Rahuma*

تقييم طين البنتونيت بتكوين الفايدية منطقة أم الرزم ، ليبيا

ديفد واتسون وميلاد رحومة

يقع تكوين الفايدية الذي يرجع إلى العصر الأوليجوسيني والميوسيني الأوسط كأعلى الوحدات الصخرية بمنطقة درنة وطبرق. ويوجد عند قاعدة التكوين فوق تكوين الأبرق مباشرة طبقة من الطين. ويتكون هذا الطين من كميات متباينة من المونتموريلونيت وأنماط الطين الأخرى مع الجلوكونيت والجبس والجير والمعادن الأخرى. وقد تم التعرف على مستحاثات دقيقة في العديد من العينات كما إحتوت واحدة على أوستراكودات وأسنان سمك القرش وعجيرات وتبدلات عضوية من معادن الفوسفات.

وتتباين الصفات الطبيعية لخلطات مختلفة من الماء والطين من عينة إلى أخرى. وتتصرف الخلطات المختلفة كسوائل لدائنية كاذبة ، بالإضافة إلى أن لها المواصفات المطلوبة في سوائل الحفر. غير أن هذه المواصفات تختلف من مكان لآخر كما تختلف عمودياً بالقطاع. وعموماً فإن عينات الجزء السفلي من القطاع لها مواصفات أفضل من نصف القطاع العلوي.

وقد كان للطين المعد من العينات مواصفات تقدر بحوالي 25 متر مكعب/للطن ولزوجة تصل إلى 73 سنتبويز. وقد تم أيضاً التعرض لنتائج تجارب إستعمال الصودا الكاوية ، CMC للتحكم في فاقد التصفية واللزوجة.

ABSTRACT

The Upper Oligocene-Middle Miocene Al Faidiyah Formation occurs as the uppermost unit in the Darnah-Tubruq area. At the base of this unit, immediately above the underlying Al Abraq Formation, is a layer of clay. This clay unit is composed of varying amounts of montmorillonite and other clays, along with glauconite, gypsum, carbonates, and other minor minerals. In several samples, microfossils have been identified, while another contains ostracods, sharks' teeth and nodules and pseudomorphs of phosphate minerals.

The physical properties of muds made up of varying amounts of this clay with water vary from sample to sample. The different mixtures behave as pseudo-plastic fluids, and show many of the required properties of drilling fluids. Their properties do, however, vary from place to place, and vertically within the section. Samples from the lower parts of the section generally have better properties than those from the upper half.

Muds have been prepared from the samples having yields as high as 25 m^3/tonne, and viscosities as high as 73 centipoises. Results of tests using caustic soda and Carboxy-Methyl-Cellulose (CMC) to control filter loss and viscosity are also reported.

INTRODUCTION

The Umm ar Rizam clay project was initiated by the Exploration Department of the Petroleum Research Centre, Tripoli, in 1981. The aim of the project is to identify resources of bentonitic material that could be used as drilling mud, thus replacing expensive foreign imports. The use of domestic muds could result in a saving of 2.5 million dinars (or foreign currency equivalent) per year in the cost of bentonite alone.

*Petroleum Research Centre, P.O. Box 6431, Tripoli, G.S.P.L.A.J.

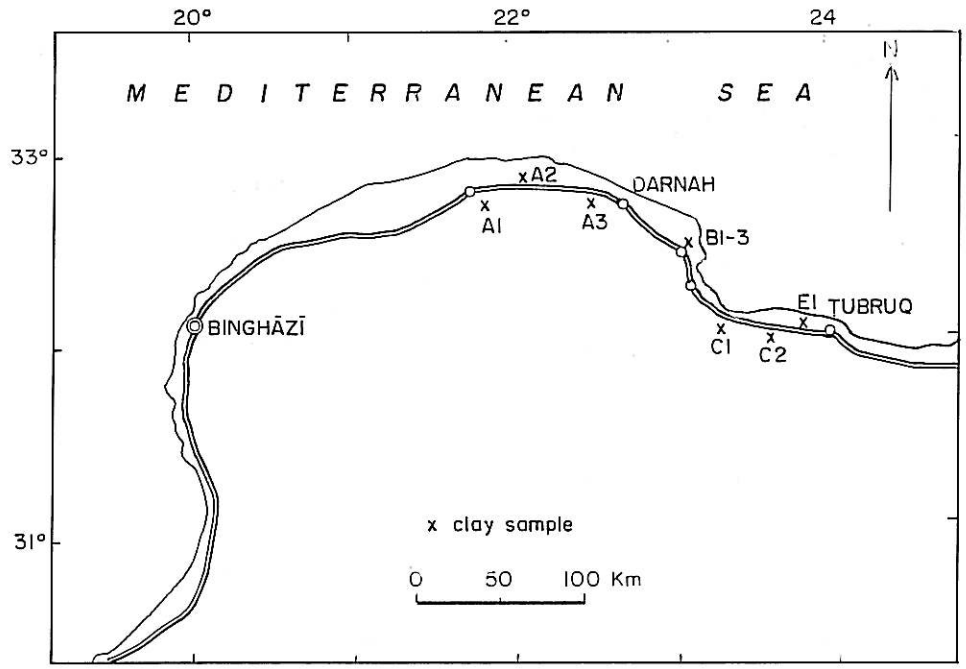


FIG. 1. Clay sample locations (1981).

Early work by Alami *et al.* (1981) (Fig. 1), Gent (1985) and others of the Petroleum Reseach Centre, consisted of searching existing maps and files from all available sources for reference to montmorillonitic clays or bentonite, and later, sampling several of the areas of interest. The result of this early work was encouraging in that, in the Umm ar Rizam area, some samples collected in the first phases proved to have properties approaching those of commercial bentonite. Follow up work resulted in the collection of additional samples from this area, some of which again gave encouraging results.

In the most recent phase of this project, carried out by present authors, more detailed sampling was done in the immediate vicinity of Umm ar Rizam (Fig. 2), along with extensive testing of the various clays collected. It is the result of this sampling and testing programme that are reported in this paper.

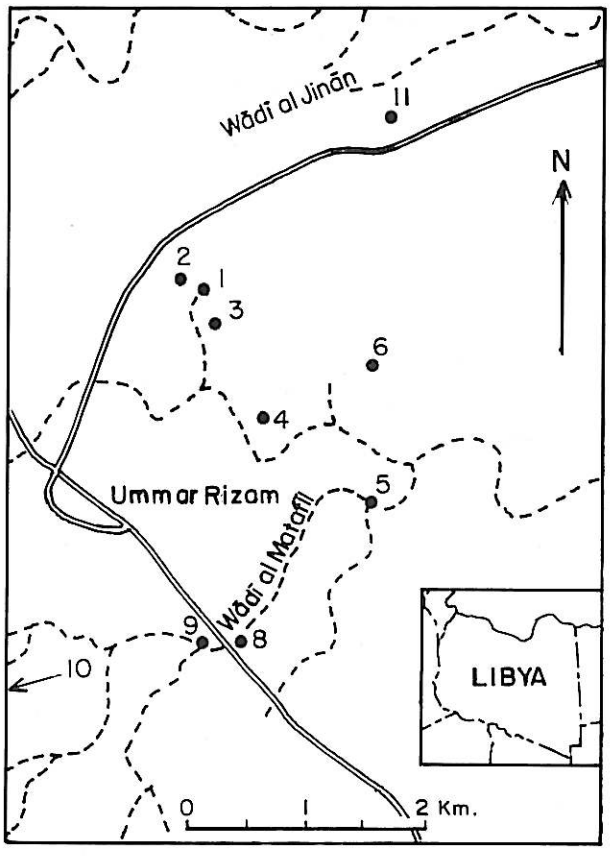


FIG. 2. Location of sampled sections (1986).

LOCATION AND ACCESS

The area of main interest in this study is centered on the village of Umm ar Rizam, approximately 60 Km SE of Darnah, and 120 Km NW of Tubruq. It is connected to both of these larger centres by a first class paved highway. A secondary paved road connects the main highway with the coast approximately 30 Km to the east. Access off the main road is either by secondary paved highway or by desert tracks, which although not maintained are good enough to allow access to virtually any area. The land surface is mainly bare stony desert devoid of vegetation aside from scattered palms and thorn bushes. Some shrubs are present in the bottoms of wadis and in areas irrigated for agricultural purposes. The wadis are generally narrow and very steep sided. They are

usually not driveable along their length, and can be very difficult to cross. Any cross-country driving must take these obstacles into account. The desert surface itself is hard and relatively smooth and conditions are such that materials and equipment can be delivered to virtually any area.

GENERAL GEOLOGY

The Darnah map sheet, on which the area of interest lies, is covered by rocks of Eocene to Middle Miocene age. The formations exposed are, in order of age, the Appolonia, Darnah, Al Bayda, Al Abraq and Al Faidiyah. They all consist of sequences of limestones, marls and siltstones, with minor amounts of dolomite (Zert, 1974).

Al Faidiyah Formation, the youngest formation on the map sheet, is the unit of interest in this study. It is a transgressive unit, bound on the lower part by a discontinuity with Al Abraq Formation. This discontinuity is marked by a bed of clay ranging in thickness from 2 to 20 metres. In the eastern and central areas of the sheet, this clay layer is montmorillonitic, and probably developed as an extensive shallow marine deposit. The montmorillonitic clay is largely devoid of macrofossils. The more marly layers immediately above and below this layer contain abundant pectens and oysters. The age of this unit has been placed as beginning at the Upper Oligocene. Al Faidiyah Formation itself continues in age to the Middle Miocene.

GEOLOGY OF THE UMM AR RIZAM CLAYS

In the area of Umm ar Rizam, the youngest unit exposed is of course the Al Faidiyah Formation. It overlies Al Abraq calcarenite. Over the area examined in this study, Al Abraq limestone was the lowermost unit seen. The limestone consists of a yellow to cream calcarenite containing abundant pelecypod, echinoid and oyster shells. In places the rock could more correctly be called bioclastic. The facies developed is typical of shallow-water shelf seas (Zert, 1974).

Immediately above Al Abraq Formation and separated from it by a discontinuity, is the bentonitic clay, representing the basal portion of Al Faidiyah Formation. In the immediate vicinity of Umm ar Rizam, Al Faidiyah Formation consists of a few metres of blocky to rubbly limestone covering the clay unit. The limestone directly on top of this clay layer is fossiliferous, and contains abundant shells of *Cardium* and *Ostrea*. Remains of corals and echinoids are also plentiful in some sections.

Beneath this fossiliferous layer, and visible only in wadi banks and the sides of depressions, is usually a layer 0.5 m thick composed mainly of glauconite pellets. These pellets range in size up to 0.5 mm in diameter, and make up 90% of the rock. The remainder is clay and occasional gypsum and carbonate.

The boundary between the glauconitic layer and the underlying clay is sharp, with no glauconite appearing mixed with the lower layer. The main clay layer varies in apparent thickness from 5 to more than 20 metres. Due to its position in the sides of wadis, the exposure is limited due to slumping of the overlying limestone, and the thicknesses are in part estimates. This clay layer usually contains more than 98% clay minerals. The remaining 2% is made up of gypsum, phosphate pellets, carbonate minerals (calcite and dolomite) and occasional opaque grains. Upon dispersion in a water and methaphosphate solution (as for API residue test), less than 1% is usually left on a 200 mesh screen. In most cases this residue is undispersed clay, but in a few samples, there are some microfossils and phosphate pellets.

Some samples collected from the near surface contain up to 10% gypsum in the form of single crystals and aggregates to 10 cm diameter. These accumulations disappear completely at depths of 0.3–0.5 m. Their appearance in some samples is attributed to evaporation and subsequent crystallization from recent ground waters.

The clay has been examined by a number of methods. Chemically it fits under the broad definition of a mixed layer clay (Table 1).

Table 1. Chemical Analysis of Umm ar Rizam and Other Clays

	Illite*	Montmorillonite*	Umm ar Rizam Clay**
SiO_2	46–57	51–65	53.9
Al_2O_3	19–31	15–34	24.9
Fe_2O_3	4–7	0–15	6.6
MgO	1–3	0.1–7	2.8
CaO	0.2–2	0–4	1.7
Na_2O	0.2–0.6	0–4	1.0
K_2O	4–6	0–2	0.32
H_2O^+	6–8	5–14	8.8

*From Weaver and Pollard (1975).
**Average of 7 analyses.

Table 2. Cation Exchange Capacities of Some Clays

Clay	Cation Exchange Capacity in ME 12/100 gr Dry Clay
Montmorillonite	70–130
Vermiculite	100–200
Illite	10–40
Kaolinite	3–15
Chlorite	10–40
Attapulgite	10–35
Umm ar Rizam (avg of 7)	84.0 ± 8.1

After Gray and Darley, 1980.

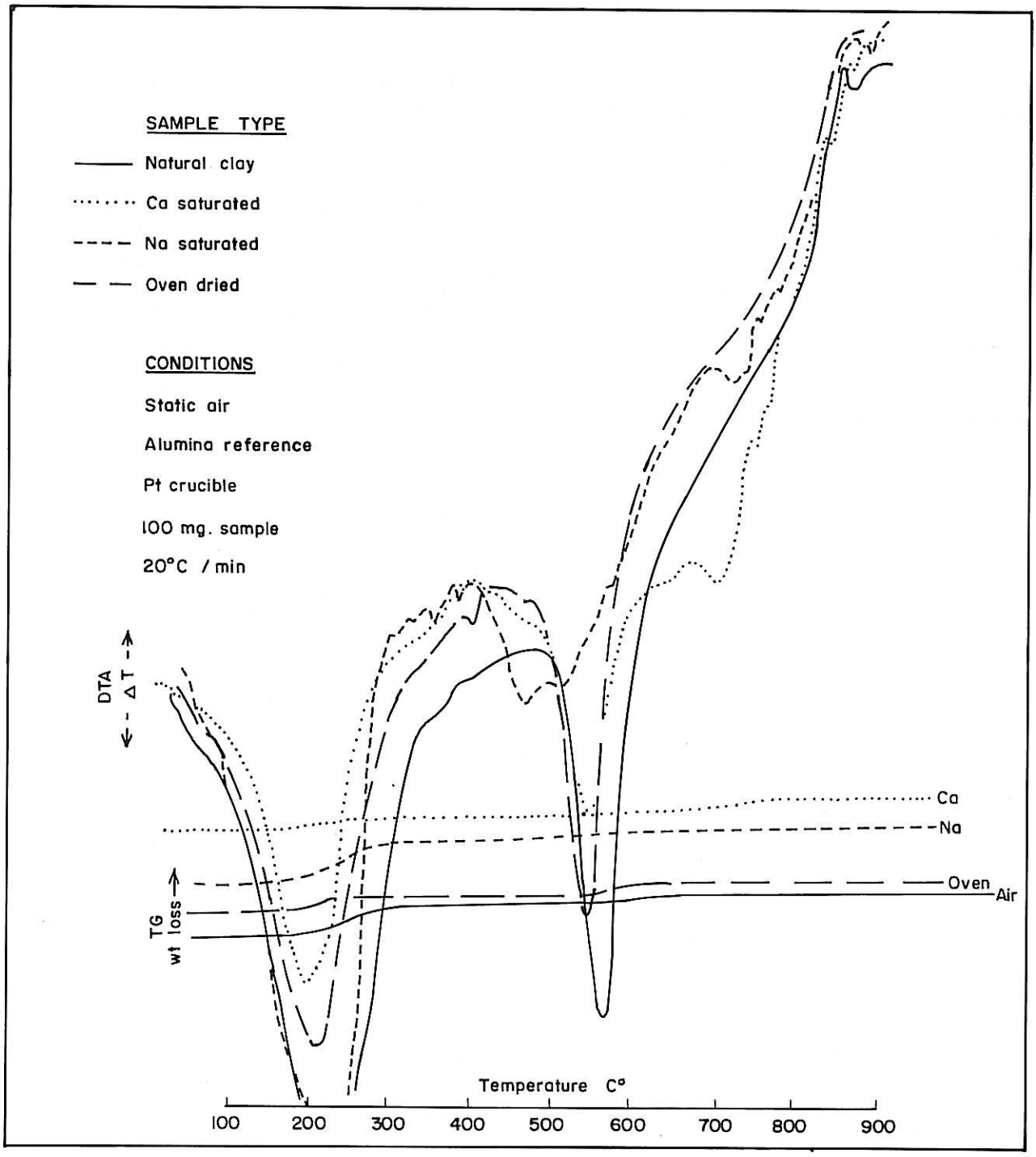


FIG. 3. DTA-TG curves-natural and treated clays.

Under the microscope it is devoid of any visible structure, with no recognizable crystals or form even to the limits of resolution of the SEM. Curves obtained by DTA-TGA (Fig. 3) are typically montmorillonite, although falling between calcium and sodium varieties in character. As may be seen in the following description of the mud-making characteristics, these too fall between the properties of calcium and sodium varieties, or between poor mud and good.

The cation exchange capacity (CEC) of the clay was determined using sodium as an index ion. The values obtained for several samples all fall within the range of values normally accepted for montmorillonite. The determined values are given in Table 2, along with values for various clay minerals.

MUD TESTING

While the chemistry of clay, along with its many other physical properties is important, it is the actual mud-making properties that are of importance to the well drilling industry. The muds made from the clay and water must have the right combinations of gel strength, viscosity and density in order to perform as necessary. In addition, a certain amount of clay must yield at least a minimum amount of mud in order to be economical.

These properties vary with the amount of clay used in the mud as well as with the type of clay. Larger amounts of clay increase the viscosity, but may also increase the mud cake thickness and have a less than desirable effect on another properties. The properties usually tested, and their recommended values are given in Table 3.

In order to evaluate the performance of the Umm ar Rizam clays as drilling mud additives, a series of standard tests were performed. These tests, carried out using API recommended methods, included measurement of apparent viscosity with a standard Fann VG meter, and filtrate loss using a standard filter press. The results of some of the tests along with the recommended values are given in Table 3.

In addition to the tests performed on the muds as collected, several additional tests were carried out to determine the effects of additives on the muds and to see if marginal materials could be upgraded at reasonable cost to make acceptable muds. These tests showed that additions of CMC soda ash and NaOH could alter the filter loss and viscosity sufficiently to make almost any of the clays tested acceptable for drilling muds. The results of these tests are summarized in Table 4.

Table 3. Physical (Mud) Properties of Clay/Water Mixtures

Sample	Apparent* Viscosity cp	Plastic* Viscosity cp	Yield m^3/tonne	Filtrate* Loss cc/30 min
API/OCMA Recommended	15 (min)	–	15 (min)	15 (max)
1a	9.5	3	13.6	27.2
1b	4	3	–	n.d.
1c	5.25	3.5	–	n.d.
1d	14	4	16.53	25.5
3	10	3	13.4	21.0
4	4.5	3	–	n.d.
6a	7.5	3	11.9	33.3
6b	9.5	6	12.0	29.0
6c	5	3	–	n.d.
6d	3.5	3	–	n.d.
6e	14	6	–	33.7
6f	18.75	6.5	18.6	32.2
8	12	4	15.8	20.3
9	9	3.5	11.3	n.d.
10	8	4	12.9	42.0
11	3.5	2	–	n.d.
12	31	7	25.4	30.0

*For 6% clay/water muds.
n.d. Not done.

Table 4. Effect of Additives on Filtrate Loss and Viscosity

	Sample 12		Sample 6a	
Test No.	Additive	Filtrate loss (cc/30 min)	Additive	Viscosity (cp)
A	Nil	36	Nil	9.5
B	0.1% CMC	20.5	0.1% NaOH	12.3
C	0.15% CMC	19	0.2% NaOH	14
D	0.2% CMC	15.5	0.3% NaOH	20
E	0.5% CMC	12.3	0.5% NaOH	29
F	1.0% CMC	9.5	1.0% NaOH	38

As can be seen from Table 4, several of the muds have sufficient viscosities and yields to be used as drilling muds. The filter losses are high but additions of CMC can reduce this loss to acceptable levels (Table 4).

CONCLUSIONS AND SUMMARY

The bentonitic beds of Al Faidiyah Formation in the area of Umm ar Rizam can be used to prepare drilling muds that pass the tests for viscosity and yield. Their properties can be upgraded by additions of small amounts of CMC in order to pass the requirements for filter loss.

The bentonite is found as a bed of varying thickness (2–20 m) over a very wide area. It appears at this time from the amount of field work done that the mud-making properties vary from place to place, but are reasonably consistent over the sort of distances that would be of concern to a mining operation. Likewise the thickness while variable is reasonably consistent over short distances.

Using an average thickness of 5 m of mineable bentonite, it has been calculated that there would be approximately a 750-year supply of bentonite per square kilometre in the Umm ar Rizam area, enough to supply Libya's needs for the foreseeable future.

ACKNOWLEDGEMENTS

The authors would like to acknowledge the support of Mr. M. Massaud and the Management of the Petroleum Research Centre.

REFERENCES

Alami, M., Rehoma, S. and Salem, G., 1981, Bentonitic clay of Al Jabal Al Akhdar, Unpublished Rep., Petrol. Res. Cent., Tripoli, 33p.

American Petroleum Institute, 1984, Specification for Oil Well Drilling Fluid Materials. API RP13A, Dallas.

Gent, M., 1985, Bentonite Project Field Trip, Unpublished Rep., Petrol. Res. Cent., Tripoli, 23p.

Gray, G.R. and Darley, H.C.H., 1980, Composition and Properties of Oil Well Drilling Fluids, 4th Ed. Gulf Publishing Company, Houston.

Weaver, C.E. and Pollard, L.D., 1975, The Chemistry of Clay Minerals Developments in Sedimentology, Elsevier.

Zert, B., 1974, Geological Map of Libya; 1:250,000. Sheet Darnah (NI34-16). Ind. Res. Cent., Tripoli, 49p.

Zomlut, R., 1985, Chemical Evaluation of Umm ar Razam Clay Deposits as a bentonite, Unpublished Rep., Petrol. Res. Cent., Tripoli, 27p.

PRJ, Vol. 4. (January 1992); P. 52–55, 3 FIGS, 6 TABLES.

KINETICS OF ORTHOVANADATE CATALYSED EPOXIDATION OF MALEIC ANHYDRIDE BY HYDROGEN PEROXIDE

I. Ahmad* and M. Degam*

حركية تفاعل الماليك إنهيدرايد مع فوق أكسيد الهيدروجين في وجود الأورثوفانيدات كعامل حفاز

إفتخار أحمد ومسعود دغيم

تم دراسة حركية وميكانيكية تحويل الماليك أنهيدرايد إلى أيبوكسيد الهيدروجين في وجود أورثوفانيدات الصوديوم كعامل حفاز.
كان التفاعل من الدرجة الأولى بالنسبة إلى الماليك إنهيدرايد والعامل المساعد وكان من الدرجة الصفر بالنسبة إلى فوق أكسيد الهيدروجين.
كما تم حساب طاقة التنشيط فكانت 68.93 ك جول/مول.

ABSTRACT

The kinetics and mechanism of epoxidation of maleic anhydride by hydrogen peroxide in the presence of sodium orthovanadate as catalyst have been studied. The reaction was found to be first order with respect to maleic anhydride and catalyst and zero order with respect to hydrogen peroxide. Based on substituent, solvent and salt effects the mechanism of epoxidation step is believed to be concerted with considerable polar (electrophilic) character. The energy of activation has been calculated to be 69.93 KJ mol^{-1}.

INTRODUCTION

Maleic anhydride is a compound which can be produced by the oxidation of butane, butenes or benzene [1]. The value of maleic anhydride can be increased by converting it to its epoxide. The epoxy of maleic anhydride should be of potential commercial interest because of its easy conversion into tin epoxysuccinates which are important plasticizer-stabilizers of polyvinil chlorides [2] as well as for cross linkable epoxy containing film forming polyamides [3]. Although organic peracids [4] are generally used for the epoxidation of alkenes, compounds having strong electron-withdrawing substituents adjacent to the double bonds are not readily epoxidised by them [5]. Recently hydroperoxides [6–10] are being used for the epoxidation of such alkenes, but these are limited to only nonaqueous medium. In these cases hydroperoxide metal [V(V), Mo(VI) and W(VI)] complexes [8–10] bring about epoxidation through metal-hydroperoxide-olefin complexes, whereas aqueous hydrogen peroxide in the presence of tungstate or molybdate epoxidises through peroxyacid [11–13]. More recently we have studied [14, 15] the catalytic activities of tungstate and molybdate ions on the epoxidation of maleic anhydride by hydrogen peroxide. This paper presents kinetic study of the epoxidation of maleic anhydride by hydrogen peroxide in the presence of sodium orthovanadate as catalyst.

*Petroleum Research Centre, P.O. Box 6431, Tripoli, G.S.P.L.A.J.

EXPERIMENTAL

All the chemicals used were the analar (B.D.H.) grade. Maleic anhydride was standardised using bromate-bromide procedure [16] and hydrogen peroxide was standardised by permanganate method [17]. The ionic strength of the reaction mixture was maintained by the addition of sodium perchlorate. The pH of the reaction mixture was adjusted by perchloric acid on the lower side and that on the upper side by triethanolamine.

The kinetics of the reaction was followed by monitoring the concentration of hydrogen peroxyde which is measured colorimetrically described elsewhere [18]. Every run was followed until reaction was at least 90% complete. After the reactants had reached thermostat temperature, the reaction was started by addition of hydrogen peroxide. The kinetics were followed by examining 5 ml aliquots of the reaction mixture for hydrogen peroxide content. The aliquots were added to 5 ml titanium sulphate solution to stop the reaction. Optical density was measured at 420 nm and the concentration of hydrogen peroxide was read from a calibration graph. The catalyst concentration was too small to affect the colorimetric estimation of hydrogen peroxide.

The epoxysuccinic acid formed in this reaction was measured quantitatively by the pyridinium chloride-pyridine method [19]. Instead of methanolic sodium hydroxide, an aqueous solution was used for titration. No tartaric acid was detected in the reaction mixture above pH 6.0. However, below pH 6.0, the test of tartaric acid [20] was positive.

RESULTS AND DISCUSSION

The progress of the reaction was followed by examining the concentration of hydrogen peroxide at different time intervals. Trial and error plots of the rate data for runs with excess maleic anhydride concentration indicate that the reaction is zero order in hydrogen peroxide. The plots of concentration of hydrogen peroxide versus time were good straight lines and their slope yields K_{obsd}. The calculated k_{obsd} were found to be independent of the concentration of hydrogen peroxide. The results are reported in Table 1. The standard deviation of K_{obsd} is 0.01.

The order of reaction with respect to sodium orthovanadate (Na_3VO_4) was determined by varying its concentration and keeping other variables constant. The plot of k_{obsd} against the concentration of sodium orthovanadate was a straight line (Fig. 1). This confirms first order dependence of rate on

Table 1. Pseudo-Zero-Order Rate for Vanadate Catalysed Epoxidation of Maleic Anhydride by Hydrogen Peroxide

$[H_2O_2] \times 10^3$ (M)	$K_{obsd} \times 10^7$ (mol dm^{-3} sec^{-1})
2.00	6.19
2.50	6.20
3.00	6.22
3.50	6.19
4.00	6.21
4.50	6.20
5.00	6.18

[MA] = 0.20 M; $[Na_3VO_4] = 5.00 \times 10^{-4}$ M; pH, 6.0; Temp., 50°C

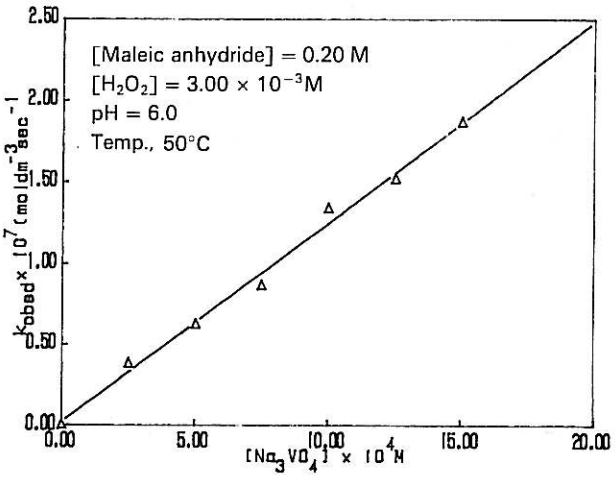


FIG. 1. First order dependence of rate on sodium orthovanadate concentration.

sodium orthovanadate concentration. The plot of k_{obsd} versus concentration of sodium orthovanadate passes through the origin which shows that there is no reaction in the absence of sodium orthovanadate. Similarly, the dependence of rate on maleic anhydride concentration was determined by varying its concentration and keeping all other variables constant. k_{obsd} thus found were directly proportional to the concentration of maleic anhydride (Table 2). This shows first order dependence of rate on maleic anhydride concentration.

Preliminary studies have shown that under our experimental conditions, hydrogen peroxide does not ring about epoxidation of maleic anhydride without sodium orthovanadate alone (without hydrogen peroxide) fails to bring about the epoxidation. This clearly suggests the involvment of some more oxygenated form of vanadium in the process as oxygen carrier. Jander and Jahr [21] have shown that in the acidic medium, orthovanadate changes into vanadium pentoxide, which according to Flood and co-workers [22] dissolves in aqueous hydrogen peroxide giving peroxyvanadic acid. It is thus presumed here that in the system under investigation, peroxyvanadic acid is the epoxidising species and in a

Table 2. First Order Dependence of Rate on Maleic Anhydride Concentration

$[MA] \times 10^2$ (M)	$k_{obsd} \times 10^7$ (mol dm^{-3} sec^{-1})	$\frac{k_{obsd}}{[MA]} \times 10^5$
20.00	6.22	0.311
30.00	9.33	0.311
40.00	12.40	0.310
50.00	15.61	0.312
60.00	18.62	0.310

$[H_2O_2] = 3.00 \times 10^{-3}$ M; $[Na_3VO_4] = 5.00 \times 10^{-4}$ M; pH, 6.0; Temp., 50°C.

rate controlling step it reacts with the unsaturated acids giving epoxysuccinic acid and regenerating vanadic acid. Vanadic acid is then reconverted into peroxyvanadic acid by hydrogen peroxide. The following seems to be the most probable mechanism:

$$H_3VO_5 \overset{K_1}{\rightleftharpoons} H_2VO_5^- + H^+ \quad (1)$$

$$\text{where, } k_1 = \frac{[H_2VO_5^-][H^+]}{[H_3VO_5]} \quad (2)$$

$$MA + H_3VO_5 \underset{K_{-2}}{\overset{K_2}{\rightleftharpoons}} \text{(intermediate complex)} \quad (3)$$

$$\text{(intermediate complex)} \xrightarrow{k_3} MAE + H_3VO_4 \quad (4)$$

MA and *MAE* are maleic anhydride and maleic anhydride epoxide, respectively.

Assuming steady-state approximation for the complex formation.

$$\text{epoxidation rate} = k'[MA][H_3VO_5] \quad (5)$$

$$\text{where, } k' = \frac{k_2k_3}{k_{-2}+k_3}$$

The catalyst (Na_3VO_4), at any stage in the process, is distributed in three forms according to eqn. (6),

$$[Na_3VO_4] = [H_3VO_5] + [H_2VO_5^-] + [\text{intermediate complex}] \quad (6)$$

The concentration of intermediate complex in eqn. (6) is negligible in comparison to other terms of eqn. (6). Hence,

$$[Na_3VO_4] = [H_3VO_5) + [H_2VO_5^-] \quad (7)$$

Substituting for $[H_3VO_5]$ from eqn. (2) and (7) in eqn. (5), we get,

$$\text{epoxidation rate} = \frac{k'[H^+][Na_3VO_4][MA]}{K_1 + [H^+]} \quad (8)$$

$$\text{or epoxidation rate} = k_{obsd} \quad (9)$$

Here,

$$k_{obsd} = \frac{k'[H^+][Na_3VO_4][MA]}{k_1 + [H^+]} \quad (10)$$

Eqn. (8) explains the observed order of reaction with respect to maleic anhydride, sodium orthovanadate and hydrogen peroxide. The results of variation of epoxidation rate with pH are shown in Table 3. The straight line plot (Fig. 2) between inverse of k_{obsd} and inverse of $[H^+]$ is in agreement with eqn. (10).

Table 3. Dependence of Rate on pH of the Medium

pH	$\frac{1}{[H^+]}$ (dm^3 mol^{-1})	$k_{obsd} \times 10^7$ (mol dm^{-3} sec^{-1})	$\frac{1}{k_{obsd}} \times 10^{-7}$
5.0	1.00×10^5	8.37	0.12
5.5	3.16×10^5	7.14	0.14
6.0	1.00×10^6	6.22	0.16
6.5	3.16×10^6	4.26	0.23
7.0	1.00×10^7	2.40	0.42

$[H_2O_2] = 3.00 \times 10^{-3}$ M; $[Na_3VO_4] = 5.00 \times 10^{-4}$ M; [MA] = 0.20 M; Temp., 50°C.

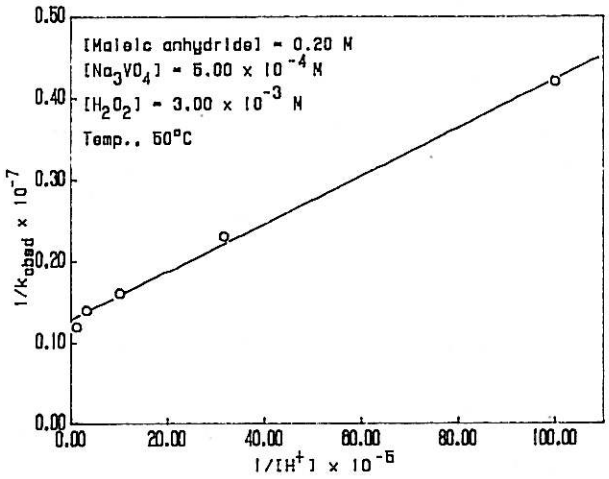


FIG. 2. Plot of inverse of k_{obs} against inverse of hydrogen ion concentration.

Increase in ionic strength did not affect the epoxidation rate (Table 4). The epoxidation rate of citraconic anhydride was performed under the same conditions as for maleic anhydride given in Table 1. In place of 0.20 M maleic anhydride citraconic acid of the same concentration was used to observe the substituent effect. The average value of k_{obsd} was found to be 7.35×10^{-7} mol dm^{-3} sec^{-1}. The faster epoxidation rate of citraconic anhydride as compared to that of maleic anhydride under identical

Table 4. Dependence of Vanadate-Catalysed Epoxidation Rate of Maleic Anhydride on Ion Strength of the Medium

Ionic Strength $\mu \times 10^4$ M	$k_{obsd} \times 10^7$ (mol dm^{-3} sec^{-1})
40.00	6.22
50.00	6.18
60.00	6.23
70.00	6.20
80.00	6.22
90.00	6.21
100.00	6.23

$[H_2O_2] = 3.00 \times 10^{-3}$ M;
$[Na_3VO_4] = 5.00 \times 10^{-4}$ M;
[MA] = 0.20 M; pH, 6.0; Temp., 50°C.

conditions shows that the presence of methyl group at the double bond is rate enhancing. This points to an electrophilic addition which is generally observed in the corresponding reaction of olefins with organic peracids and in other three-centre-type additions [23, 24]. The epoxidation rate decreases (Table 5) as the percentage of water in alcohol-water mixture decreased (dielectric constant lowered) but no linear relation between epoxidation rate and dielectric constant was obtained. Solvent and salt effects described above give an insight into the nature of the transition state of the oxygen transfer from the peracids to the double bonds of the olefinic substrate as described elsewhere [25].

The reaction was studied at six different temperatures ranging from 35°C to 60°C, and the results are given in Table 6. The plots of log k_{obsd} against reciprocal of temperature gave a straight line. The energy of activation was calculated from the slope of this plot to e 68.93 kJ mol^{-1}.

Table 5. Dependence of Vanadate-Catalysed Epoxidation Rate of Maleic Anhydride in Ethanol-Water Mixture on the Composition of the Solvent

% of ethanol	Dielectric Constant	$k_{obsd} \times 10^7$ (mol dm^{-3} sec^{-1})
0	78.5	6.22
15.4	69.5	5.89
31.5	60.0	5.31
50.0		4.65

$[MA] = 0.20$ M; $[Na_3VO_4] = 5.00 \times 10^{-4}$ M; $[H_2O_2] = 3.00 \times 10^{-3}$ M; Temp., 50°C; pH = 6.0.

Table 6. Effect of Temperature on Epoxidation Rate

Temperature (K)	$\frac{1}{T} \times 10^3$	$k_{obsd} \times 10^7$ (mol dm^{-3} sec^{-1})	$7 + \log k_{obsd}$
333	3.00	25.88	1.4130
328	3.05	17.78	1.2499
323	3.10	13.40	1.1271
318	3.14	7.08	0.8500
313	3.19	4.76	0.6776
308	3.25	3.33	0.5224

$[MA] = 0.20$ M; $[Na_3VO_4] = 10.00 \times 10^{-4}$ M; $[H_2O_2] = 3.00 \times 10^{-3}$ M; pH = 6.0.

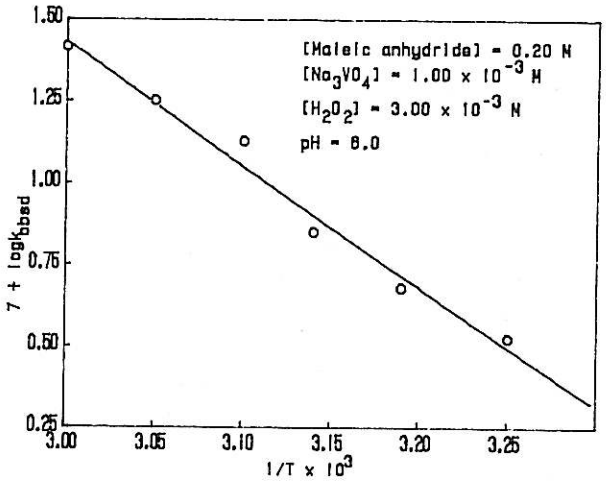


FIG. 3. Plot of log k_{obs} vs. reciprocal of absolute temperature.

ACKNOWLEDGEMENT

The authors are thankful to the Management of the Petroleum Reseach Centre for providing facilities to conduct this work.

REFERENCES

[1] Lowenheim, F.A. and Moran, M.K., 1975, Industrial Chemicals, 4th ed., John Wiley and Sons, 514–518.
[2] Bavley, A. and Knuth, C.J., 1961, U.S. Patent, 2972595, Feb. 21.
[3] Campbell, T.W. and McDonald, R.N., 1963, J. Polymer Sci., Part A1, 2525.
[4] Swern, D., 1949, Chem. Rev., **45**, 1.
[5] Payne, G.B., 1959, Fifth Petroleum Congress Proceedings, New York, Section IV, Paper 16, p. 185.
[6] Johsberger, T., Miller, D., Herman, F. and Indicator, N., 1971, J. Org. Chem, **36**, 4078.
[7] Howe, G.R. and Hiatt, R.R., 1971, J. Org. Chem., **36**, 2493.
[8] Sheng, M.N. and Zajacek, J.G., 1968, Adv. Chem, Ser., **76**, 418.
[9] Su, C., Reed, J.W. and Gould, E.S., 1973, Inorg. Chem., **12**, 337.
[10] Gould, E.S., Hiatt, R.R. and Irwin, K.C., 1968, J. Amer. Chem. Soc., **90**, 4573.
[11] Raciszewski, Z., 1960, J. Amer. Chem. Soc., **82**, 1267.
[12] Sapunov, V.N. and Lebedev, N.N., 1966, Zh. Org. Khim., **2**, 273.
[13] Beg, M.A. and Ahmad, I., 1975, J. Catal., **39**, 260.
[14] Ahmad, I., Tumi, S.O., Bashish, M. and ElAbib, A.R., 1989, Hyd. Proc., 51.
[15] Ahmad, I., Degam, M and Labib., 1991, Pet. Res. J., **3**, 53.
[16] Lucas, H.J. and Pressman, D., 1938, Ind. Engg. Chem., Anal. Ed., **10**, 140.
[17] Kolthoff, I.M., Sandell, E.B., Meehan, E.J. and Stanley, B., 1969, in "Qualitative Chemical Analysis", pp. 834, Macmillan Co. Collier Macmillan Ltd., London.
[18] Reichert, J.S., McNeight, S.A. and Rudel, H.W., 1939, Ind. Engg. Chem., Anal. Ed., **11**, 194.
[19] Jungnickel, J.L., Peters, E.D., Polgar, A., Weiss, F.T., Proskauer, E.S. and Weissberger, A., 1953, Organic Analysis, Wiley (Interscience), New York, Vol. I, pp. 136.
[20] Perkin, M.F., 1924, "Qualitative Chemical Analysis", Longmans, Green and Co., New York, N.Y., pp. 219.
[21] Remy, H., 1956, in "Treatise in Inorganic Chemistry", Elsevier, Amsterdam, Vol. II, pp. 100.
[22] Flood, P., Lewis, T.J. and Richards, D.H., 1963, J. Chem. Soc. 5024.
[23] Swern, D., 1957, Org. React., **7**, 378.
[24] Skell, P. and Garner, A., 1956, J. Amer. Chem. Soc., **78**, 5430.
[25] Allan, G.G. and Neogi, A.N., 1970, **19**, 256.

PRJ, Vol. 4. (January 1992); P. 56–58, 2 FIGS, 2 TABLES.

CHARACTERIZATION OF METHANOL-UTILIZING BACTERIA AND YEAST AS A SINGLE CELL PROTEIN PRODUCT

M. Bushwereb* A. Al-Misuraty* and S. Al-Jelani*

تقييم الخميرة والبكتريا (النامية على الميثانول) كمصدر لبروتين وحيد الخلية

مجاهد أبوشويرب ، عز الدين المصراتي وسعد الجيلاني

إستعملت تقنية النمو المستمر (المخمر) للكائنات الدقيقة الحية لدراسة معدل النمو ومحتوى الخلية لكل من البكتريا مثايلوموناس كلارا Methylomonas Clara والخميرة كانديدا بويوديني Candida boidinii. وجد أن أحسن معدل للنمو كان عند التركيز 2 % من الميثانول مع البكتريا وإنخفض المعدل عندالتركيز الأعلى من الميثانول.

معدل النمو للخميرة تحسن مع إزدياد تركيز إضافة الميثانول فازداد المعدل مع إزدياد التركيز (1 % ، 2 % و3 %).

كما وجد أن أعلى نسبة من البروتين والدهن كانت عند التركيز 2 % من الميثانول بالنسبة للبكتريا (مثايلوموناس كلارا) فكانت نسبة البروتين (71.6 %) ونسبة الدهن (4.1 %). ولم تظهر إختلافات في نسبة المحتوى للخلية بالنسبة للخميرة (كانديدا بويوديني).

ABSTRACT

A continuous culture technique was used to study the growth rate and cell contents of methanol-utilizing bacteria Methylomonas clara and yeast Candida boidinii. The changes in propagation of the culture have been investigated. The optimal growth and biomass yield of Methylomonas clara occured at 2% methanol concentration, beyond that an inhibition in growth was observed. However, the specific growth rate and cell yield for Candida boidinii increased with increasing methanol concentration 1%, 2% and 3%. The maximum contents of protein and fat were observed at 2% methanol concentration for Methylomonas clara (71.6%) and (4.1%) respectively. While, no differences in cell contents were observed with Candida boidinii.

INTRODUCTION

Microorganisms are protein sources of growing importance. The microorganisms cultivated on carbohydrates and hydrocarbons will be produced on a large scale in the near future. The importance of yeast and bacteria as test organisms for the study of biological phenomena are well known. Many investigation have been devoted to reveal the effect of nutritional, environmental, and genetical factor on the growth of yeast and bacteria cells, behaviour of the cells and their cell composition (Levin and Cooney, 1973; Haber *et al.*, 1983; Jara *et al.*, 1983; Hamdani *et al.*, 1987; Tani *et al.*, 1988; Lim and Tani, 1988).

Methanol, ethanol and *n*-paraffine are attractive raw materials for the production of fermentation products such as single cell protein, amino acids, organic acids and antibiotics because of their low cost, high purity, high water solubility (methanol) and because they can be easily and cheaply produced.

The existence of methanol assimilating yeast and bacteria is relatively a recent subject of investigation. The microbial technology is still lagging, especially the growth physiology of the involved organism.

Some efforts have been made to illustrate some of the parameters affecting the methanol utilization by yeast (Fonda and El-Masry, 1981) and bacteria (Abu-

*Petroleum Research Centre, P.O. Box 6431, Tripoli, G.S.P.L.A.J.

Ruwaida *et al.*, 1990). This work is undertaken with the objective to determine the growth propagation rate and cellular contents of Methylomonas clara and Candida boidinii for a biomass production as a single cell protein products.

MATERIAL AND METHODS

Microorganisms

Bacteria, Methylomonas clara strain ATCC No. 31226 and Yeast, Candida boidinii strain ATCC No. 56507 were used throughout this study.

Cultivation

The cultivation was carried out at 30°C in a 10 liter MBR fermentor (MCS 10, MBR Bio reactor Ltd. Switzerland). The dissolved oxygen concentration in the medium expressed in percentage was (20%). The rotation speed of the impeller was between 200 to 400 rpm.

The minimal salts medium used for the growth of bacteria contained, (per liter of distilled water),: $Na_2HPO_4 \cdot 2H_2O$, 2.75 g; KH_2PO_4, 1.36 g; $MgSO_4 \cdot 7H_2O$, 0.04 g; $(NH_4)_2SO_4$, 2.0 g; Fe_3C_2, 10 mg; NaCl, 2 g. The trace elements were added to the medium at 1 ml per liter which contains (in mg) $ZnSO_4 \cdot 7H_2O$, 0.08; $MnSO_4 \cdot 4H_2O$, 0.03; $CuCl_2 \cdot 2H_2O$, 0.03; $NiCl \cdot 6H_2O$, 0.02; $CaCl_2 \cdot 6H_2O$, 0.1; $CaCl_2 \cdot 2H_2O$, 0·2 and H_3BO_3, 0·2.

The pH of the medium was adjusted between 7 to 7.1.

The yeast was grown on the following medium (g/liter):

Bacto-yeast extract	3
Malt extract	3
Bacto pepton	5
Bacto dextrose	10

The pH of the medium was set up at 4.44. The methanol concentrations in the feeds were 1%, 2% and 3%.

Analytical Methods

Growth was measured turbidimetrically at 610 nm while referring to a standard free media curve. Dry weight was estimated after drying overnight at 80°C. The protein was estimated by the macro-Kjedahl method (AOAC, 1980). The fat content was determined by diethyl ether extraction method (AOAC, 1980). The soluble carbohydrates was estimated as nitrogen free extract (NFE) method (AOAC, 1980).

RESULTS AND DISCUSSION

The results showed that a methanol feed concentration up to 2% produced the highest growth and yield coefficient, but also high cellular protein content when Methylomonas clara was used.

Changes of cell concentration of Methylomonas clara during the batches cultivation at 1% and 2% methanol concentration in the biomass fermentor are illustrated in Fig. 1. The lag phase has extended with increase in the methanol concentration.

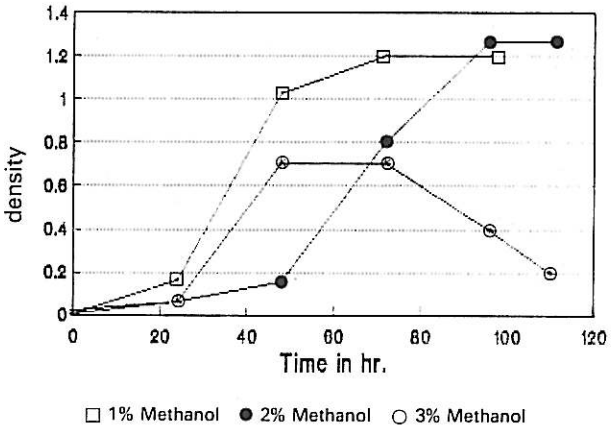


FIG. 1. Effect of methanol on growth rate of Methylomonas clara.

The specific growth rate and cell yield decreased with increasing methanol concentration, while the maximum content of crude protein was observed at the concentration of 2% methanol. However, 3% methanol concentration inhibited the growth rate of this organism. Changing the methanol concentration from 1% to 2% increased the crude protein and fat 62 to 71.63% and 3.05 to 4.1% respectively, while the carbohydrate and ash were decreased. The cellular contents of the protein, fat, carbohydrates and ash were determined (Table 1).

Growth behaviour of Candida boidinii is illustrated in Fig. 2.

The lag time became longer with increasing methanol concentration. The growth rate increased with increasing methanol concentration, while no differences were observed on cellular contents such as crude protein and fat (Table 2). Inhibition of

Table 1. The Effect of Methanol Concentrations on Crude Protein, Fat, Carbohydrates, Ash and Moisture Contents in Methylomonas Clara (in Percentage)

Methanol	1%	2%
Moisture	4.74	6.49
Protein	62.00	71.60
Fat	3.05	4.10
Carbohydrates	26.26	17.30
Ash	8.69	7.00

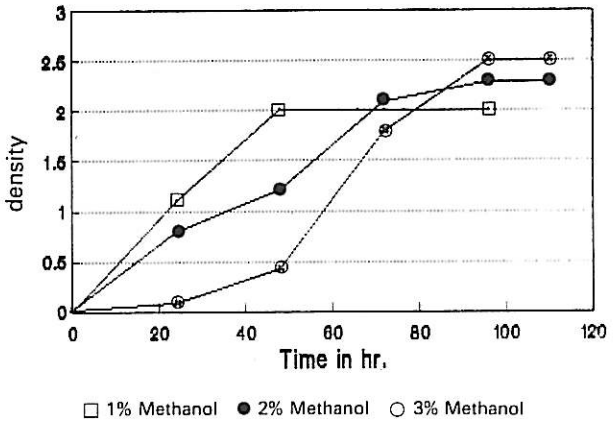


FIG. 2. Effect of methanol on growth rate of Candida Boidinii.

Table 2. The Effect of Methanol Concentrations on Crude Protein, Fat, Carbohydrates, Ash and Moisture Contents in Candida Boidinii (in Percentage)

Methanol	1%	2%	3%
Moisture	5.3	4.1	3.4
Protein	40.25	40.20	39.2
Fat	8.07	8.10	7.5
Ash	7.01	6.3	5.0
Carbohydrates	44.67	45.4	46.9

growth rate was observed at 3% methanol concentration. A similar observation has been reported for other methanol utilizing bacteria (Kim and Ryu, 1976). However, unlike Methylomonas clara, the 3% methanol concentration in the feed did not inhibit the growth rate of Candida boidinii.

CONCLUSION

The Methylomonas clara culture gave a maximum yield at 2% methanol concentration beyond which the yield decreased. The decrease in yield at high methanol concentration is associated with a slight increase in the cellular contents of protein and fat.

The optimal concentration for Candida boidinii was not defined and at 3% methanol concentration did not inhibit their growth.

The present investigation resulted in defining the optimal concentration of methanol as the sole carbon source in the medium used for growing Methylomonas clara. The methanol inclusion in the medium supported satisfactory levels of growth, yield and product. The cellular contents of crude protein (71.6%) for Methylomonas clara and (40%) for Candida boidinii was within acceptable levels for single cell protein producing cultures (Krug *et al.* 1979).

ACKNOWLEDGEMENT

The authors are grateful to the Petroleum Research Centre for providing the necessary facilities to carry out this work.

REFERENCES

Abu-Ruwaida, A.S., Banat, I.M. and Hamdan, I.Y., 1990, Appl. Microbiol, and Biotechnol. 32: 550–555.

AOAC, 1980, Association of Official Analytical Chemists, 13th Edn., ed. Horwitz, W., AOA Washington, D.C.

Fonda, M.S. and El-Masry, H.G., 1981, Parameters Affecting Methanol Utilization by Yeasts. Zbl. Bakt. 11 Abt. 136, 417–432.

Haber, C.L., Allen, L.N., Zhao, S. and Hanson, R.S., 1983, Methlotropic Bacteria: Biochemical Diversity and Genetic, Science 221: 1147–1153.

Hamdan, I.Y., El-Nawawy, A.S., Banat, I.M., Al-Awadhi, N.M., 1987, Process and Microorganisms for Producing Single Cell Protein, Patent application submitted to U.S. patent office. Serial No. 07/120322, Nov. 1987.

Jara, P., Allais, J.J., Baratti, J., 1983, Isolation and Characterization of a Methanol Utilizing Yeast with High Cell Yield, Eur. J. Appl. Microbiol. Biotechnol., **17**, 19–23.

Kim, J.H., Ryu, Dy, 1976, Optimization of Medium and Maximization of Biomass Productivity in Production of Single Cell Protein from Methanol, J. Ferment. Technol., **54**, 427–436.

Krug, E.R., Lim, W.J., Tsao, G.T, 1979, Single Cell Protein from C1 Compounds, Annu. Rep. Ferment Process 3, 141–195.

Levin, D.W. and Coony, C.L., 1973, Isolation and Characterization of Thermotolerant Methanol Utilizing Yeast, Appl. Microbiol., **26**, 982–990.

Tani, Y., Lim, W.J. and Yang, H.C., 1988, Isolation of L-Methionine Enriched Mutant of a Methylotropic Yeast Candida Boidinii, J. Ferment, Technol., **66**, 153–158.

Wang-J. and Tani, Y., 1988, Production of L-Methionine Enriched Cells of Mutant Derived from a Methylotropic Yeast, Candida Boidinii, J. Ferment. Technol., Vol. 66, No. 6, 643–647.

PRJ, Vol. 4. (January 1992); P. 59–62, 5 FIGS, 2 TABLES.

Short Note

A COMPUTER PROGRAM TO SIMULATE TWO-PHASE PIPELINE FLOW

M.M. Elgarni*, H.H. Beck* and N.A. Faruqi*

منظومة حاسوبية لمحاكاة الإنسياب خلال خطوط الأنابيب ثنائية الطور

محمد القرني ، هيثم حسن بك ونور الدين الفاروقي

يزداد هبوط الضغط خلال الإنسياب الثنائي الطور للمخاليط الهيدروكربونية نتيجة للتأثير المتبادل بين الطورين ، وتظهر تعقيدات أخرى نتيجة إلى تجمع كتل من السائل خصوصاً في تجاويف الأنابيب الطويلة الممتدة على الأرض أو قاع البحر، ولذلك تعد المعرفة الوثيقة بقطاعات الضغط وتشكيل نمو كتل السائل ضرورية لتصميم ومحاكاة خطوط الأنابيب الثنائية الطور. تعرض الورقة منظومة حاسوبية لإنجاز ذلك.

INTRODUCTION

Two-phase flow is commonly encountered during the transportation of hydrocarbon mixtures through land based or subsea pipelines. An important task during the design and simulation of pipelines is to predict pressure and temperature variations along the pipe length and to estimate build-up of liquid slugs at different locations in particular in the hollows of the pipelines. The information for the liquid build-up is required to compute both pressure variations as well as the volume of slugs during pigging operation. The above information is also vital in the mechanical design of pipeline and pipe supports and in the stress analysis. A rigorous approach to this problem involve dividing the whole pipe length into several finite length elements (FLE) and carrying out in each of them phase equilibrium, heat transfer and pressure drop calculations sequentially. Depending upon the available data and the objectives of the task the calculations may have to be carried starting from the upstream end, downstream end or from some intermediate locations. In view of the coupled nature of the physical processes and consequently the calculation techniques, digital computer application is essential to perform the computations. This paper presents general organization and calculation logic of a computer program developed to simulate two-phase flow line carrying hydrocarbon mixtures. The program has been tested by using IBM PC AT on a 30 miles long pipeline for which data was available in the literature [4].

*Petroleum Research Centre, P.O. Box 6431, Tripoli, G.S.P.L.A.J.

EQUILIBRIUM AND TRANSFER PROCESS MODEL EQUATIONS

The equilibrium flash calculations have been performed by using SRK equation of state (Table 1) [8] for computing the k-values. The physical and thermodynamic properties are estimated using a number of techniques given in the literature [1, 3–9].

The hydrodynamics of the two-phase calculations is based on Beggs and Brill Models [2], as shown in Table 2. The information for the friction factor and pipeline roughness is obtained from White [10].

Frequently the hydrocarbon mixtures contain both defined and undefined components. The program is written with capability to process the undefined

Table 1. Soave Equation of State

$$P=-\frac{RT}{V-b}-\frac{a\alpha}{V(V+b)}$$

Parameters

$a_i=0.42747R^2T_{ci}/P_{ci}$

$b_i=0.08664RT_{ci}/P_{ci}$

$\alpha_i=1.202\ \exp(-0.30288\ T_r)$ (for Hydrogen)

$\alpha_i=[1+(0.48508+1.55171W_i-0.15613W_i^2)(1-T_{ri}^{0.5})]^2$ (for other components)

$A_i=a\alpha P^2/R^2T^2$

$B_i=bP/RT=0.08664P_r/T_r$

$a\alpha=\sum\sum Y_iY_i(a\alpha)_{ij}$

$b=\sum Y_ib_i$

$A=\sum\sum Y_iY_iA_{ij}$

$B=\sum Y_iB_i$

$(a\alpha)_{ij}=(1-k_{ij})\sqrt{(a\alpha)_i(a\alpha)_j}$

$k_{ij}=0$ for hydrocarbons pairs and hydrogen

$A_{ij}=(1-k_{ij})(A_iA_j)^{0.5}$

$Z^3-Z^2+(A-B-B^2)Z-AB-0$

$Z=$smallest positive value for liquids

$Z=$largest positive value for vapours

Table 2. Equations for Liquid Holdup

Horizontal Flow Pattern	Horizontal Holdup ($H_L(0)$)	C^+ (Uphill)	C^- (Downhill)
Segregated	$\frac{0.98\ \lambda^{0.4846}}{N_{FR}^{0.0868}}$	$(1-\lambda)\ln\left[\frac{0.011N_{LV}^{3.539}}{\lambda^{3.768}N_{FR}^{1.614}}\right]$	$(1-\lambda)\ln\left[\frac{4.7N_{LV}^{0.1244}}{0.3602N_{FR}^{0.5056}}\right]$
Intermittent	$\frac{0.845\lambda^{0.5351}}{N_{FR}^{0.0173}}$	$(1-\lambda)\ln\left[\frac{2.96\lambda^{0.305}N_{FR}^{0.0978}}{N_{LV}^{0.4473}}\right]$	As above
Distributed	$\frac{1.065\lambda^{0.5824}}{N_{FR}^{0.0609}}$	0.0	As above

mixture into one or more pseudo components, if provided in any one of the following form:

(1) Complete TBP and density of mixture
(2) GLC analysis giving carbon number distribution
(3) ASTM D-86 data along with density
(4) Density and molecular weight.

The critical properties and physical properties of the pseudo components are estimated using the relationships available in the literature [1, 2–10].

Program Organization and Calculation Logic

The general organization of the program is schematically explained in Fig. 1a, whereas Fig. 1b provides the calculations flow chart. The program is organized into a main program which controls the computations, takes in input and gives out output. The input information is distributed among various subroutines using "COMMON" statement. As it is obvious from Fig. 1, the program could be used in different cases:

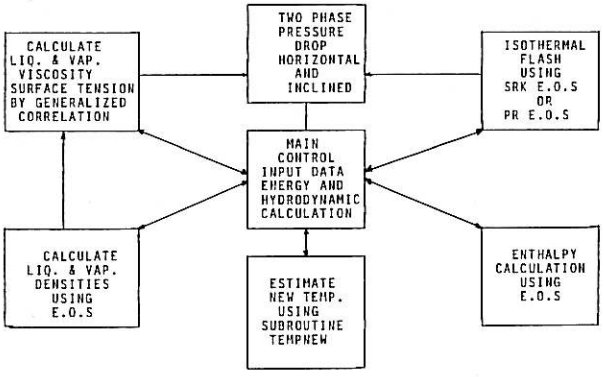


FIG. 1a. General organization for two phase flow calculation.

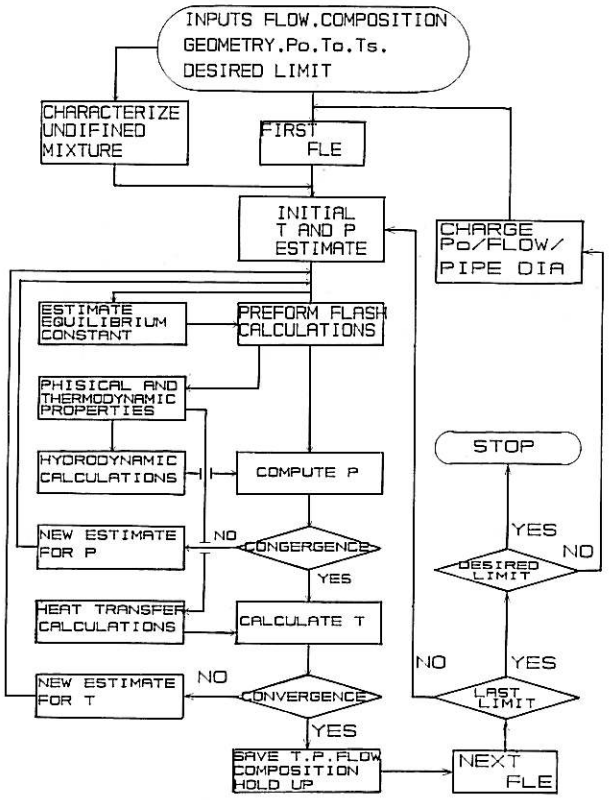


FIG. 1b. Flow chart for calculations of a single pipe.

(A) To simulate a single pipeline having single physical input and single physical output:

In this case the program could simulate the pipeline on stand alone basis and to carry out any of the following tasks.

(1) Upstream conditions are provided and it is required to estimate the intermediate and downstream conditions.
(2) The program must determine the upstream condition (or downstream) if mixed down stream/ upstream conditions are available. For example it is required to compute total flow rate if delivery and upstream pressures are specified. In this case the program performs trial and error calculations until the convergence is achieved.
(3) To simulate a pipeline having one or more tie-in lines and/or branches. In the case of tie-in lines the flow rate and composition will change.

(B) Simulate a system of pipelines or to optimize a single pipeline conditions in conjunction with another:

In this case the program could not be used on stand-alone basis. It should be used as a back-up package or subroutine.

RESULTS AND DISCUSSION

A reference case for two-phase flow has been provided by Maddox and Erbar [4] for testing purposes. Complete geometrical, flow and compositional details are provided for a 30 miles long and 15 inch size pipeline. The flow rate is 100 MM SCF/day of gas and 67.3 barrels/day of liquid.

The data is provided for two cases:

(1) Smooth pipe
(2) Rough pipe (roughness 0.005 ft)

Fig. 2 gives the pressure profile for the rough pipe. The results obtained from the program are compared by the data provided by Maddox and Erbar [4]. The computed and given delivery pressures are 790 psia and 775 psia respectively. The agreement is within $\pm 2\%$. Fig. 3 provides the results for non-adiabatic condition. The heat transfer coefficient has been taken as 0.1 Btu/(hr) (sq. ft) (deg. F). This represents an average value for an insulated pipeline. A comparison between Fig. 2 and Fig. 3 indicates that the pressure differences between the adiabatic and non-adiabatic case are a function of the absolute pressure.

The pressure drop for both cases remain identical as long as the total pressure remains above 700 psia.

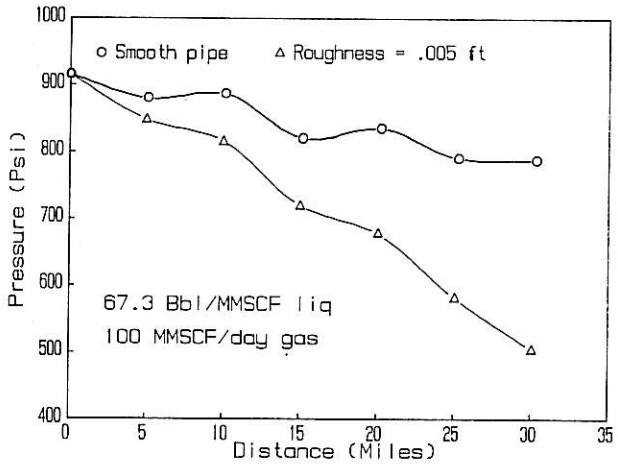


FIG. 2. Pressure profile for two phase flow (no heat transfer, 15 inch inclined pipe).

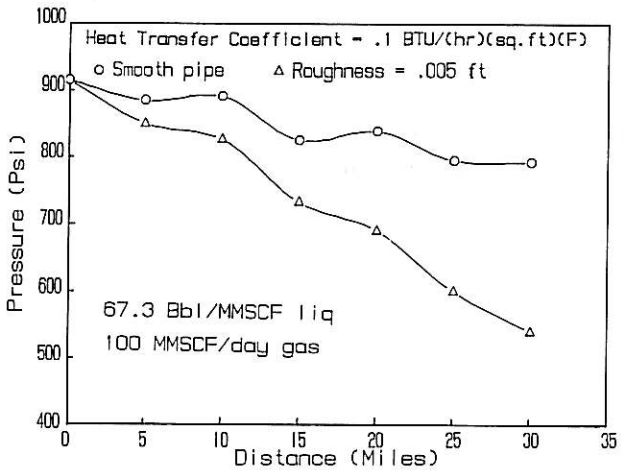


FIG. 3. Pressure profile for two phase flow (15 inch inclined pipe), with heat transfer.

Below 700 psia high temperatures and lower pressure encountered in the adiabatic case have lead to higher pressure drop. It may thus be inferred that operating a gas phase rich and liquid defficient line at high pressure offer advantages from the pressure drop point of view (and consequently lower pumping power).

Fig. 4 and Fig. 5 present the temperature profiles.

An increase in the heat transfer coefficient from 0.0 (adiabatic) to 0.2 Btu/(hr) (sq/ft) (Deg. F) has lead to a 3 fold increase in the cooling. Asymptotic behavior is

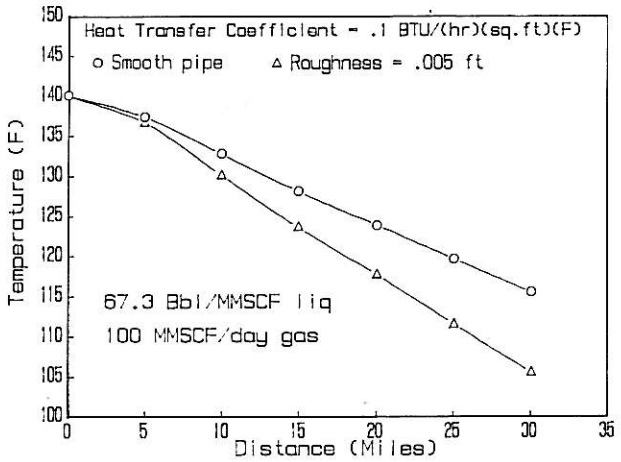


FIG. 4. Temperature profile for two phase (15 inch inclined pipe).

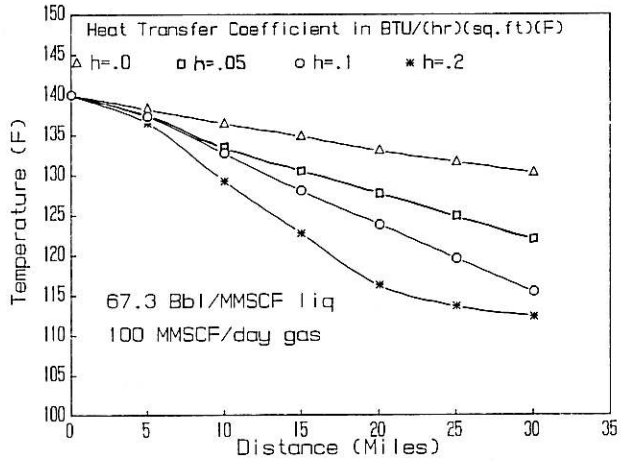


FIG. 5. Effect of heat transfer coefficient (on temperature of two phase flow inclined 15 inch pipe).

apparent for the case of $h=0.20$ at temperatures below 112°F. For the longer pipes the operation may approach isothermal conditions.

CONCLUSIONS

(1) A simulation program has been presented which has applications in simulating two-phase pipelines on either stand-alone basis or as a subroutine of another program.

(2) The program reproduced the results of a reference case wih an accuracy of $\pm 2\%$.

ACKNOWLEDGEMENT

The authors wish to express their thanks to the Petroleum Research Centre for providing the computer facilities used in this work.

REFERENCES

[1] API, 1976, "American Petroleum Institute", Technical Data Book "Petroleum Refining", Chapters 1–10.

[2] Beggs, H.L. and Brill, J.P., 1975, "A study of two-phase flow in inclined pipes", Transaction AIME, **255**, 172.

[3] Kesler, M.G. and Lee, B.I., 1976, "Hydrocarbon Processing", **55**, 153.

[4] Maddox, R.N. and Erbar, J.N., 1982, "Gas Conditioning and Processing, Vol. II, Campbell Petroleum Series, Oklahoma.

[5] Pederson, K.S., Per Thomassen and A. Fredenslaud, 1984, Thermodynamics of Petroleum Mixtures Containing Heavy Hydrocarbons" Ind. Eng. Chem. Process Des. Dev., **23**, 163–170.

[6] Peng, D.Y. and Robinson, D.B., 1976, "A New Two Constant Equation of State, Ind. Eng. Chem. Fundamentals, **15**, 59–64.

[7] Riazi, M.R. and Thomas E. Daubert, 1986, "Prediction of Molecular Type Analysis of Petroleum Fractions and Coal Liquids", Ind. Eng. Chem. Process. Dev., **25**, 1009–1015.

[8] Soave, G.L., 1972, "Equilibrium constants from a modified Relich-Kwang equation of state" Chem. Eng. Science, **27**, 1197–1203.

[9] Walas, S.M., 1985, "Phase Equilibria in Chemical Engineering" Butterworth Publishers, Boston. p. 53–56, 509–514.

[10] White, F.M., 1986, "Fluid Mechanics", 2nd ed., McGraw-Hill Book Co., New York, p. 313.

PRJ, Vol. 4. (January 1992); P. 63–67, 5 FIGS.

Short Note

BUTADIENE REACTIONS USING THE EROS 5.0 COMPUTER PROGRAM

T. Elgomati* and K. Rafeiner**

تفاعلات البوتاديين باستخدام برنامج الحسوب EROS 5.0

طارق القماطي وكلاوس رافينر

تم دراسة تفاعلات البوتاديين مع متفاعلات مختلفة ، باستخدام برنامج الحسوب EROS 5.0 الذي تم برمجته وتطويره من قبل البروفسور قاستيقر ومجموعته بجامعة ميونخ التقنية .

وقد تم بالفعل الحصول على مجموعة كبيرة من النتائج الإيجابية لمجموعة من المركبات التجارية بتفاعل البوتاديين والماء والكلور والأمونيا وسيانيد الهيدروجين والهيدروجين .

INTRODUCTION

This study is intended to provide a picture of the probable products that can be produced when butadiene reacts with different reagents.

Industrial processes are largely determined by thermodynamic considerations. Only if a reaction is exothermic can the search for an appropriate catalyst begin. Therefore, as a guide to the evaluation of the different reaction pathways and products, the heats of reaction are investigated.

Butadiene is considered as one of the most important starting materials under (C_4–C_5) [1]. As a monomer and a comonomer it was used for synthesis of elastomer thermoplastics and dispersion. Also because of the fact that it is an inexpensive byproduct, makes it one of the most important starting materials in industry.

Gasteiger [5, 6] and his group have been working in writing and developing the EROS program (Elaboration of Reaction for Organic Synthesis) for the last 15 years. This program system can be used for the production of organic reactions and for the design of organic synthesis.

*Chemistry Dept., Al Fateh University, Tripoli, G.S.P.L.A.J.
**Institut für Org, Chemie, Boltz Monnstr., D-8046 Garching, Germany.

PREDICTION OF REACTION-DESIGN FOR SYNTHESIS

EROS [4] (Elaboration of Reactions for Organic Synthesis) is a system of computer programs which generates sequences of organic chemical reactions. It can be applied to two different types of problems depending on how the reactions are interpreted.

In a forward strategy it is assumed that the chemical reactions proceed in the same direction as they are obtained from the program. From the starting materials, that are inputs, their products in a chemical reaction can be predicted. The following types of problems can be studied.

- Prediction of the products of a chemical reaction
- Prediction of metabolic pathways
- Prediction of the degradation of a chemical in the environment
- Search for the synthetic uses of an industrial byproduct

- Elucidation of the structure of a reaction product
- Generation of all isomers with a given empirical formula

If the reactions, as output by the program, are considered to be reverses of chemical reactions, i.e. retrosynthetic steps, then the program can be used for the planning of synthesis. In such a backward (retrosynthetic) strategy the input structure is the target of a synthesis, and one is searching for reactions and precursors leading to this compound. By such an approach, problems of synthesis design can be studied. These include:

- Design of chemical synthesis, ranging from laboratory procedures to large scale industrial processes
- Study of biochemical pathways

It is an essential feature of EROS that reactions are not taken from a database of known reactions. Rather, chemical reactions are perceived as bond-breaking and making, and electron-shifting processes. This allows the generation of all conceivable reactions, irrespective of whether a reaction is known or not. Thus, novel reactions may be found.

EROS can be applied to seek answers to two fundamental questions of major importance to an organic chemist. First, how can a desired compound be synthesized and second what is the product of such reaction?

Obviously, answering these two questions requires a deep insight into organic chemistry. Reaction prediction asks for a knowledge of the course of organic reactions, a knowledge of chemical reactivity. Synthesis design requires, on top of these capabilities, to develop strategies and plan for approaching a synthesis problem. Incomplete as our knowledge as chemists is in these fields, it cannot be expected that a computer program can solve these problems straight away.

Because of the difficulties of predicting the outcome of complex organic reactions and planning of the synthesis of organic compounds, all means to solve these problems must be considered.

Therefore, the utilization of the computer by chemists to tackle problems of reaction prediction and synthesis design is essential.

In this sense, EROS should be considered as an instrument for the chemist to analyse and seek solutions to the problems at hand. Various options are offered to the user to specify initial conditions. The more a chemist makes use of these options to specify clearly the initial conditions, the closer he gets to the optimum results.

GENERATION OF REACTIONS

An essential feature of the logic behind EROS is to use electron shifting schemes as generators for chemical reactions. The electrons that are shifted in a chemical reaction may be located in bonds (breaking or making of bonds) or they may be free electrons on atoms. Thus it becomes clear how important it is to take into account all valence electrons. Since, in chemical reactions, electrons may be converted from free electrons to bonding electrons, or vice versa. Working with formal reaction schemes allows the generation of all conceivable chemical reactions, irrespective of whether they are known or without precedence. Additionally, novel (and promising) reactions are obtained and it is up to the chemist to try to verify them in the laboratory. In this way, new inventions may be initiated.

Reaction schemes are not unfamiliar to an organic chemist. In fact, he uses them routinely in the discussion of reaction mechanisms. There, the electron shifts occurring in a reaction are indicated by curved arrows.

In EROS Version 5.0 several such reaction schemes are contained. They correspond to overall bond change patterns observed frequently and found in important organic reactions. They can be selected by the user or are invoked by default. For example, a very common reaction scheme involves the breaking and making of two bonds (reaction generator RG 22: Fig. 1).



FIG. 1. An important reaction scheme: breaking and making two bonds.

GENERATION OF REACTIONS – THE OPTION "REAGEN"

Working with complete sets of formally possible reaction generators, as was done in the EROS precursor system CICLOPS, leads to reactions of various complexity (mechanistic steps and complete reactions) and varying chemical importance. Thereby, the system becomes rather inaccessible to general evaluation procedures. In EROS 5.0 therefore, only carefully selected reaction schemes are used. Although this leads to neglecting certain chemical reactions types, the selection of the schemes is such that the majority of chemically important organic reactions are encompassed. This applies to the presently known reactions but it is believed that this will also be true for new reactions. The selection of reaction schemes is supported by statistical analyses.

The reaction schemes contained in EROS comprise changes in the electron distribution which are normally considered as complete chemical reactions. Thus, starting with neutral molecules. But they are also applicable to reactions of charged and other reactive intermediates. Note that these reaction schemes give

only the overall result of the electron shifts in a reaction. They are not concerned with the timing of the bond breaking and making. Thus, both concerted and stepwise processes are represented by these reacting schemes.

Presently there are two reaction schemes in EROS 5.0. Two bonds are broken and two are made in this reaction scheme (Fig. 2).

Note that both conceivable permutations for bond making are considered. This reaction scheme comprises the majority of organic reactions: substitution, addition, and elimination reactions, as well as other types, such as certain electrocyclic reactions.

In the reaction scheme (Fig. 3) three bonds are broken and three bonds are made.

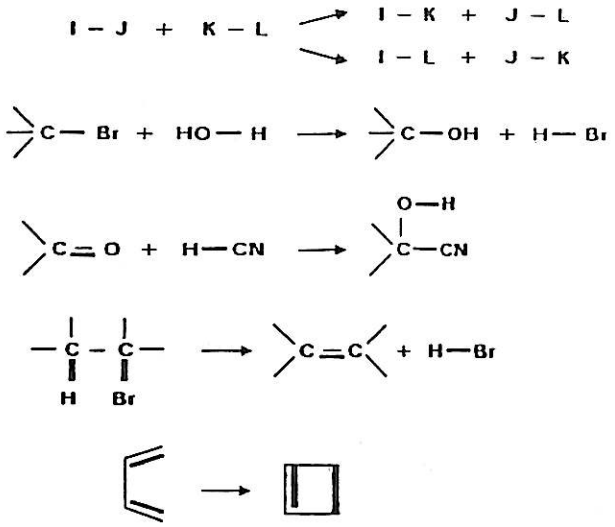


FIG. 2. Reaction scheme RG 22, breaking and making two bonds.

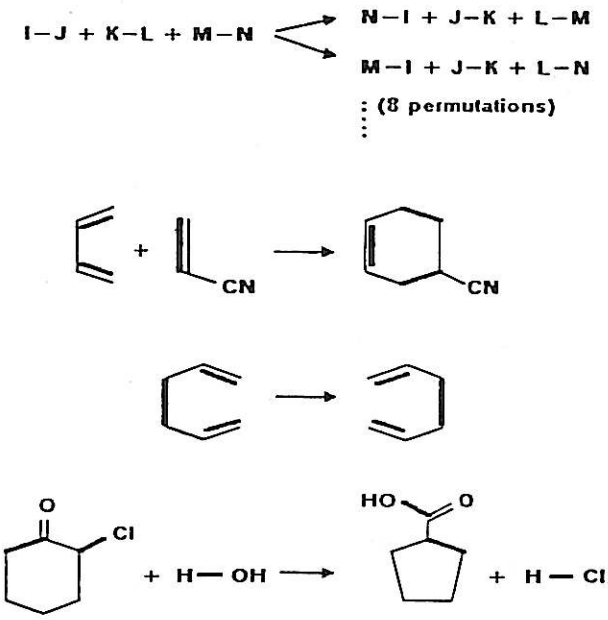


FIG. 3. Reaction scheme RG 33, breaking and making three bonds.

Many important reactions follow this electron shifting pattern e.g. the Diels–Alder reaction or the Cope rearrangement. As an example for a stepwise process the Favorski rearrangement is given.

Several reactions were studied as described in the following paragraph starting from butadiene and reacting with different reagents [2, 3]. This is shown in Fig. 4.

These reactions gave a good range of products from which we then chose the logical and the probable ones. We considered reaction enthalpy as the most important factor. Only exothermic reactions were selected, since they are thermodynamically favored. From this point of view the products were chosen as shown in Fig. 5.

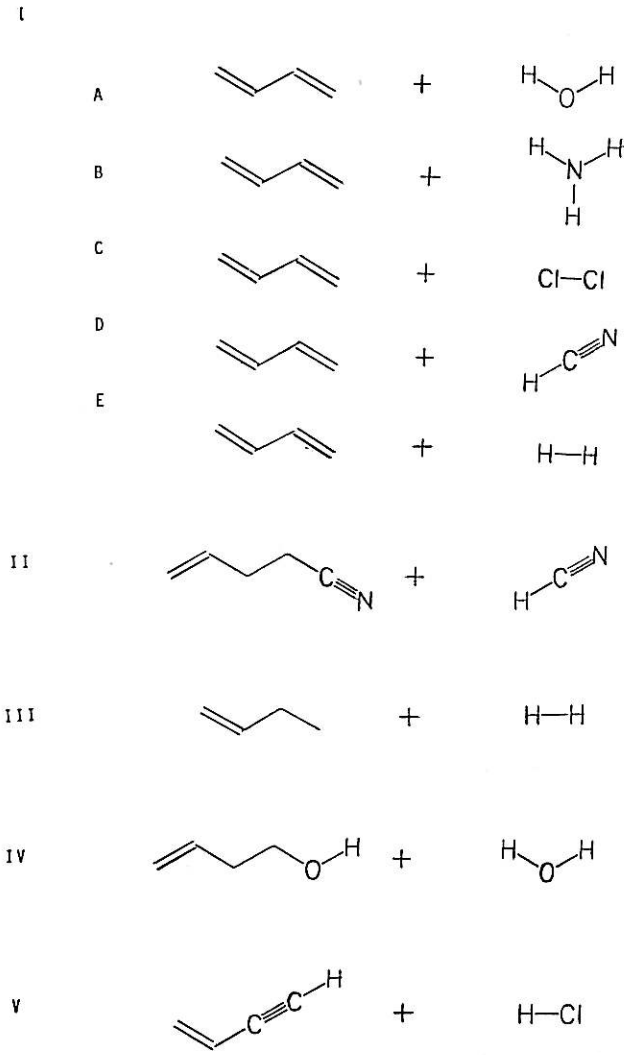


FIG. 4. The studied reaction of butadiene with different reagents and some other relevant reactions.

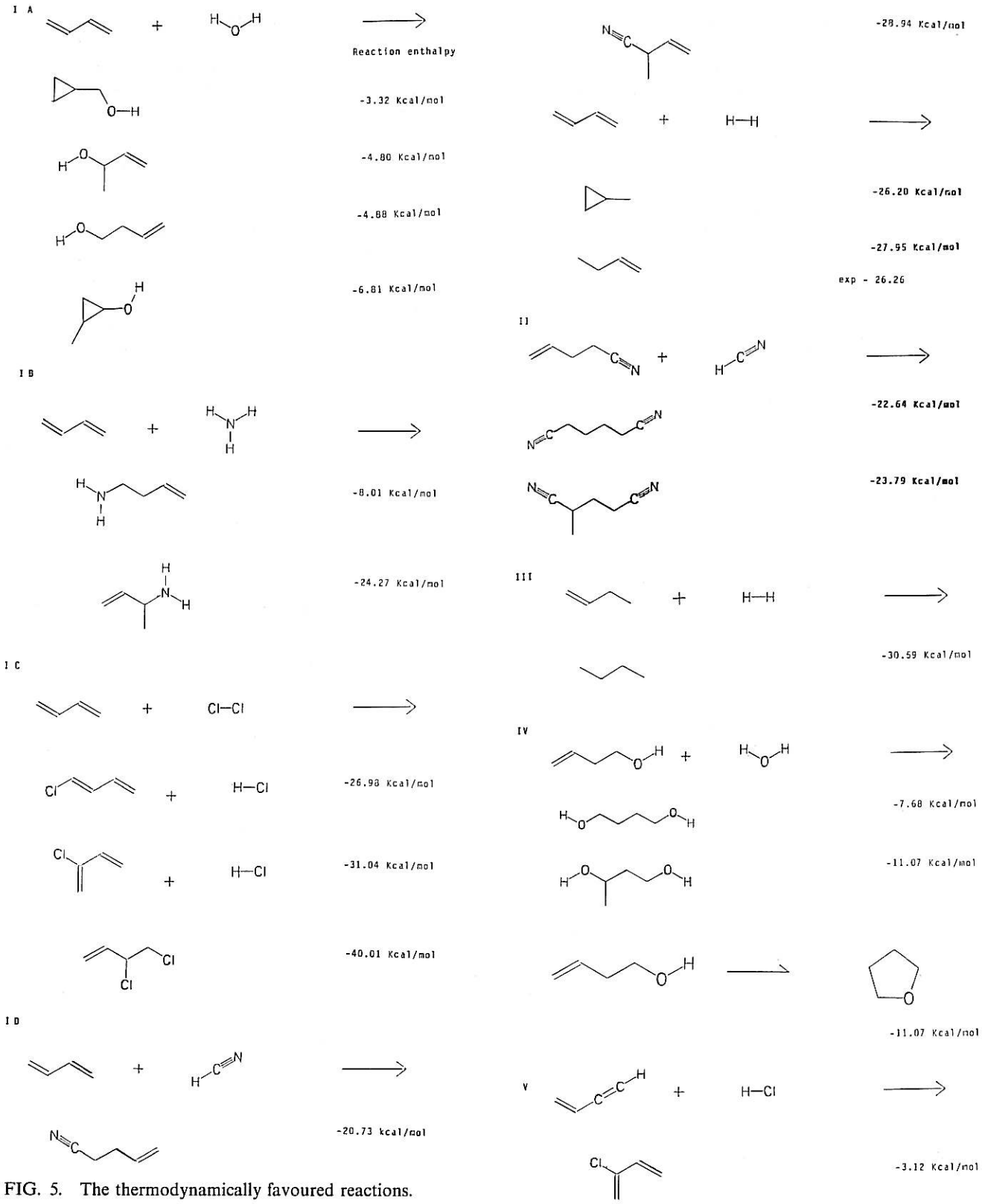


FIG. 5. The thermodynamically favoured reactions.

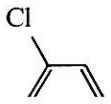
CONCLUSION

EROS can be used to study potential products derived from butadiene

(a) $+H_2O$ 1.4 butane-diole, tetrahydrofuran } commercial products

(b) $+NH_3$ incomplete study
only a first level intermediate follows reaction of these intermediates with other reagents e.g. with O_2.

(c) shows application of EROS to both addition and substitution of butadiene with chlorine.
Chloroprene commercial products.



for synthetic rubber exothermic reaction, can also be obtained in a two step procedure through addition and elimination of HCl.
Alternative processes from vinylacetylene are also favorable and commercially proven.

(d) $+HCN$ adiponitrile commercial products.

(e) $+H_2$ for comparison with experimental $Hf°$

The calculated heats of reaction [2, 3] show which reactions are thermodynamically favoured (exothermic) and therefore it is of interest to look for suitable catalyst to realise such a reaction.

ACKNOWLEDGEMENT

We would like to express our deep appreciation and gratitude to Prof. Dr. J. Gasteiger for his guidance and valuable discussions in preparing this work.

REFERENCES

[1] Weissermel, K. and Arpe, H. -J., 1978, Industrielle Organische Chemie, Verlag chemie. Weinheim. New York.

[2] Cox, J.D. and Pilcher G., 1970, Thermochemistry of Organic & Organometallic Compounds, Academic Press.

[3] Pedley, Naylor and Kirby, 1977, Thermochemical Data of Organic Compounds, Sussex NPL Computer analysis thermochemical data: organic and metalorganic compounds Sussex University.

[4] Gassteiger, J., Hutchings, M.G., Christoph, B., Gann L., Hiller, C., Low P., Marsili, M., Saller. H. and Yuki, K., 1987, A New Treatment of Chemical Reactivity: Development of EROS, an Expert System for Reaction Prediction and Synthesis Design, Chemische Institutes, Technische Universitat, München. Topics in current chemistry, vol. 137, p. 21–73, Springer Verlag, Berlin Heidelberg.

[5] Gasteiger, J., 1984, Chapter: Syntheseplanung, in "Computer in der Chemie", (Ziegler, E., Ed.) Springer Verlag Heidelberg, p. 207–257.

[6] Gasteiger, J., Marsili, M., Hutchings, M.G., Saller, H., Löw, P., Röse, P. and Raffeiner, K., 1990, Journal of Chemical Information and Computer Sciences, 30.

PRJ, Vol. 4. (January 1992); P. 68–71, 5 FIGS, 2 TABLES.

Short Note

STUDY OF CORROSION DAMAGE TO CU/NI CHLORINATOR LINE BY SEA WATER

M.L. Mehta* and A.T. Hassan*

دراسة حول تآكل خط أنابيب تزويد الكلور

م . ل . مهتا وعبد الفتاح حسن

تعرّض جزء من خط تزويد الكلور في بعض المنشآت إلى تحفر بسبب تأثير وسط محدث (ماء البحر) . وقد أجريت الإختبارات للكشف عن الأضرار التي تعرض لها السطح كما تم تحليل مخلفات التآكل كيميائياً وذلك لتحديد أسباب العطب .

BACKGROUND AND CASE HISTORY

The chlorinator line which failed was delivering sea water and hypochloride to the stilling tube of sea water lift pump 29/X–OIC to treat sea water continuously with 2 ppm of hypochloride to control microorganism. After every five to six hours, shock treatment of about 5 ppm of hypochloride for half an hour was also being given. This chlorinator line was 38 mm ($1\frac{1}{2}$ inch) in diameter with a wall thickness of 1.5 mm. Its material is reported to be 90–10 copper-nickel alloy. A flow velocity of 0.45 m/sec (1.5 ft/sec) was used. At times this line was shut down and thus flow was not always continuous.

Failure in the form of perforation/leak occurred at some distances from the outlet of the chlorinator line after it had been in operation for $1\frac{1}{2}$ years.

The objective of this study is:

(i) To investigate nature/type of corrosion damage and cause of perforation.
(ii) To determine chemical composition to check whether the material of chlorinator line is as per specification.

*Petroleum Research Centre, P.O. Box 6431, Tripoli, G.S.P.L.A.J.

LABORATORY INVESTIGATIONS

(A) Visual observations
(B) Microscopic examination
(C) Analysis of corrosion product layer found on the alloy surface
(D) Chemical composition of tube material

(A) Visual Observations

Failed section of the chlorinated tube in the as-received condition is shown in Fig. 1. It had been cut



FIG. 1. As received failed section of chlorinator line showing extensive pitting, channels and perforation.

longitudinally and then flattened. The internal surface shows extensive pitting corrosion and formation of channels/grooves. Pits are shallow and degree of pitting is different in different regions. Colour of the surface film formed on the alloy substrate is mostly dark brown in colour and in some regions such as original substrate film is dark brown, spotty and not very adherent. The area surrounding the perforation is partly covered with the film and has finer pits but no channels (Fig. 1). Thickness was measured at different locations and are marked in Fig. 1. In the region surrounding the leak thickness had been reduced to 0.5 mm compared with original thickness of 1.5 mm indicating considerable corrosion in this localized area.

(B) Metallographic Examination

The morphology of localized attack tend towards horse-shoe morphology (Fig. 2 a,b). Initially pits are formed as seen in Fig. 3a and then these pits grow to emerge into one another leading to the observed morphology. These horse-shoe attack propagate further leading to channel formation as illustrated in Fig. 3b. Within the horse-shoes cracked corrosion product layer was detected as in Fig. 4. In perforated/leaked region shallow horse shoe morphology of attack is observed (Fig. 5), but no channels/grooves were formed.

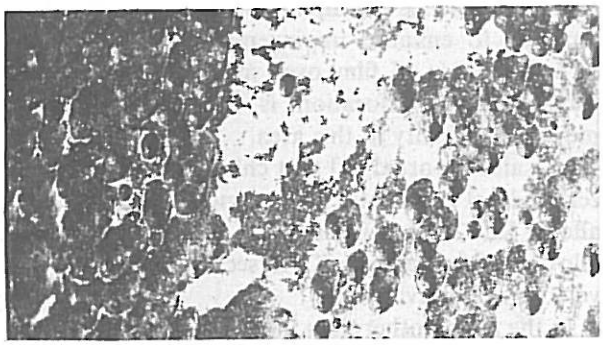


FIG. 2(a). Corrosion attack tending towards horse-shoe morphology. ×6.4.



FIG. 2(b). Corrosion attack tending towards horse-shoe morphology. ×16.

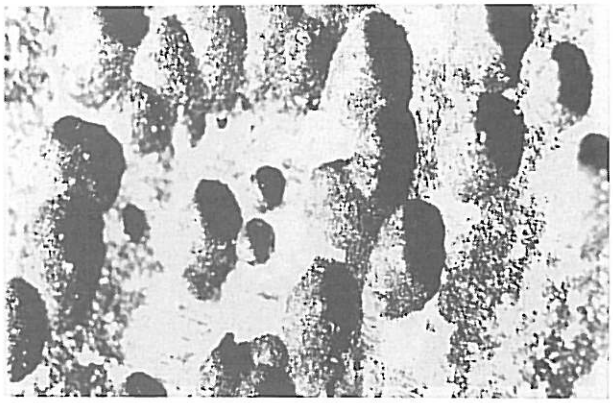


FIG. 3(a). Showing early stages of pit formations in original substrate and growth of pits into horse-shoe morphology and channel formation.

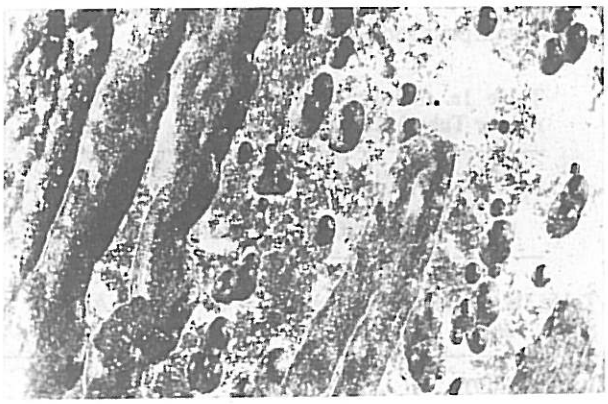


FIG. 3(b). Side-way growth of channels leading to wider channel. ×16.

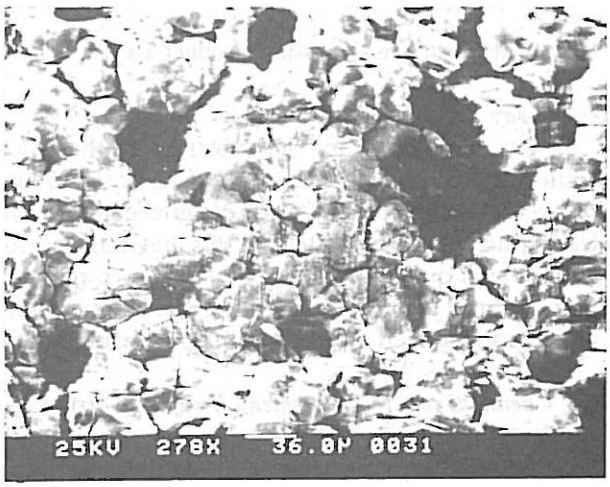


FIG. 4. Scanning electron micrograph showing cracked corrosion product within a horse-shoe.

(C) Chemical Composition

The chemical composition of the material was determined using atomic absorption spectrometer and is given in Table 1a. It confirms the material to be 90-10 Cu/Ni alloy. As per standard designation for

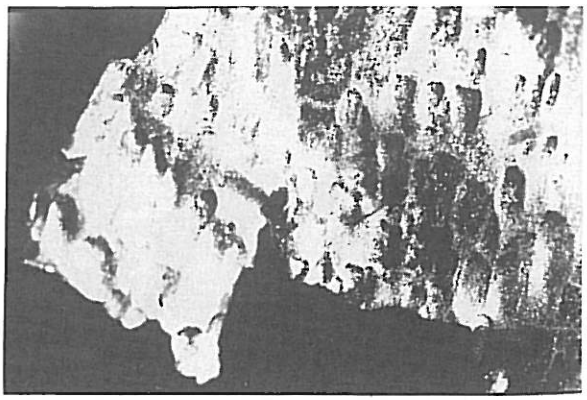


FIG. 5. Horse-shoe morphology of corrosion attack at the perforation site. ×6.4.

copper and copper alloys the composition in Table 1a corresponds to copper alloy number C 70600 whose composition is listed in Table 1b.

Table 1a. Chemical Composition of the Chlorinator Tube Material (wt%)

Ni	Fe	Mn	Cr	Cu
11.0	1.91	0.66	0.029	balance

Table 1b. Chemical Composition of the Copper Alloy No. C 70600

Copper alloy No.	Cu	Pb	Fe	Zn	Ni	Mn
C 70600	86.5%	0.05%	1.0–1.8%	1.0%	9–11%	1.0%

(D) Analysis of the Corrosion Product Layer

(a) X-ray diffraction analysis

It was scrapped from the substrate of the failed section shown in Fig. 1. Since the film was thin and only a very small quantity of the material could be collected, the diffraction pattern of this material was not of very high quality. Analysis of the pattern revealed that scrapped material constituting corrosion product layer was identified to consist of coprous sulphide.

(b) Chemical test to supplement X-ray diffraction results

Sodium azide test for the identification of sulphide in the corrosion product layer was carried out. Nitrogen gas bubble were evolved upon immersing corroded pieces of Cu/Ni alloy in the sodium azide-iodine reagent indicating the presence of sulphide in the product.

Upon standing the test solution along with corroded pieces the solution became nearly colourless as the reaction, $NaN_3 + I_2S \xrightarrow{S} 2NaI_3 + 3N_2$ approaches to completion as iodine converts to NaI. This observation confirms that sulphide is present in the corrosion product scrapped from the substrate. In the above reaction sulphide acts as a catalyst.

DISCUSSION

The results of the present investigations reveal formation of sulphide surface film on the alloy substrate and suggest the presence of sulphide in the sea water flowing through the chlorinator line. When cuprous sulphide forms as the principal corrosion product layer on the copper alloy surface as in the present case it lacks passivity [1]. It is reported [2] that even the presence of sulphide as low as 0.007 ppm in the sea-water causes localized sulphide induced attack. Increasing level of sulphide accelrates the attack. It is well established [3] that the conventional Cu/Ni alloys are known to perform adhersely in polluted sea water, pollutant being sulphide.

Flow velocity in the chlorinator line is 0.45 m/sec (1.5 ft/sec) and is much lower than minimum flow velocity required to result in erosion-corosion. Perforation in the chlorinator line has been caused by localized impingement attack. It is difficult to establish the cause of the localized enhancement of flow required.

One of the main causes of localized impingement attack in a straight tube as in the present case is some sort of partial internal logdement causing local turbulence. Presence of sulphide in sea water has been reported to enhance impingement attack. The observed absence of film over most of the area surrounding the perforation is indicative of higher prevailing velocity in this area.

It is also reported [4] that chlorine dosing above a certain level accelerates impingement attack in Cu/Ni alloys. Safe level is 0.2 mg/l for 90-10 copper-nickel alloy at a flow velocity of 9 m/sec. Data at lower flow velocity is not available.

In the region other than the impingement area bulk flow velocity has been smaller as indicated by the morphology of attack. Ellison and Wen [5] have proposed three fundamentally different mechanisms for the interaction between fluid flow and corrosion, namely convective mass transfer controlled corrosion, phase transport controlled corrosion, and erosion-corrosion. The horse-shoe morphology is indicative of mass transfer controlled corrosion [6]. The reaction rate is controlled by connective mass transfer. Any flow disturbances will cause shallow pits or grooves in areas with locally high mass transfer.

CONCLUSIONS

(i) Formation of cuprous sulphide film on alloy substrate is detected and indicates the presence of sulphide in the sea water.

(ii) Corrosion damage to chlorinator tube is attributed to accelerated attack induced by the presence of sulphide in the sea water.

ACKNOWLEDGEMENT

The authors would like to thank the Petroleum Reseach Centre Management for their support and encouragement.

REFERENCES

[1] Encyclopedia of Industrial Chemical analysis, 1973, Vol. 18, p. 393.
[2] Gilbert, P.T., 1982, Materials Performance, Vo. 21, p. 47.
[3] Syrett, B.C., 1981, Materials Performance, Vol. 20, p. 50.
[4] Francis, R., 1982, Materials Peformance, Vol. 21, p. 44.
[5] Ellison, B.T. and Wen, C.J., 1981, Am. Inst. Chem. Eng. Symp. Ser., Vol. 77, p. 161.
[6] Sybergr, T., 1987, Br. Corros. J., No. 2, p. 83.

PRJ, Vol. 4. (January 1992); P. 72–74, 2 FIG, 4 TABLES.

Short Note

DETERMINATION OF TRACE METALS IN SOME GAS OIL FRACTIONS OF LIBYAN CRUDE OILS BY ELECTROTHERMAL ATOMIC ABSORPTION SPECTROMETRY

I. Busheina, I. Ahmad, H.M. Kut, N. Bawash and S. Zayed

تحديد العناصر في بعض قطفات وقود الديزل المنتج من النفط الخام الليبي بإستعمال الإمتصاص الذري (الكهروحراري)

إسماعيل بشينة ، إفتخار أحمد ، حسن الكت ، نادية بعوش وصلاح زايد

تم إستعمال جهاز الإمتصاص الذري (الكهروحراري) لتحديد آثار العناصر في قطفات وقود الديزل المنتج من النفط الخام الليبي. فقد تم تحديد كمية الحديد ، النيكل ، النحاس ، الفانيديوم ، الكروم والرصاص في هذه القطفات.

INTRODUCTION

Trace metals in crude oil and their products are commonly determined by atomic absorption spectrophotometry. The presence of some metals (e.g. Ni, Cu, Fe, As) in the crude oil causes poisoning of the catalysts used in refining processes, and other metals (e.g. V) cause corrosion problems, thus reducing the efficiency of the refining plant [1–3]. On the other hand, the nature and level of metals in the oil can be used for identification of the source of the oil. The presence of copper in refined products promotes formation of gums and lacquers during heating or storage and thus accelerates the deterioration of these products and reduces the storage stability [4]. Vanadium concentration above 2 ppm in fuel oils can lead to severe corrosion turbine blades and deterioration of refractory furnace linings and stacks.

Most of the metallic species in petroleum products are present as volatile organometallic compounds, salts, fine metallic particles and coloidal suspensions.

*Petroleum Research Centre, P.O. Box 6431, Tripoli, G.S.P.L.A.J.

Atomic absorption trace methods [4] are known to determine the concentrations of trace metals in petroleum fractions. In many cases, to use atomic absorption equipment effectively, it would be necessary to destroy the organic matter and concentrate the metal content. The solution to the problem involved designing a simple method of decomposing the petroleum products' organic matter, while retaining the trace elements in an easily soluble flux, with a low blank, and solubilizing a maximum number of elements in one simple preparation.

Middleton and Stuckey [5] published work about dry ashing at 350°C with HNO_3, holding Ag, As, Cd, Co, Cr, Cu, Fe, Mo, Pb, Sr, and Zn. Gorsuch [6] published a study of recovery of fourteen different trace elements from organic material. He summarized some 250 investigations reported in the literature, to aid him in a choice of methods to study. The most common method found was direct dry ashing; second most common was wet digestion with nitric and sulphuric acids. Methods reported giving efficient trace element recovery, following destruction of organic matter, were dry ashing with sulphuric acid,

nitric acid, or magnesium compounds. An alternative approach arises from the comprehensive report by Gorsuch on the recovery of trace elements after wet and dry ashing. It has been shown [7] that all the wanted metallic elements are retained after dry ashing at 500°C provided a suitable ashing aid such as p-toluene sulphonic acid is employed. The metals are extracted from the residual ash with nitric acid, and cesium chloride is used as ionization buffer.

This paper presents the analysis of six trace metals in some gas oil range fractions obtained from Libyan crude oils by atomic absorption spectrophotometer using graphite furnace tube. p-toluene sulphonic acid was employed as ashing aid.

EXPERIMENTAL

Reagents and Materials

All chemicals used were of high purity analytical grade. Standard solutions of different elements of interest were prepared by appropriate dilution from stock standards supplied by VHG Labs, Inc, Manchester. High purity deionized water was used throughout the sample preparations. All solutions were stored in precleaned polypropylene containers. Export blend crude oil samples were collected at source and the appropriate fractions were collected from laboratory scale fractionation column. The fractions studied were 220–280°C and 280–340°C boiling ranges.

Apparatus

Atomic Absorption Spectrophotometer (Varian AA 1475) coupled with Varian GTA-95 graphite tube atomizer was used throughout this study. The instrument has also facilities of background correction and automatic sampling. The unit contains Epson recorder (model RX-80) attached to the atomic absorption spectrophotometer. Varian high intensity, hollow cathode lamps were used for all the elements analysed. The GTA furnace operation conditions used for each element are shown in Table 1.

Table 1. Conditions of Furnace Setting

Element	Wave length (nm)	Temperature Setting (in °C)	
		Start temp.	Plateau temp.
Cu	384.8	75–120	2300
Cr	357.9	75–120	2500
Pb	217.0	75–120	2000
Fe	248.3	75–120	2300
V	318.5	75–120	2700
Ni	232.0	75–120	2400

Procedure

A known weight of about 20.000 g of sample was placed in a platinum crucible together with 1.0 g p-toluene sulphonic acid and then dry ashed in a muffle furnace at 500°C for 60–90 minutes. The residue was brought to room temperature. Then 10 ml of 25% nitric acid was added, warmed gently and filtered into 50 ml volumetric flask, washed with further 10 ml of 25% nitric acid, added 5 ml of 1% cesium chloride solution and finally made up to the mark with distilled water. The blank solutions were prepared for each sample in duplicate. Calibration solutions were prepared from stock standards to contain the same concentrations of nitric acid (5%) and cesium chloride (0.1%) as the sample solutions. Table 2 represents the experimental condition used for the determination of different elements in various samples.

Table 2. Experimental Conditions for Determination of Different Elements

Element	Conc. range ($\mu g\, g^{-1}$)	Wave length (nm)
Cu	0.0060–0.1400	324.8
Cr	0.0004–0.0100	357.9
Pb	0.0800–1.1000	217.0
Fe	0.0200–0.7000	248.3
V	0.0400–0.1000	318.5
Ni	0.0500–1.1000	232.0

The weight of the sample was taken accurately weighed about 20.0000 g in each sample.

RESULTS AND DISCUSSION

The calibration plots of copper, chromium and iron were straight lines while for lead, vanadium and nickel were smooth curves. All plots pass through the origin. The calibration curves, as an example, for copper and lead are shown in Fig. 1a and Fig. 1b respectively.

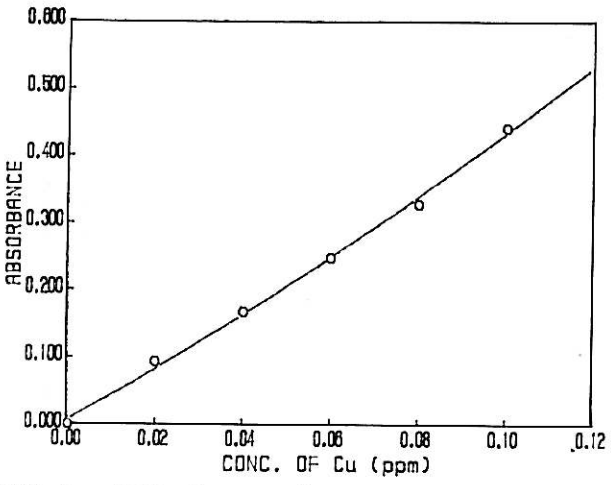


FIG. 1a. Calibration curve for copper.

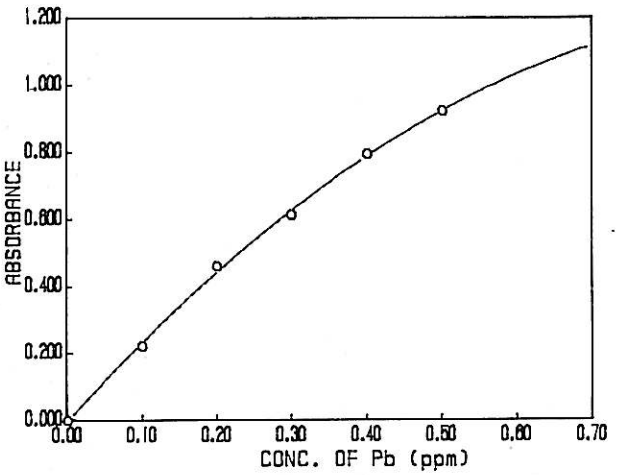


FIG. 1b. Calibration curve for lead.

The characteristic mass for each element at the operation condition stated are shown in Table 3. Results for the determination of Cu, Cr, Fe, Pb, Ni and V in twelve gas oil range fractions of export grade Libyan crudes are shown in Table 4.

These results indicate that the maximum content of copper (0.2230 $\mu g\, g^{-1}$) is found in sample 2B. The chromium content is in the range of 0.0004–0.0427 $\mu g\, g^{-1}$. Iron content is maximum (0.6930 $\mu g\, g^{-1}$) in sample 3B and minimum (0.0200 $\mu g\, g^{-1}$) in sample 6A. Nickel content was found maximum (1.0980 $\mu g\, g^{-1}$) in sample 4B and minimum (0.0590 $\mu g\, g^{-1}$) in sample 4A while sample 5A contains less than detection limit (0.0074 $\mu g\, g^{-1}$). The vanadium content ranges from 0.0400 to 0.1450 $\mu g\, g^{-1}$. Comparing these results with trace metal content in gas oils of other middle east crudes [8] show that Libyan gas oils contain less trace contents.

This study demonstrates that trace elements can be determined with good performance by using dry ashing procedure with the help of p-toluene sulphonic acid as an ashing aid. Acceptable precision and less interference was observed when using aqueous solution as standard for calibration graph. The results obtained in this work would help in studying the presence of some trace elements and their distribution in gas oil fractions.

Table 3. Working Sensitivities of Different Elements

Element	Wave length (nm)	Standard Conc. range ($\mu g\, g^{-1}$)	Sensitivity ($\mu g\, g^{-1}$)
Cr	357.9	0.0200–0.1000	0.0008
Fe	248.3	0.1000–0.6000	0.0005
Cu	324.8	0.0200–0.1000	0.0010
Ni	232.0	0.5000–3.000	0.0074
Pb	217.0	0.1000–0.5000	0.0021
V	318.5	0.5000–4.0000	0.0216

ACKNOWLEDGEMENT

The authors are thankful to the management of Petroleum Research Centre for providing facilities and encouragement.

REFERENCES

[1] Capacho-Delgado, L. and Manning, 1966, D.C., Atom. Absorp. N. Newslatt., **5**, 1.
[2] Chakarbarti, C.L. and Hall, G., 1973, Spectrosc. Lett, **6**, 385.
[3] Omang, S. H., 1971, Anal. Chim. Acta, **56**, 470.
[4] Hassan, S.S.M., 1984, Organic Analysis Using Atomic Absorption Spectrometry, Ellis Horwood Ltd., England, 328.
[5] Middleton, G. and Stuckey, R.E., 1954, Analyst, **79**, 138.
[6] Gorsuch, T.T., 1959, Analyst, **84**, 135.
[7] Vigler, M.S. and Gaylor, V.F., 1972, Appl. Spect., **28**, 342.
[8] Oil and Gas Journal data Book, 1987, published from Oil and Gas Journal.

Table 4. Trace Metal Concentrations in Different Samples

Crude Fraction	Temp. Range (°C)	Trace metal content (in $\mu g\, g^{-1}$) Copper (Cu)	Chromium (Cr)	Iron (Fe)	Lead (Pb)	Nickel (Ni)	Vanadium (V)
1A	220–280	0.0219	0.0055	0.1740	1.0520	0.2090	0.0950
1B	280–340	0.0052	0.0013	0.1000	0.1637	0.1600	0.0900
2A	220–280	0.0639	0.0427	0.5130	0.1570	0.3700	0.0550
2B	280–340	0.2230	0.0137	0.0700	0.1720	0.1990	0.0750
3A	220–280	0.0052	0.0078	0.4020	0.2700	0.1990	0.1070
3B	280–340	0.1390	0.0220	0.6930	0.0107	0.8470	0.0620
4A	220–280	0.0453	0.0151	0.2260	0.0870	0.0590	0.0520
4B	280–340	0.0059	0.0142	0.4520	0.1009	1.0980	0.0970
5A	220–280	0.0260	0.0165	0.1250	0.0848	0.0370	0.1450
5B	280–340	0.0052	0.0215	0.1320	0.1880	0.1500	0.0820
6A	220–280	0.0379	0.0004	0.0200	0.1210	0.0750	0.0720
6B	280–340	0.0052	0.0160	0.4240	0.1980	0.1250	0.0400

Trace metal content (in $\mu g\, g^{-1}$)